# Structural Studies in a Proterozoic Gneiss Complex and Adjacent Cover Rocks, West Needle Mountains, Colorado

by

Richard G. Gibson

dissertation submitted to the Faculty of the
Virginia Polytechnic Institute and State University
in partial fulfillment of the requirements for the degree of
Doctor of Philosophy
in
Geological Sciences

APPROVED:

C. Simpson, Co-chairperson

K. A. Eriksson, Co-chairperson

L. Glover III

A. K. Sinha

D. A. Hewitt

October, 1987

Blacksburg, Virginia

**Structural Studies in a Proterozoic Gneiss Complex and Adjacent Cover Rocks, West Needle Mountains, Colorado**

by

Richard G. Gibson

C. Simpson, Co-chairperson

K. A. Eriksson, Co-chairperson

Geological Sciences

(ABSTRACT)

Proterozoic rocks in the Needle Mountains include ca. 1750 Ma amphibolite-grade, metavolcanic and metaplutonic gneisses and ca. 1690 Ma granitoids that comprise basement to the siliciclastic Uncompahgre Group. The mafic and felsic gneisses underwent synkinematic metamorphism and two phases of isoclinal folding and foliation development during $D_B$, prior to emplacement of the ca. 1690 Ma plutons. $D_{BC}$ deformation caused folding of $D_B$ fabrics in the gneisses, development of a sub-vertical, east-striking foliation in the granitoids, and generation of a macroscopic sigmoidal foliation pattern throughout the area prior to 1430 Ma. $D_{BC}$ structures in the basement are correlated with macroscopic structures in the Uncompahgre Group, which was deformed into an east-trending cuspate synclinorium during this event. Gently plunging mineral lineations and asymmetric kinematic indicators in the basement record a component of dextral strike-slip shearing in domains of east-striking foliation and sinistral shearing in areas of northeast-striking foliation. A model for $D_{BC}$ involving the development of conjugate strike-slip shear zones in response to north-northwest shortening is most consistent with the kinematic and fabric orientation data.

A zone of phyllite, derived largely from basement, occurs everywhere along the basement-cover contact. Kinematic indicators along and near the contact record upward movement of the cover relative to basement on each side of the synclinorium and imply that the cover rocks are parautochthonous. Stratigraphic facing of the cover rocks away from basement supports the interpretation of this contact as an unconformity at the base of the Uncompahgre Group. Alteration of the basement rocks along this contact involved hydration and the loss of CaO, MgO, $SiO_2$, and $Na_2O$. The phyllite zone is interpreted as a metamorphosed and deformed regolith that localized out-of-synform movement while the basement and its parautochthonous cover were folded together during $D_{BC}$.

Rocks in the Needle Mountains comprise part of the Colorado Province, one of several terranes that were possibly accreted to the Archean Wyoming Craton during the Proterozoic. Age constraints on the timing of deformation indicate that $D_B$ and $D_{BC}$ are representative of two regionally extensive deformational episodes. Pre-1700 Ma deformation is attributed to the assembly of volcanogenic terranes and their accretion to the Wyoming Craton along the Cheyenne Belt. Post-1700 Ma deformation resulted from regional north-northwest crustal shortening induced by tectonic interactions along the southern margin of the Colorado Province. These results support the hypothesis that terrane accretion was important in the Proterozoic crustal evolution of southwestern North America.

# Acknowledgements

This work was funded by teaching assistantships from the Department of Geological Sciences, a Cunningham Research Fellowship from Virginia Polytechnic Institute and State University (1986-1987), and National Science Foundation grant EAR-8507052 to C. Simpson. I would like to thank C. Simpson, K. A. Eriksson, and for their close interaction during all phases of this research. L. Glover III, A. K. Sinha, and D. A. Hewitt made constructive criticisms on portions of the manuscript. Field assistance was provided by . Additional thanks to and the rest of my fellow graduate students who have provided support, encouragement, and ideas during the course of this project.

# Table of Contents

# List of Illustrations

# List of Tables

# Chapter 1: Proterozoic Cuspate Basement-Cover Structure, Needle Mountains, Colorado

## INTRODUCTION

In many compressional orogenic belts, decollement zones of significant displacement are present within lithologic units along or near basement-cover contacts (Price and Mountjoy, 1970; Gee; 1980; Tirrul, 1983). However, in other settings where basement is folded together with its autochthonous to parautochthonous cover (Ramsay, 1967; Platt, 1980; Hoffman et al., 1984), zones of locally intense deformation also may occur near basement-cover interfaces (Gratier and Vialon, 1980; Jacob et al., 1983; Tricart and Lemoine, 1986). The distinction between deformation zones that result from large-scale translation of rock units and those that may form as a mechanical response to folding is critical to evaluation of basement-cover relations. In Precambrian terranes, where cover sequences commonly occur as deformed remnants surrounded by basement, this distinction is especially important for developing tectonic models.

Deformed, post-1700 Ma siliciclastic cover sequences in southwestern North America are present as inliers within older, volcano-plutonic basement complexes. A variety of basement-cover relations have been recognized throughout this region (Barker, 1969; Grambling and Codding, 1982; Tewksbury, 1985; Karlstrom and Conway, 1986). In central Arizona, the Mazatzal Group unconformably overlies ca. 1740 Ma basement and was involved in north-directed, thin-skinned thrusting (Puls and Karlstrom, 1985; Karlstrom and Conway, 1986). Metasedimentary rocks of the

Ortega Group in north-central New Mexico were deformed with basement into north-directed fold nappes (Grambling and Codding, 1982). Within the Needle Mountains of southwest Colorado, the area of this detailed study (Fig. 1-1), the cover rocks of the Uncompahgre Group have been interpreted to either (1) unconformably overlie ca. 1750 Ma basement (Barker, 1969) or (2) be in contact with basement along major south-directed thrusts (Tewksbury, 1985).

In the northwestern Needle Mountains (Fig. 1-1), we undertook a detailed stratigraphic and structural analysis of Proterozoic basement and cover rocks in order to place constraints on their contact and age relations and resolve the apparent conflict in tectonic transport direction relative to terranes of similar age in New Mexico and Arizona. Evaluation of new and previously published data leads to a re-interpretation of the structural evolution of this area. The model presented in this paper may be applicable to other terranes where similar basement-cover relations exist.

## STRATIGRAPHIC UNITS

The basement complex in the northwestern Needle Mountains (Fig. 1-1) is composed of (1) amphibolite-grade, compositionally layered and non-layered gneisses derived from mafic to felsic volcanogenic and plutonic rocks and (2) weakly foliated quartz diorite to granite intrusive rocks that cross-cut a prominent foliation within the gneisses (Barker, 1969). Rb-Sr and U-Pb isotopes yield ages of 1740-1760 Ma for the protoliths of the gneiss complex and 1680-1700 Ma for the granitoid plutons (ages recalculated from Silver and Barker, 1968; Barker et al., 1969; Bickford et al., 1969).

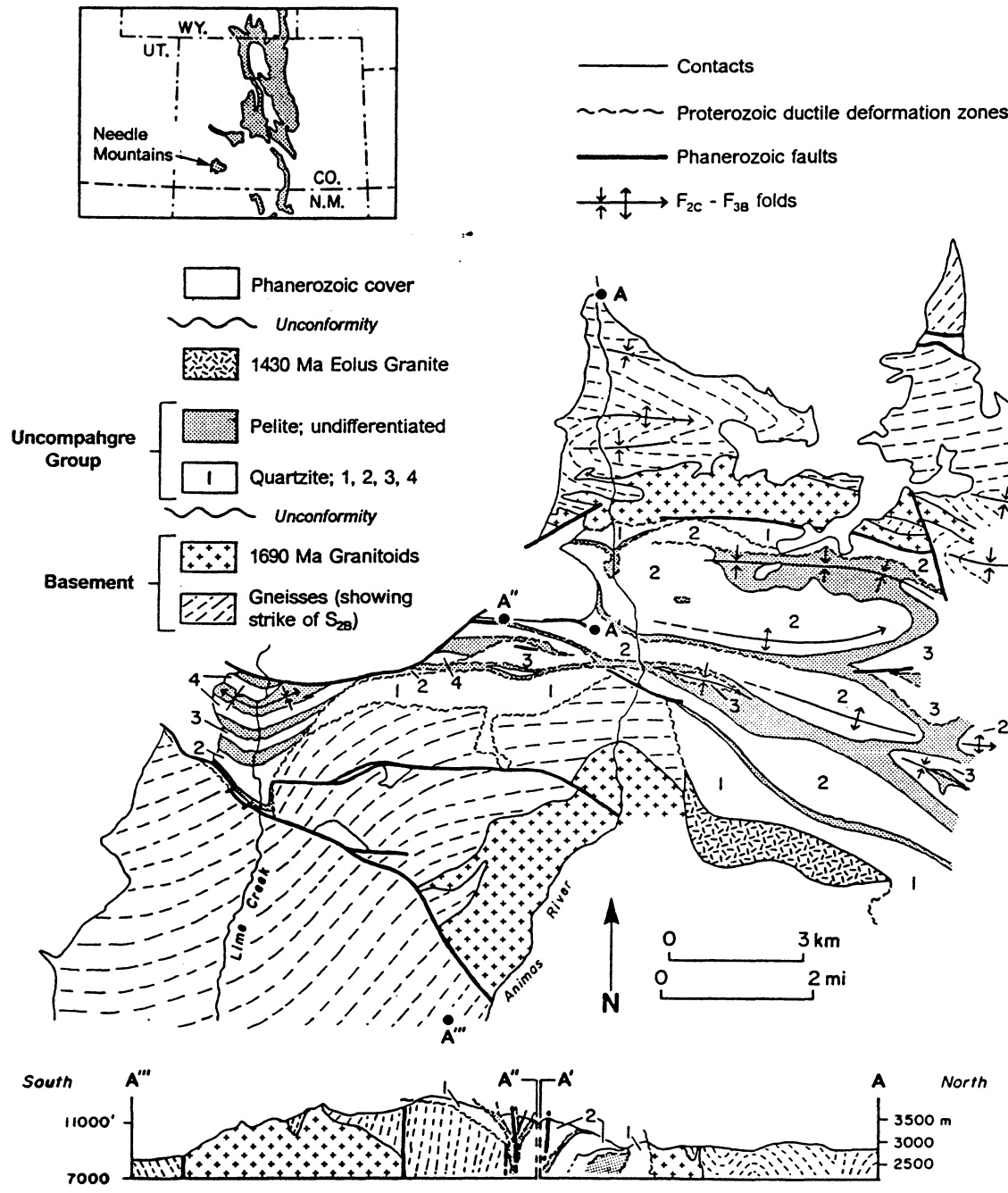


Figure 1-1: Geologic map and cross section of study area. Eastern and southeastern margins of map area from Barker (1969) and Tewksbury (1985). Inset shows location of Needle Mountains and other areas of Early to Middle Proterozoic outcrops (stippled).

The Uncompahgre Group occupies an east-trending belt bounded by basement and consists of four alternating packages of quartzite and pelite; the total thickness is approximately 3 km (Fig. 1-1; stratigraphic subdivisions defined in Harris and Eriksson, 1987). Individual quartzite and pelite units, which are distinguishable from one another based on a sequential ordering of facies, may be correlated throughout the map area. Abundant primary sedimentary structures provide control on younging directions within stratigraphic units. The age of the Uncompahgre Group relative to basement is uncertain because of localized deformation along basement-cover contacts and the absence of clasts of the underlying basement in the cover rocks. If the Uncompahgre Group unconformably overlies basement, as suggested by Barker (1969), then its maximum age would be equivalent to the ca. 1690 Ma granitoids. However, if basement-cover contacts are major thrusts, as proposed by Tewksbury (1985), then the Uncompahgre Group may be as old or older than basement gneisses. A minimum age for the Uncompahgre Group is provided by the cross-cutting, undeformed, 1410-1450 Ma Eolus Granite (Silver and Barker, 1968; Barker, 1969; Bickford et al., 1969).

## STRUCTURAL GEOLOGY

Two polyphase pre-1430 Ma deformational events ($D_B$ and $D_{BC}$) can be distinguished within the study area. $D_B$ is exclusive to basement whereas $D_{BC}$ structures are the product of an event that affected both basement and cover (Gibson and Simpson, 1986; Harris et al., 1986). An early phase of metamorphism ($M_1$) resulted in the growth of synkinematic garnets during $D_B$. Post-$D_{BC}$, $M_2$ metamorphism produced muscovite + chlorite ± andalusite ± chloritoid within the Uncompahgre Group and along basement-cover contacts, and retrograde assemblages within the basement

(Barker, 1969). The chronology of tectonic features and metamorphism is outlined in Figure 1-2.

### $D_B$ Structures Within Basement

A well-developed planar mineral alignment ($S_{1B}$) is parallel to lithologic contacts everywhere except in mesoscopic, isoclinal $F_{1B}$ fold hinges. $F_{2B}$ folds are close to isoclinal, have a weak axial planar $S_{2B}$ mineral alignment, deform $S_{1B}$, and are cross-cut by the ca. 1690 Ma granitoids. $D_B$ structures are truncated along contacts with the Uncompahgre Group.

### $D_{BC}$ Structures Within Basement and Cover

The oldest structures within the Uncompahgre Group are deformation zones localized within stratigraphic intervals of interbedded pelite and quartzite up to 50 m thick or individual pelitic beds < 15 cm thick. Structures in the thicker deformation zones include mesoscopic, tight to isoclinal, locally rootless folds ($F_{1C}$) that have axial-planar slaty cleavage, $S_{1C}$ (Tewksbury, 1981, 1985; Harris et al., 1986). Narrower bedding-parallel deformation zones exhibit a sigmoidal foliation ($S_{1C}$) defined by elongate detrital grains, quartz ribbons, and aligned white mica + hematite. Shear zone geometry and local stratigraphic duplication within individual quartzite units indicate that north-directed thrusting produced these structures.

Macroscopic, upright, subhorizontal, east-trending, tight to open folds ($F_{2C}$ and $F_{3B}$; Figs. 1-1 and 1-2) deform $D_B$ structures in basement (Gibson and Simpson, 1986) and the bedding-parallel deformation zones within the Uncompahgre Group (Tewksbury, 1981, 1985). Circa 1690 Ma granitoids in the basement contain a

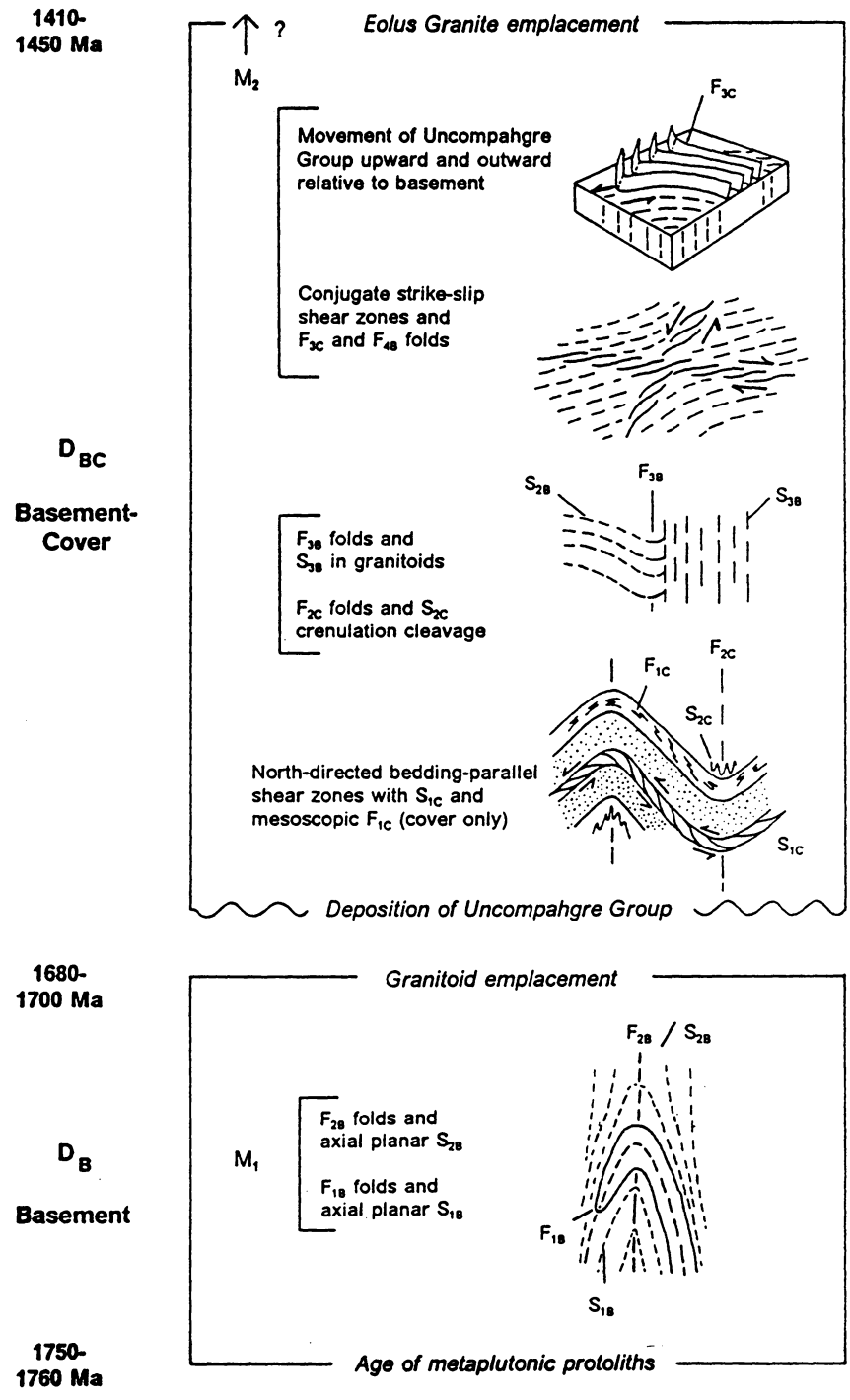


Figure 1-2: Chronology of deformation, plutonism, and metamorphism in the study area. Time scale is nonlinear. Peak of $M_2$ postdates $D_{BC}$, but minimum age is uncertain.

subvertical, east-striking, $S_{3B}$ foliation parallel to $F_{3B}$ axial surfaces. In the cover, an axial-planar spaced cleavage ($S_{2C}$) is associated with $F_{2C}$ folds.

Foliation surfaces ($S_{1B}$-$S_{3B}$) in basement gneisses and ca. 1690 Ma granitoids contain a subhorizontal mineral lineation that is parallel to the long axes of deformed clasts in metavolcaniclastic rocks. Asymmetric quartz *c*-axis fabrics and rare subvertical, mesoscopic shear zones or shear bands indicate predominantly dextral, noncoaxial flow in domains of east-striking foliation, and sinistral shear in zones of northeast-striking foliation (see map pattern of $S_{2B}$ foliation in Fig. 1-1). These directions and senses of movement resemble those observed in conjugate ductile shear zones (cf. Ramsay, 1980) and imply north-northwest to south-southeast shortening.

Steeply dipping, east- and northeast-striking zones of localized deformation within the Uncompahgre Group (Fig. 1-1) are characterized by attenuated and truncated stratigraphic units and phacoidal or crenulation fabrics in pelites. Asymmetrically pulled-apart psammitic beds, shear bands, and gently to moderately plunging mineral lineations indicate dextral oblique movement along east-striking zones and sinistral oblique slip within northeast-striking zones (Fig. 1-1). These senses of movement concur with the pattern observed in the basement.

Steeply plunging, macroscopic $F_{3C}$ and mesoscopic $F_{4B}$ folds in the vicinity of Lime Creek (Fig. 1-1) geographically coincide with zones of sinistral shearing in both the basement and cover. These structures are interpreted to be the product of reorientation of older structural elements into a northeast-striking, sinistral shear zone.

## $D_{BC}$ Structures Along Basement-Cover Contacts

Contacts between the basement and Uncompahgre Group are marked by a zone of quartz-muscovite phyllite or phyllonite that is generally less than 2 m thick but locally up to 12 m thick (Barker, 1969; Tewksbury, 1985). Within the adjacent Uncompahgre Group, conglomerates and pebbly sandstones become increasingly foliated and grade into these micaceous lithologies. In basement gneisses and granitoids, mineral assemblages are altered to phyllosilicates + Fe-Ti oxides; relict foliations ($S_{1B}$ or $S_{2B}$) are either deflected into parallelism with the contact or overprinted by a spaced to continuous muscovite foliation that is subparallel to the contact.

The northern basement-cover contact is vertical to steeply north-dipping, whereas the southern contact is convex upward, and subhorizontal at topographically highest elevations (Fig. 1-1, cross section). Cover rocks, typically of the basal unit (quartzite 1; Fig. 1-1), always young away from the contacts. On the southern contact east of Lime Creek, Proterozoic sinistral offset of stratigraphic units in the cover resulted in the juxtaposition of quartzite 2 and basement (Fig. 1-1). Along the northern contact east of the Animas River, a Phanerozoic fault places granitoids against quartzite 2 of the Uncompahgre Group (Fig. 1-1).

Shear bands within phyllonites along the southern contact record north-side-up, dip-slip motion; < 10 cm-thick shear zones within the basal 50 m of the Uncompahgre Group quartzites show oblique dextral and north-side-up movement. Fabrics in phyllites along the northern contact usually display a lack of consistent asymmetry. At one locality along the northern contact west of the Animas River (Fig. 1-1), a basal quartz-pebble conglomerate of the Uncomaphgre Group is in direct contact with retrograded gneiss and granite. The outcrop exhibiting this probable

unconformable contact is bounded on the north and south by south-side-up deformation zones.

## DEFORMATION MODEL

Previous deformation models for the Needle Mountains have implied that the Uncompahgre Group is either parautocthonous (Barker, 1969) or allochthonous (Tewksbury, 1985) relative to basement. Tewksbury (1985) inferred a south-directed sense of tectonic transport from the apparent ramp-flat geometry of the phyllonite zone that defines the southern basement-cover contact (Fig. 1-1, cross section). Bedding-parallel deformation zones refolded about upright folds ($F_{2C}$) were interpreted by Tewksbury (1981) to be the product of progressive south-directed thrusting. This model requires a consistent north-side-up sense of movement on both the northern and southern basement-cover contacts. Major inconsistencies between Tewksbury's (1981, 1985) model and our data include (1) predominantly north-directed movement on pre-$F_{2C}$ deformation zones within the Uncompahgre Group and (2) opposing senses of dip-slip movement along the northern and southern basement-cover contacts.

An alternative model for $D_{BC}$ in the northwestern Needle Mountains is illustrated in Figure 1-3. The Uncompahgre Group was deposited unconformably on a previously deformed gneiss complex intruded by ca. 1690 Ma granitoids. Subsequent deformation was initially thin-skinned and produced north-directed, bedding-parallel deformation zones and local stratigraphic duplication (Fig. 1-3a). The preservation of intact stratigraphic order within the Uncompahgre Group, especially in the western and eastern parts of the study area (Fig. 1-1), suggests that this deformation did not involve large-scale stratigraphic duplication at the scale of the map area. With further

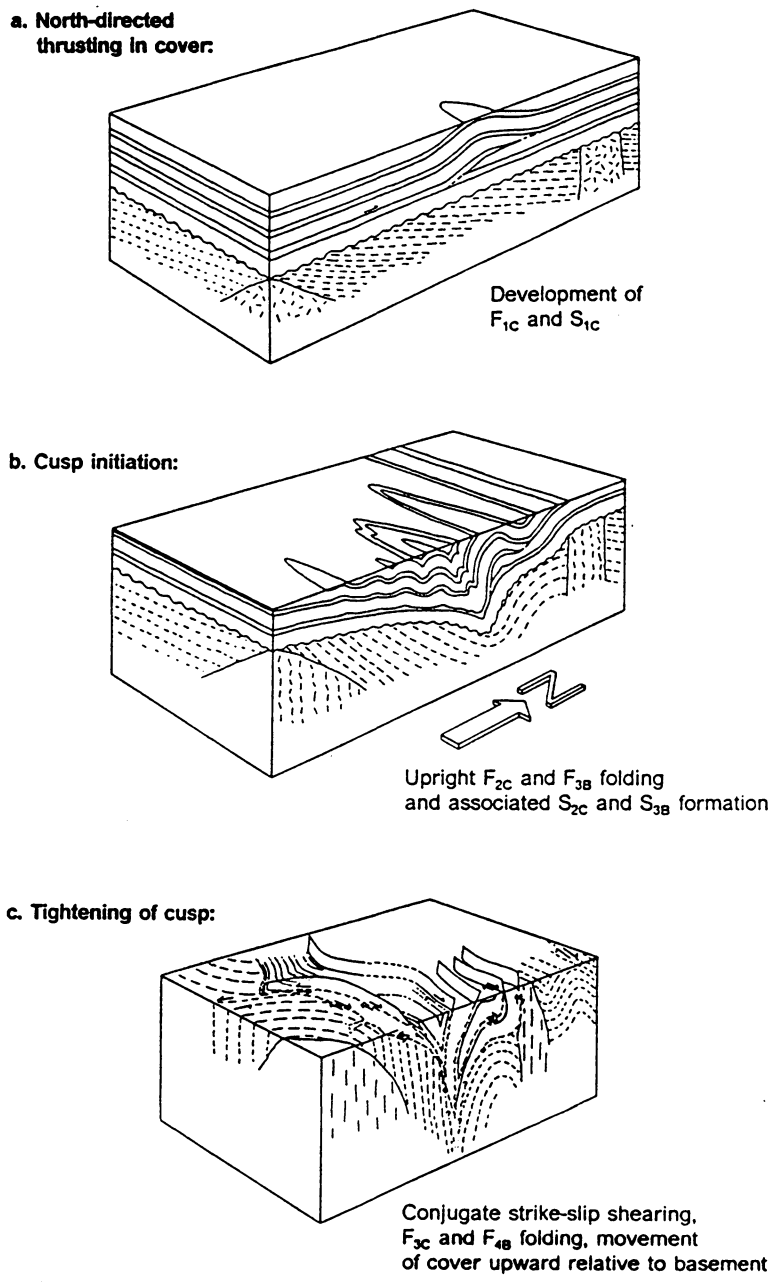


Figure 1-3: Interpretive model for $D_{BC}$ deformation in northwestern Needle Mountains. North-directed thrusting (a) was preceded by deposition of Uncompahgre Group unconformably upon basement. Pre-$D_{BC}$ basement fabric orientation is unknown. Cover structures in (b) patterned after observed deformation style in eastern part of map area.

compression, upright folding ($F_{2C}$, $F_{3B}$) of basement and cover began and the unconformity surface was deformed into a cusp-shaped geometry with convex-upward limbs (Fig. 1-3b). This type of structure is typically interpreted to reflect the greater viscosity of one unit (basement) relative to the other (cover) during folding (Ramsay, 1967; Dieterich, 1970). The final increments of deformation involved strike-slip shearing within all lithologic units and tightening of the cusp with upward movement of the Uncompahgre Group relative to basement (Fig. 1-3c). Decoupling of cover from basement during cuspate folding probably occurred because of contrasting rheological properties and the presence of a mechanically weak micaceous layer along the contact (probable unconformity). This process may be analogous to the detachment along lithologic contacts that is necessary to accommodate space problems during concentric folding of layered sequences (cf. Dahlstrom, 1977).

Although our data are consistent with the Uncompahgre Group being deposited unconformably on basement, few clasts in the basal Uncompahgre Group can be linked to a local basement provenance. However, potential source rocks for chert and iron formation clasts in the Uncompahgre Group (Harris and Eriksson, 1987) do exist in basement terranes in southwest Colorado (e.g. Barker, 1969; Afifi, 1981). The absence of locally derived felsic gneiss and amphibolite clasts may be due to a distant provenance and/or deep weathering of these lithologies to sand- and clay-sized fractions (e.g. Stallard, 1986). A weathered horizon is a possible protolith for the hydrated aluminous rocks found along the basement-cover contacts.

Cross sections of the Uncompahgre Group outcrop belt (Figs. 1-1 and 1-3c) cannot be restored to their undeformed state by using standard section balancing techniques (e.g., Dahlstrom, 1969) because of the movement of stratigraphic units into and out of the plane of section during the final phase of $D_{BC}$. It is also not possible to estimate the magnitude of displacement along basement-cover contacts be-

cause they are parallel to bedding in the Uncompahgre Group and no other marker units are present at this interface.

The age of $D_{BC}$ deformation can only be bracketed between pluton emplacement at approximately 1690 and 1430 Ma. It is possible, therefore, that the various phases of $D_{BC}$ do not represent a continuum of deformation. However, a single progressive event most simply explains the observed relationships.

## IMPLICATIONS

Basement-cover contacts in the northwestern Needle Mountains, previously interpreted as south-directed thrusts (Tewksbury, 1985), are reinterpreted as unconformities that localized deformation during cuspate infolding of cover into basement following limited north-directed, thin-skinned thrusting. This movement pattern is consistent with north-directed tectonic transport documented in approximately coeval rocks of northern New Mexico (Grambling and Codding, 1982) and central Arizona (Puls and Karlstrom, 1985; Karlstrom and Conway, 1986). The style of Proterozoic deformation in the Needle Mountains is apparently analogous to that of the Alpine external massifs and their cover (Ramsay, 1967; Gratier and Vialon, 1980; Tricarte and Lemoine, 1986) and the Tree River fold belt and internal zone of the Wopmay Orogen (Hoffman et al., 1984; King, 1986).

Cuspate structures may be more common than previously recognized in geologic terranes where cover sequences occur as isolated remnants within basement. Deformation zones along basement-cover interfaces in such settings may form as a geometrical product of folding, and may not necessarily represent loci of large-scale tectonic translation.

# Chapter 2: Proterozoic Polydeformation in Basement Rocks of the Needle Mountains, and its Regional Tectonic Implications

## INTRODUCTION

Proterozoic rocks in western North America occur in northeast-trending provinces that decrease in age discontinuously southward from Archean rocks of the Wyoming Craton (Condie, 1982). These age provinces have been interpreted as regions of juvenile crust that were accreted to the Wyoming Craton episodically throughout the Early and Middle Proterozoic (Condie, 1982; Nelson and DePaolo, 1985). The oldest of these terranes, the Colorado Province (Bickford et al., 1986), bounds the Wyoming Craton along the Cheyenne Belt (Karlstrom and Houston, 1984) in southern Wyoming and extends south and west into northern New Mexico and central Arizona (Fig. 2-1). The central part of this province is composed largely of metamorphosed 1700-1800 Ma pelitic and immature psammitic rocks whereas the northwestern and southeastern portions are dominated by approximately coeval rocks of volcanogenic origin (Tweto, 1980). Granitoid plutons, ranging in age from approximately 1750 Ma to 1000 Ma intrude the metamorphic rocks (Tweto, 1980).

Structural studies along the northern and southern margins of the Colorado Province have shown that northward nappe translation was an integral part of their structural development (Grambling and Codding, 1982; Karlstrom and Houston, 1984; Puls and Karlstrom, 1985; Karlstrom and Conway, 1986; Grambling and Ward, 1987; Deubendorfer and Houston, 1987). In contrast, the kinematic significance of structures in the interior of the Colorado Province, where moderately to steeply dipping

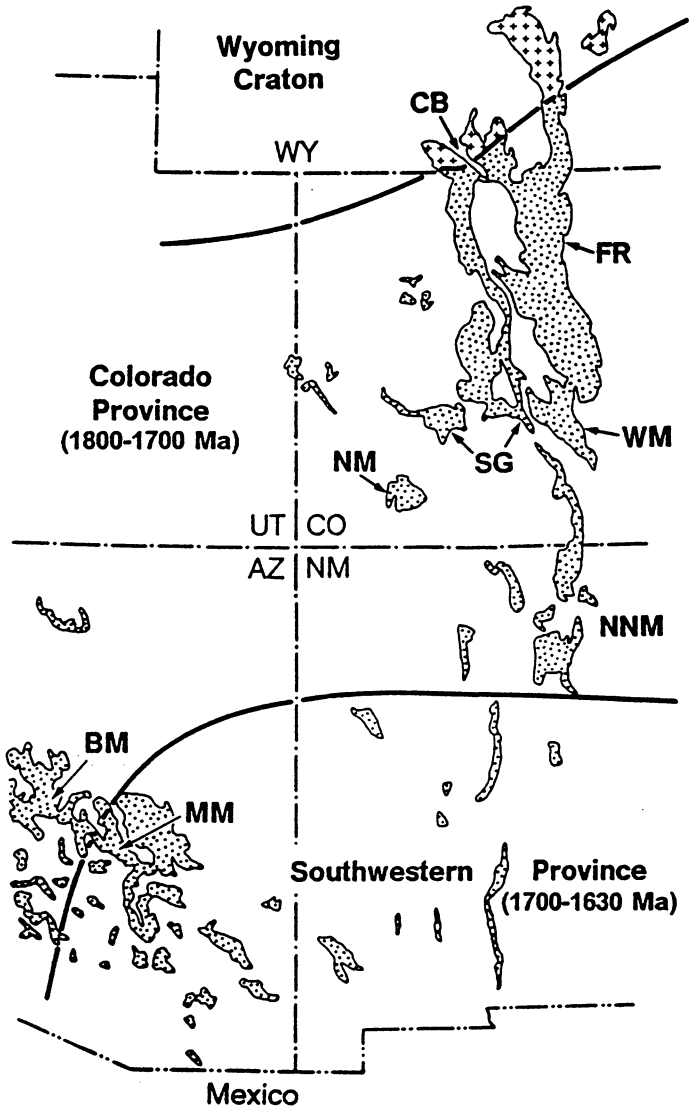


Figure 2-1: Map (after Condie, 1982) showing areas of Early to Middle Proterozoic (stippled) and Archean (crosses) outcrop in the southwestern United States with age provinces as defined by Bickford et al. (1986). Locations mentioned in text include Bradshaw Mountains (BM), Cheyenne Belt (CB), Front Range (FR), Mazatzal Mountains (MM), Needle Mountains (NM), northern New Mexico (NNM), Salida-Gunnison area (SG), and Wet Mountains (WM).

foliations lack a regionally consistent orientation (Tweto, 1980; Reed et al., in press), is uncertain. Although polyphase folding sequences have been described for a few portions of the central Colorado Province (e.g. Taylor, 1976; Braddock and Cole, 1979), no regional deformation chronology exists.

This paper contains an evaluation of the sequence, absolute chronology, and kinematic significance of structures in an internal portion of the Colorado Province. The northwestern Needle Mountains region (Fig. 2-1) was selected for 1:12500 scale mapping and structural analysis because three lithologic/stratigraphic sequences with contrasting deformation histories are preserved (Barker, 1969; Tewksbury, 1985; Harris et al., 1987) and existing radiometric age data (Silver and Barker, 1968; Barker et al., 1969; Bickford et al., 1969) may be used to bracket ages of deformation. The data presented in this paper are interpreted in terms of two distinct deformational episodes. The older event produced penetrative fabrics in rocks older than 1700 Ma whereas the younger one affected all three sequences and resulted from north-northwest crustal shortening prior to 1430 Ma. These results are discussed with regard to data from other portions of the Colorado Province in order to evaluate regional deformation patterns.

## GEOLOGIC SETTING

The Needle Mountains comprise a 1100 $km^2$ (425 $mi^2$) exposure of Proterozoic rocks in southwestern Colorado (Figs. 2-1, 2-2a). Tilted and gently folded Cambrian to Pennsylvanian strata unconformably overlie the Precambrian rocks on the south and west whereas Oligocene volcanogenic rocks of the San Juan volcanic field occur to the north and east (Tweto, 1979). The area of detailed mapping covers approxi-

Figure 2-2:

a) Generalized geologic map of the Needle Mountains after Barker (1969); boxed area enlarged in (b).

b) Geologic map of northwestern Needle Mountains; CBP - Coal Bank Pass, HML - Highland Mary Lakes, ML - Molas Lake, SP - Snowdon Peak.

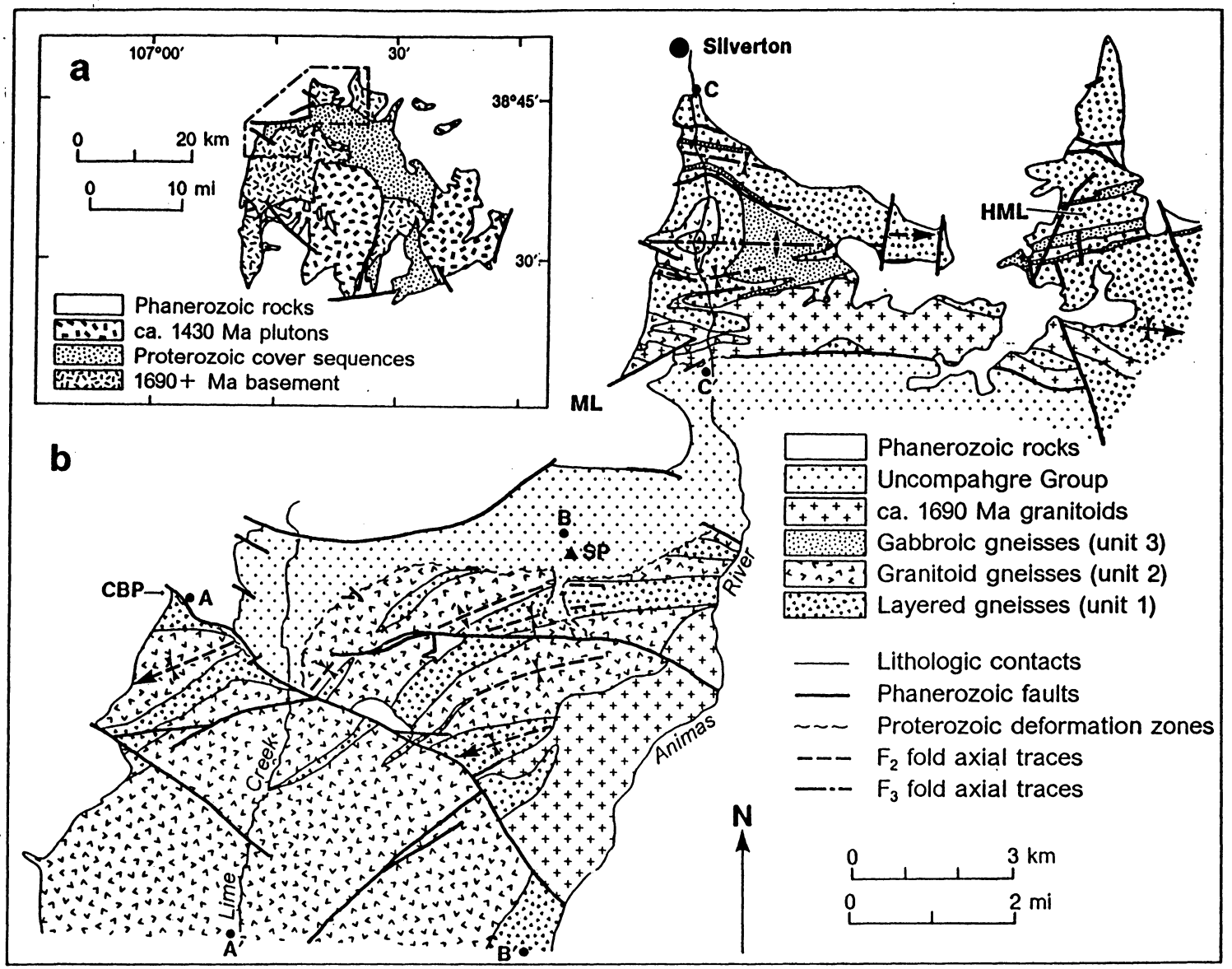
a
107°00′
30′
38°45′
30′
0
20 km
0
10 mi
Phanerozoic rocks
ca. 1430 Ma plutons
Proterozoic cover sequences
1690+ Ma basement
Silverton
C
C′
HML
ML
b
B
SP
CBP
A
River
Animas
Lime Creek
A′
B′
Phanerozoic rocks
Uncompahgre Group
ca. 1690 Ma granitoids
Gabbroic gneisses (unit 3)
Granitoid gneisses (unit 2)
Layered gneisses (unit 1)
Lithologic contacts
Phanerozoic faults
Proterozoic deformation zones
F2 fold axial traces
F3 fold axial traces
N
0
3 km
0
2 mi

mately 140 km$^2$ (55 mi$^2$) in the northwestern corner of the mountain range, south of the town of Silverton (Fig. 2-2a).

Numerous Phanerozoic faults, defined by zones of cataclasis and iron-staining, cross-cut the Proterozoic rocks but do not significantly disrupt Precambrian geologic relationships. Paleozoic stratigraphic variations across faults in the vicinity of Coal Bank Pass and Molas Lake (Fig. 2-2b) indicate episodic movement throughout the Paleozoic and into the Pennsylvanian during which the Needle Mountains stood as a topographic highland (Baars and See, 1968). North- and east-striking faults in the area south and southeast of Silverton (Fig. 2-2b) locally displace the basal portion of the Tertiary volcanic sequence and are, therefore, interpreted to have ceased movement during the Oligocene.

Proterozoic rocks in the Needle Mountains (Fig. 2-2a) include 1) a metamorphosed volcano-plutonic complex intruded by ca. 1690 Ma granitoid plutons (basement complex); 2) conglomerates, quartzites, and pelites of the Uncompahgre Group and Vallecito Conglomerate (cover sequences); and 3) undeformed ca. 1430 Ma granite and gabbro plutons that intrude both the basement and cover (Barker, 1969). Within the map area (Fig. 2-2b), basement rocks occupy two areas separated from one another by an east-west trending synformal outcrop belt of the Uncompahgre Group (Barker, 1969; Harris et al., in press). These areas of basement outcrop are referred to as the northern and southern basement domains. Contacts between the basement and cover are marked by narrow phyllonite zones (Barker, 1969; Tewksbury, 1985). Although the earliest workers in the region (Cross et al., 1905; Barker, 1969) considered the Uncompahgre Group to be younger than the basement, Tewksbury (1985) proposed that the units are in thrust contact along the phyllonite zones and that their relative ages are, therefore, unconstrained. However, Harris et al. (in press) showed that the basement and Uncompahgre Group share part

of the same deformation history and that the sense of tectonic transport along basement-cover contacts is inconsistent with the thrust belt model of Tewksbury (1985). They argued that the Uncompahgre Group is parautochthonous and was deposited unconformably on the ca. 1690 Ma granitoids and previously deformed metavolcanic rocks. The phyllonite zones were generated by differential movement of lithologic units during folding of the cover together with basement. Structures within the Uncompahgre Group and along basement-cover contacts are discussed in Harris (1987) and Chapter 3. In this paper, the lithologies and structures within the basement complex are described and a model developed to explain its polyphase structural evolution.

## LITHOLOGIC UNITS OF THE BASEMENT COMPLEX

Cross et al. (1905) and Barker (1969) recognized two mappable gneissic units, the Twilight Gneiss and Irving Formation, in addition to granitoid plutons within the basement complex. Quartzo-feldspathic gneisses in the western half of the southern basement domain were previously mapped as the Twilight Gneiss whereas amphibolites and associated lithologies exposed farther east and in the northern basement domain were included in the Irving Formation. Because northeast-striking lithologic belts may be traced continuously across the inferred north-south trending contact between the Twilight Gneiss and Irving Formation (cf. Fig. 2-2b with Fig. 2-2 of Barker, 1969), these unit names are not used here. The gneisses are, instead, subdivided on the basis of lithology and the presence or absence of outcrop-scale compositional layering. The mineralogy, texture, and field characteristics of the map units are summarized in Table 2-1.

Table 2-1: Characteristics of map units within gneiss complex; numbers in parentheses in Mineralogy column are approximate modal abundances of each mineral.

| Mineralogy | Texture | Field Characteristics |
|---|---|---|
| **Unit 1: Layered Gneiss** | | |
| a. pl(10-60) + qtz(20-50) + bt(tr-40) ± grt(≤10) ± ms(≤25) ± ksp(≤10) | bt ± ms foliation; 0.05-1mm grain size; some porphyroblastic grt | centimeter to meter scale layering defined by variable mica content; gradational into dacite porphyry, breccia, and flow-banded metadacite; locally contains ≤15mm-long ellipsoidal quartz aggregates ("eyes") or prominent pressure shadows around garnets |
| b. hb(5-70) + pl(10-60) ± bt(≤35) ± qtz(≤25) ± ep(≤20) ± grt(≤5) ± act(≤20) | hb ± bt foliation; 0.05-1.0mm grain size | centimeter to decimeter scale layering defined by variable ep or pl content; locally relict amygdules, pillow structures, and volcaniclastic textures |
| c. qtz(80-95) + mt(5-20) ± grt(≤2) | mt foliation; 0.1-1mm grain size | ≤200m-long lenses within 1a and 1b; strongly magnetic |
| d. pl(40-60) + bt(10-25) + ged(2-10) + qtz(5-15) ± cum(≤20) ± grt(≤10) | massive to weakly foliated; 1-4mm grain size radiating amphibole crystals | restricted to areas of intense tectonic disruption west of Lime Creek |
| **Unit 2: Granitoid Gneiss** | | |
| a. pl(25-45) + qtz(20-40) + bt(8-20) ± hb(≤35) ± ksp(≤11) ± ep(≤2) ± grt(≤2) | ribbony foliation; 0.05-1mm grain size; 10-20mm long grain aggregates; locally porphyroclastic | abundant ellipsoidal mafic inclusions elongate parallel to foliation; commonly interlayered with amphibolite (1b or 3b) |
| b. pl(25-50) + qtz(30-40) + bt(tr-10) ± ksp(≤25) ± ep(≤10) | weakly to strongly foliated; 0.05-1mm grain size; 3-7mm long grain aggregates | homogeneous in outcrop; locally contains layers of 3b; interlayered with 1b along contacts |
| **Unit 3: Gabbroic Gneiss** | | |
| a. hb(60-75) + pl(15-40) + ttn(tr-5) ± ep(≤5) ± chl(≤1) ± qtz(≤1) | weakly to strongly foliated; 1-4mm grain size; ≤10mm long grain aggregates; locally porphyroclastic | homogeneous in outcrop; contacts locally truncate layering in 1b; gradational into medium- to coarse-grained metagabbro |
| b. hb(60-75) + pl(25-40) ± grt(≤2) | ≤2mm grain size; 1-2mm diameter pl ± grt aggregates | as 1-3m thick layers within units 1 and 2; layers locally cross-cut mafic inclusions in 2a |

Compositionally layered gneisses (unit 1, Table 2-1) are the most abundant rocks in the northern basement domain and also occur as ≤1 km wide bands within granitoid gneisses (unit 2, Table 2-1) of the southern domain. They commonly comprise predominantly felsic (unit 1a) or mafic (unit 1b) subunits. Lenses of siliceous gneiss (unit 1c) crop out locally within the northern domain whereas orthoamphibole-bearing gneiss (unit 1d) is restricted to the area south of Coal Bank Pass (Fig. 2-2b). In the vicinity of the Highland Mary Lakes (Fig. 2-2b), layered gneisses are gradational into a sequence of pillowed (Barker, 1969) and amygdaloidal metabasalt (Fig. 2-3a), felsic porphyry, flow-banded metarhyolite/dacite, and volcaniclastic breccia (Fig. 2-3b). Throughout the rest of the map area, recognizable volcanogenic textures are restricted to small, apparently low strain lenses (Fig. 2-3a). Quartz "eyes" in some of the felsic gneisses (unit 1a) have been interpreted as relict igneous phenocrysts (Barker, 1969).

Granitoid gneisses (unit 2; Table 2-1), distinguished from unit 1 by their typical lack of outcrop-scale compositional layering and the presence of 3-20mm long mineral aggregates, predominate in the southern basement domain. In a few areas, two compositional varieties are recognized. Tonalitic to granodioritic gneisses (unit 2a; Table 2-1) characteristically contain biotite- and hornblende-rich inclusions which impart a layered appearance where they are abundant (Fig. 2-3c). Leucotonalitic, leucogranodioritic, and granitic gneisses (unit 2b; Table 2-1) lack these mafic inclusions and occur locally as dikes intruding both units 1 and 2a Fig. 2-3d). Much of unit 2 cannot be subdivided because all gradations between these two end-members exist. Contacts between units 1b and 2 are commonly transitional and characterized by intercalated, discontinuous layers of granitoid gneiss and amphibolite (25-75%).

Gabbroic gneiss (unit 3, Table 2-1) occurs as layers 25-200 m thick within unit 1 of the northern domain and as 1-3 m thick layers within unit 2 of the southern do-

Figure 2-3: Primary features in the gneisses.

a) plagioclase + epidote-filled amygdules preserved in weakly foliated lens in amphibolite (unit 1b);

b) felsic volcaniclastic breccia (unit 1a);

c) mafic inclusions in unit 2a truncated by amphibolite layer of unit 3b;

d) dike of unit 2b cross-cutting mafic inclusion in unit 2a and deformed by $F_1$ fold with axial planar $S_1$.

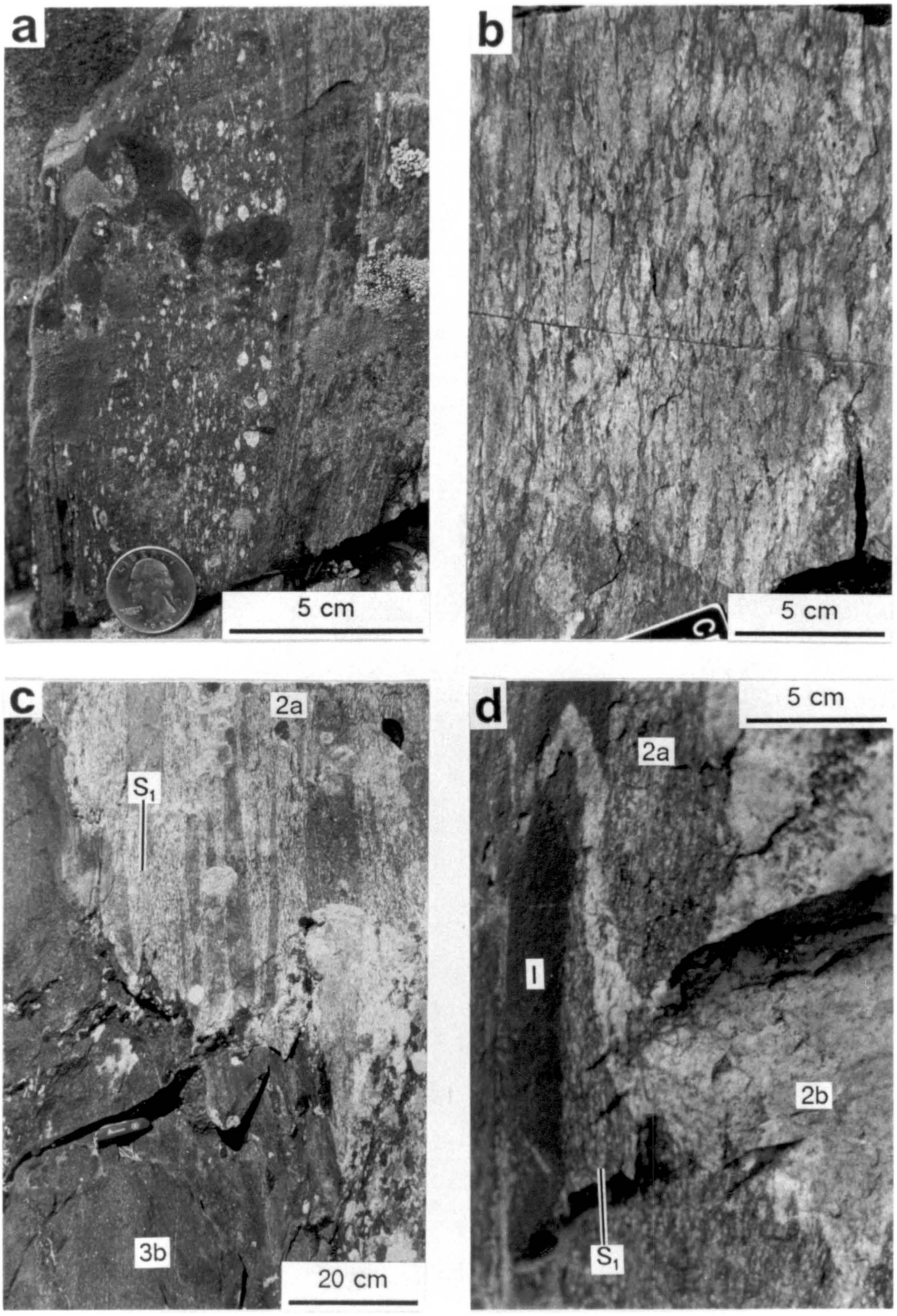
a
5 cm
b
5 cm
c
2a
S1
3b
20 cm
d
5 cm
2a
I
2b
S1

main. Near the Highland Mary Lakes (Fig. 2-2b), unit 3a (Table 2-1) is gradational into bodies of medium- to coarse-grained metagabbro with contacts discordant to compositional layering in unit 1a. Layers of unit 3b (Table 2-1) locally cross-cut mafic inclusions contained in unit 2a (Fig. 2-3c).

Barker et al. (1969) derived a Rb-Sr isochron age of 1767 ± 35 Ma[1] from twelve whole-rock samples of the Twilight Gneiss. These data were collected from rocks of both units 1 and 2 of this study and suggest that these two units are of similar age. A 1753 ± 20 Ma U-Pb zircon age (Silver and Barker, 1968) for rocks of unit 2 in both the northern and southern basement domains is consistent with the Rb-Sr data and is interpreted as a formation age of the protolith. A slightly older age for part of unit 1 may be indicated by the fact that U-Pb data from one layered gneiss lithology plots to the right of the discordia defined by data from unit 2 (data of L. T. Silver discussed in Barker, 1969). Units 1 and 3 from the northern basement domain have not been dated.

The gneisses in the northwestern Needle Mountains are interpreted as a deformed volcano-plutonic complex comprised of a volcanogenic sequence (unit 1), ca. 1750 Ma granitoid plutons (unit 2), and gabbroic dikes (unit 3). Rarely preserved primary features in units 1a and 1b suggest that their protoliths included felsic and subaqueous mafic flows, felsic and mafic volcaniclastic deposits, and hypabyssal felsic intrusions. Siliceous gneisses (unit 1d) may have been chert deposits. Textural homogeneity, mafic inclusions and locally preserved intrusive relationships indicate derivation of unit 2 from granitoid plutons that intruded the volcanogenic sequence. Radiometric dating (Silver and Barker, 1968) yields an approximate age of 1750 Ma for these plutons and cross-cutting relationships suggest that the more leucocratic in-

---

[1] Age dates presented in this paper are recalculated using decay constants of Steiger and Jager (1977) where necessary.

trusive phases (unit 2b) are generally younger than the tonalitic phases (unit 2a). Unit 3 is interpreted as deformed bodies of gabbro that intruded both the volcanogenic rocks and ca. 1750 Ma plutons.

Similar volcano-plutonic complexes are exposed throughout the southern Colorado Province and include the 1790-1740 Ma Yavapai Series in central Arizona (Anderson et al., 1971; Karlstrom and Conway, 1986), 1720-1750 Ma Moppin Series and Pecos Greenstone belt in northern New Mexico (Robertson and Moench, 1979; Wobus, 1984; Williams et al., 1986), and rocks of the Salida-Gunnison area in central Colorado (Bickford and Boardman, 1984). In the Salida-Gunnison area, Bickford and Boardman (1984) identified two temporally distinct bimodal metavolcanic sequences that are intruded by mafic dikes. The older Dubois succession (Condie and Knoper, 1986; Bickford, 1986) yields zircon U-Pb ages of 1780-1760 Ma and is intruded by the 1751 Ma Powderhorn Granite; the younger Cochetopa succession (Condie and Knoper, 1986; Bickford, 1986) yields ages of 1730-1745 Ma. Because metavolcanic rocks in the northwestern Needle Mountains are intruded by ca. 1750 Ma plutons (unit 2), they are tentatively correlated with the Dubois succession of the Gunnison area. However, not all of the metavolcanic rocks in the map area are in direct or unambiguous intrusive contact with these plutons and it is possible that representatives of the Cochetopa succession are also present.

Younger granitoid plutons within the study area include the Tenmile Granite, an ovoid body centered on the Animas River canyon within the southern basement domain, and the Whitehead Granite, a complex of dikes and small intrusive bodies localized in a 1.5 km wide, east-west trending zone immediately north of the Uncompahgre Group outcrop belt (Fig. 2-2b). Both of the intrusive bodies cut the prominent foliation in the gneisses and are themselves weakly foliated. Numerous pegmatite dikes in rocks west of Lime Creek (Fig. 2-2b) display similar relationships

to the surrounding gneisses and are also considered as part of this assemblage. The plutons are predominantly quartz monzonite (Barker, 1969) to granite in composition and several intrusive phases may be recognized in some outcrops. The Tenmile and Whitehead Granites yield zircon U-Pb ages of 1694 ± 20 Ma (Silver and Barker, 1968). Whole-rock Rb-Sr age determinations include 1680 ± 50 Ma on the Tenmile Granite and 1640 ± 74 Ma on the Whitehead Granite (Bickford et al., 1969).

## STRUCTURAL FEATURES

When examined in the field, rocks of the gneiss complex typically display only a single penetrative foliation that is generally parallel to compositional layering. Despite this apparent simplicity, four fold generations can be distinguished on the basis of their mutual geometric relationships and cross-cutting relationships with granitoid bodies. The characteristics and chronology of folds and foliations discussed below are summarized in Table 2-2.

### $F_1$, $F_2$, and Related Fabrics

The oldest structures in the basement gneisses are tight to isoclinal $F_1$ folds that deform primary lithologic contacts (Fig. 2-3d) and are associated with an axial planar alignment ($S_1$) of biotite, muscovite, amphibole, and elongate quartz and feldspar grains. In unit 2, $S_1$ is defined by quartz and feldspar ribbons and $F_1$ folds are recognizable only where deformed quartz veins or mafic layers (inclusions or dikes?) are present. Lithologic contacts nearly always parallel $S_1$.

$F_2$ folds deform $S_1$ and are most common in the southern basement domain. The most obvious macroscopic $F_2$ structure in the area is outlined by outcrop belts

Table 2-2: Summary of tectonic fabric generations in basement.

| Deformation | Folds | Foliations |
|---|---|---|
| $D_{BC}$ | $F_4$ - steeply plunging; variable axial surface orientations; gentle to tight; only occur west of Lime Creek | none |
| | $F_3$ - upright; east-trending; gently to moderately plunging; open to tight; occur only in northern domain | $S_3$ - in granitoids only; aligned biotite grains, quartz lenses and feldspar megacrysts |
| $D_B$ | $F_2$ - gently plunging; recumbent to upright; close to isoclinal | $S_2$ - biotite or amphibole grains oblique to $S_1$ in $F_2$ hinges; indistinguishable from $S_1$ on $F_2$ limbs (composite $S_2$ fabric) |
| | $F_1$ - gently plunging; recumbent to upright; tight to isoclinal | $S_1$ - penetrative mineral alignment parallel to $F_1$ axial surfaces; quartz and feldspar ribbons in unit 2 |

Figure 2-4: Cross-sections and fabric orientation data for a) southern domain west of Lime Creek; b) southern domain south and east of Snowdon Peak; and c) northern domain along Animas River. Note isoclinal $F_2$ folds (arrowed) in the hinge and along limbs of upright $F_3$ folds in (c). Map symbols as in Figure 2-2b except for gneiss units, which show $S_1$ orientation and are differentiated by numbers in parentheses corresponding to the map units. Orientation data as indicated below each projection contoured at 1, 2, 4 (stippled), and 8 (black) points per (100/n)% area. Other symbols: + $F_1$ fold axes, x $F_1$ axial surfaces, ▲ $F_2$ (+ $F_3$ in (c)) fold axes, Δ $F_2$ (+ $F_3$ in (c)) axial surfaces, • mineral lineation on $S_3$.

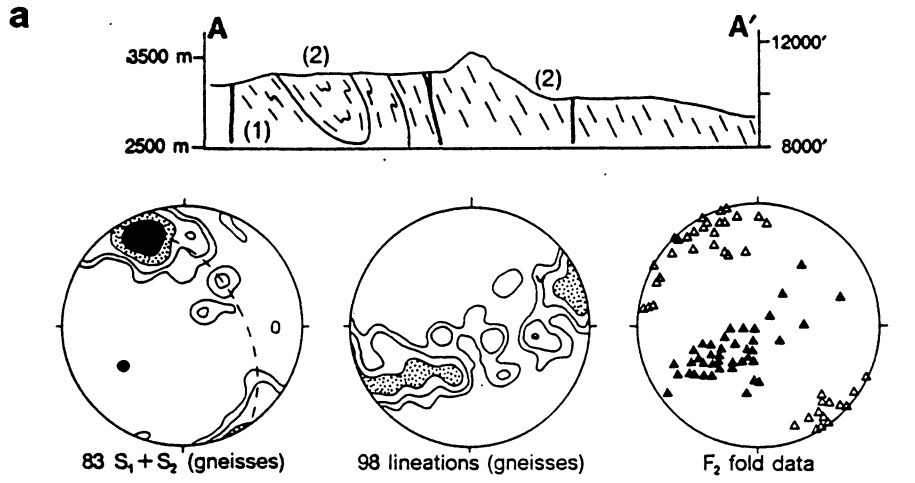
a
A
A′
3500 m
2500 m
(1)
(2)
(2)
12000′
8000′
83 S₁+S₂ (gneisses)
98 lineations (gneisses)
F₂ fold data

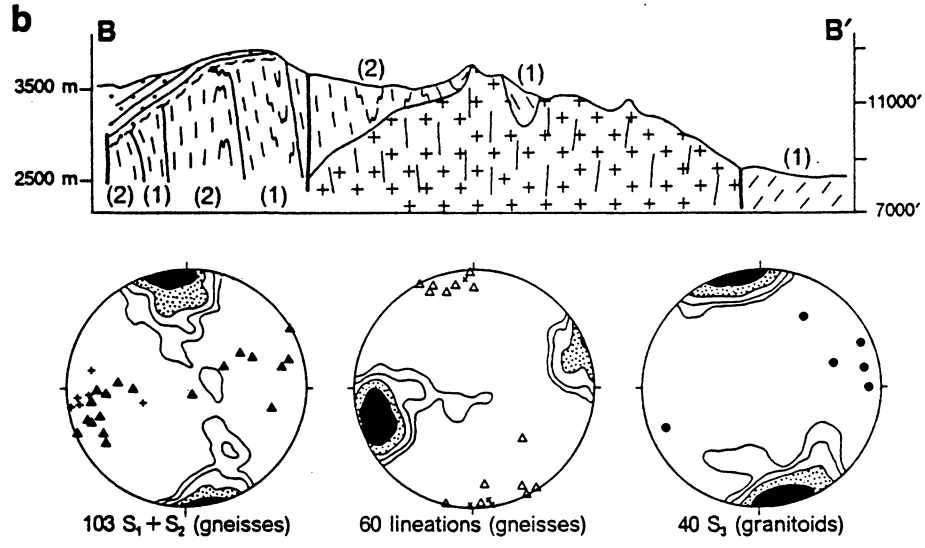
b
B
B′
3500 m
2500 m
(2) (1) (2) (1)
(2)
(1)
(1)
11000′
7000′
103 S₁+S₂ (gneisses)
60 lineations (gneisses)
40 S₃ (granitoids)

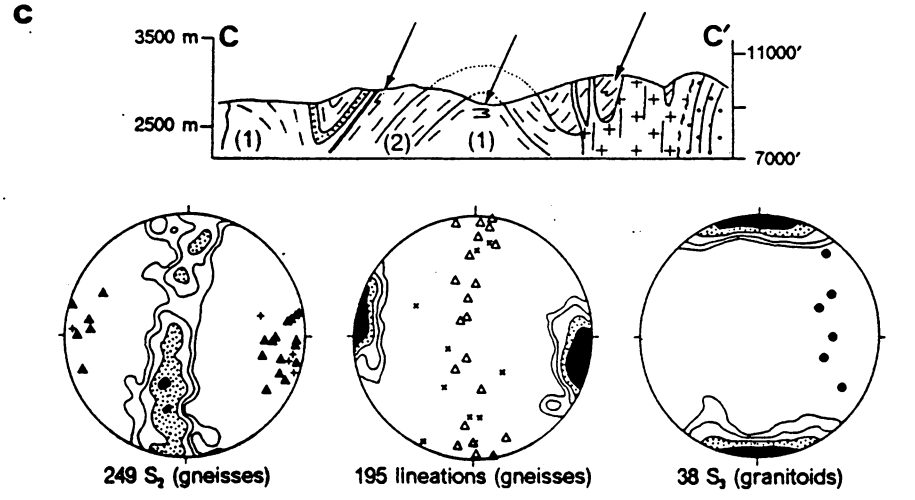
c
3500 m
C
C′
2500 m
(1)
(2)
(1)
11000′
7000′
249 S₂ (gneisses)
195 lineations (gneisses)
38 S₃ (granitoids)

of unit 1 south of Coal Bank Pass (Fig. 2-2b). $S_1$ measurements from unit 2 in the core of this structure define a β axis plunging 38° toward 238° and mesoscopic $F_2$ folds in this area plot along a partial southeast-dipping girdle but cluster around this β axis (Fig. 2-4a). Lithologic alternation south of Snowdon Peak (Fig. 2-2b) is also the product of a series of upright, subhorizontal $F_2$ antiforms and synforms (Fig. 2-4b). Mesoscopic $F_2$ folds are close to isoclinal (Fig. 2-5a) and contain an axial-planar foliation ($S_2$) that is defined in thin section by the alignment of biotite or amphibole grains at high angles to $S_1$ (Fig. 2-5b). On $F_2$ fold limbs, $S_1$ and $S_2$ are indistinguishable and comprise a composite foliation that is referred as $S_2$ throughout this paper.

In the northern domain, east-trending, open to isoclinal folds with a variety of axial surface orientations deform $S_1$ (Fig. 2-4c). The occurrence of recumbent, isoclinal folds in the hinge of an upright, macroscopic antiform (Fig. 2-4c) indicates that at least two post-$S_1$ fold generations are present. Rare, rootless isoclines that deform $S_1$ and have limbs parallel to the penetrative gneissic fabric are interpreted as $F_2$. The prominent foliation in the gneisses of the northern domain is, therefore, also considered to be $S_2$ and to have resulted from the transposition of $S_1$.

The variation in strike of $S_2$ throughout the map area defines a sigmoidal pattern (Fig. 2-6a) that is mimicked by the distribution of lithologies (Fig. 2-2b). The dip of $S_2$ is typically in excess of 60°. $F_2$ folds and $S_2$ are cross-cut by the Tenmile and Whitehead Granites (Figs. 2-4b, 2-5c, 2-5d) and truncated by ductile deformation zones along contacts with the Uncompahgre Group (Figs. 2-2b, 2-4b).

### $F_3$ and Related Fabrics

Upright folds with half-wavelengths of 0.5-2 km in the northern domain are considered $F_3$. These deform $S_2$ and produce the girdle distribution of poles to $S_2$ and

Figure 2-5: Fold generations in the gneisses.

a) $F_2$ folds deforming $S_1$ in unit 1b;

b) $S_1$ preserved in $F_2$ crenulations; foliations defined by biotite; plane light photomicrograph;

c) $S_2$ in unit 1a cross-cut by dike of Whitehead Granite containing $S_3$ parallel to $F_3$ axial surface; vertical outcrop face;

d) folded pegmatite in amphibolite containing $S_2$;

e) $F_4$ fold deforming amphibolite layer in unit 2b; horizontal outcrop surface.

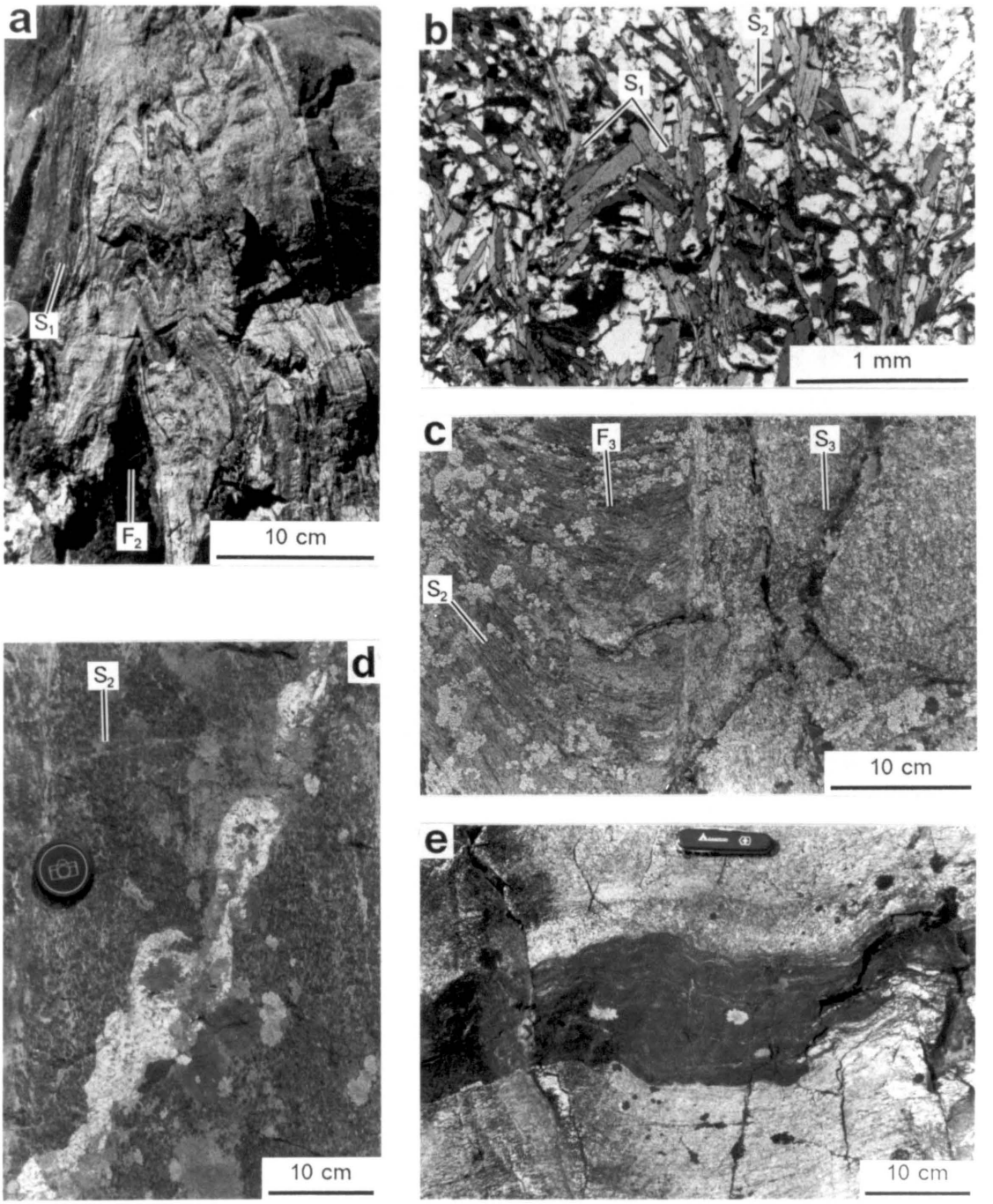
a
$S_1$
$F_2$
10 cm
b
$S_2$
$S_1$
1 mm
c
$F_3$
$S_3$
$S_2$
10 cm
d
$S_2$
10 cm
e
10 cm

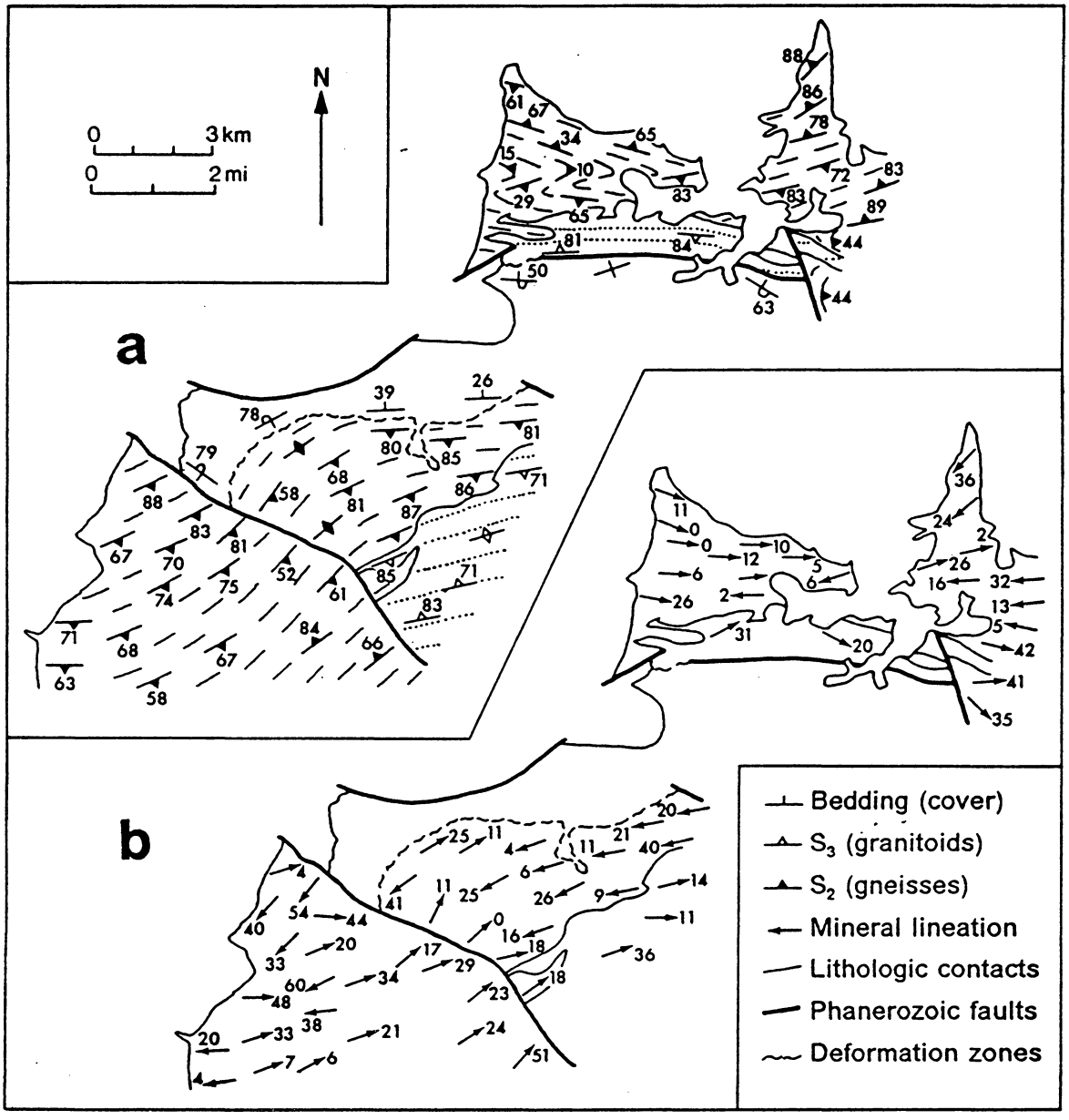


Figure 2-6: Maps showing variation in orientation of foliations (a) and mineral lineations (b) across map area. Foliations shown in (a) are $S_2$ in gneisses (dashed lines) and $S_3$ in granitoids (dotted lines).

post-$S_1$ axial surfaces (Fig. 2-4c). The $\beta$ axis for $F_3$ plunges at 10° toward 100° in the vicinity of the Animas River and is subparallel to mesoscopic $F_1$ and post-$S_1$ fold axes (Fig. 2-4c). $F_3$ axes steepen to 45° toward 095° in the area south of the Highland Mary Lakes. Mesoscopic $F_3$ folds range from gentle to tight and have asymmetries consistent with their positions on macroscopic structures. Map-scale $F_3$ folds define the pattern of lithologic belts throughout the northern basement domain and are the major structures visible in cross sections of this area (Fig. 2-4c). The concentric map pattern of lithologic units centered on the Animas River (Fig. 2-2b) is a topographic effect generated by the intersection of an $F_3$ antiform with the north-south trending river canyon. Dikes of the ca. 1690 Ma Whitehead Granite are folded by $F_3$, boudinaged on fold limbs, and contain a variably developed, east-striking, subvertical foliation, $S_3$ (Figs. 2-4c, 2-5c). Although no $F_3$ folds have been identified in the southern domain, the ca. 1690 Ma Tenmile Granite contains an east-northeast to east-striking foliation similar to $S_3$ in the Whitehead Granite (Fig. 2-4b).

### $F_4$ Folds

West of Lime Creek in the southern domain, pegmatite dikes which locally transect $F_2$ folds are themselves mildly folded (Fig. 2-5d). In addition, tight folds with east-striking axial surfaces and gentle to open folds with north-northeast striking axial surfaces (Fig. 2-5e) locally refold $F_2$ in this area and are collectively referred to as $F_4$. Unlike those of $F_3$, the axes of demonstrable $F_4$ folds typically plunge steeply and are not coaxial with $F_1$ and $F_2$ (Fig. 2-7). Although $F_4$ folds do not affect the map pattern of the area, they may account for the variation in strike of steeply dipping $F_2$ axial surfaces (Fig. 2-4a).

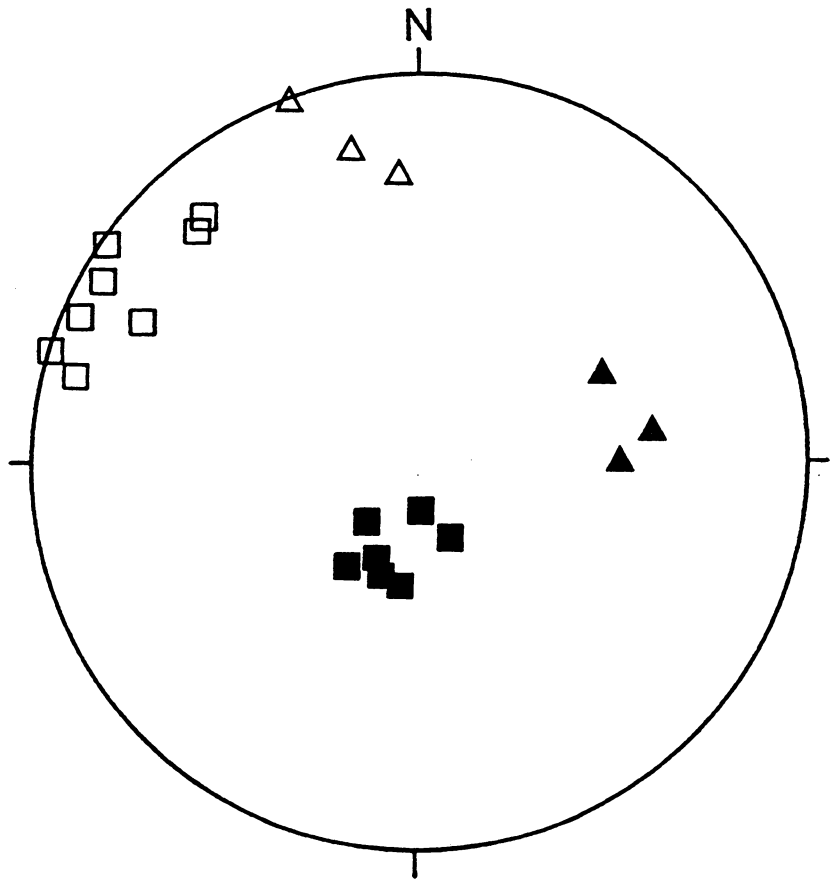


Figure 2-7: Fold orientation data from outcrop in Figure 2-5e showing orientations of $F_2$ (diamonds) and $F_4$ (squares) folds; solid symbols - fold axes, open symbols - axial surfaces.

## Mineral Lineation

A mineral lineation defined by quartz and feldspar ribbons, biotite, or amphibole occurs on $S_2$ in the gneisses throughout the entire study area. In both the northern domain and southern domain east of Lime Creek, it generally plunges less than 40° (Fig. 2-6b), coincides with $F_1$, $F_2$, and $F_3$ axes, and is never folded. The plunge of the mineral lineation is most uniform (0-20°) on $S_2$ surfaces which strike 100° to 125° and is more variable on northeast-striking surfaces (compare lineation patterns in Figs. 2-4b and 2-4c). In a few places south of Snowdon Peak (Fig. 2-2b), granitoid gneisses in the hinges of $F_2$ folds contain a predominantly L-tectonite fabric that contrasts with the typical L-S tectonite found on fold limbs. Although the mineral lineation on $S_2$ is truncated along contacts with the Tenmile and Whitehead Granites, a weak, gently east-plunging biotite lineation is also locally present on $S_3$ surfaces in granitoids (Fig. 2-4b).

In the southern basement domain west of Lime Creek, lineations are variable in both trend and plunge and define a steeply southeast-dipping girdle coincident with the typical orientation of $S_2$ (Fig. 2-4a). Lineations on $S_2$ are locally folded about open $F_4$ folds.

## Shear Fabrics

On surfaces orthogonal to the foliation and parallel to the mineral lineation, both the gneisses and granitoids typically display fabrics with apparent orthorhombic symmetry. However, shear bands and shear zones up to 5 cm wide locally cross-cut $S_2$ (Fig. 2-8a, b) in unit 2 along and west of Lime Creek, and unit 3 in the vicinity of the Highland Mary Lakes. Subhorizontal mineral lineations and foliation reorientation

into these steeply dipping (> 65°) zones indicate predominately strike-slip motion. In the northern domain, rare dextral shear zones strike 105° to 159° whereas sinistral zones strike 038° to 066° (Fig. 2-8c). Conjugate shear zones occur in unit 3a near the Highland Mary Lakes.

Within the southern domain, sinistral shear fabrics oriented 030° to 072° predominate whereas dextral zones are subordinate and more variable in orientation (Fig. 2-8c). Several south-dipping zones in the southern domain have steeply plunging lineations and reverse dip-slip movement. These generally have a more easterly strike than sinistral strike-slip zones (Fig. 2-8c). A single ≤ 1 m thick zone of mylonite derived from the Tenmile Granite occurs along the northeast-striking, western margin of this pluton. Type I S-C fabrics (Lister and Snoke, 1984) and a mineral lineation plunging 33° toward 008° indicate sinistral, oblique-slip movement.

## METAMORPHIC TEXTURES AND MICROSTRUCTURES

Within the basement gneisses, feldspar occurs as equant, strain-free 0.05-1 mm grains and polycrystalline grain aggregates or ribbons (Fig. 2-8b). Biotite grains which define all tectonic fabrics display only minor undulatory extinction and no kinking. Amphiboles in the deformed metagabbros have core and mantle textures (White, 1976) consisting of porphyroclasts with patchy extinction surrounded by recrystallized grains that lack optically visible strain features. Quartz occurs as polygonal aggregates of either 1) equant grains with unit extinction and planar boundaries (Fig. 2-8b) or 2) irregularly shaped grains with serrated, interpenetrating boundaries and internal subgrains. Mineral assemblages and grain size in the gneisses are not affected by their proximity to the hinges of any generation of folds or to mesoscopic shear fabrics (Figs. 2-5b, 2-8b).

Figure 2-8: Shear fabrics in the gneisses.

a) sinistral shear zone in unit 2b west of Lime Creek;

b) photomicrograph showing dextral shear bands and recrystallized microstructure in unit 2; partially crossed nicols;

c) rose diagrams showing strike of mesoscopic shear fabrics; black - sinistral, stippled - dextral, ruled - reverse.

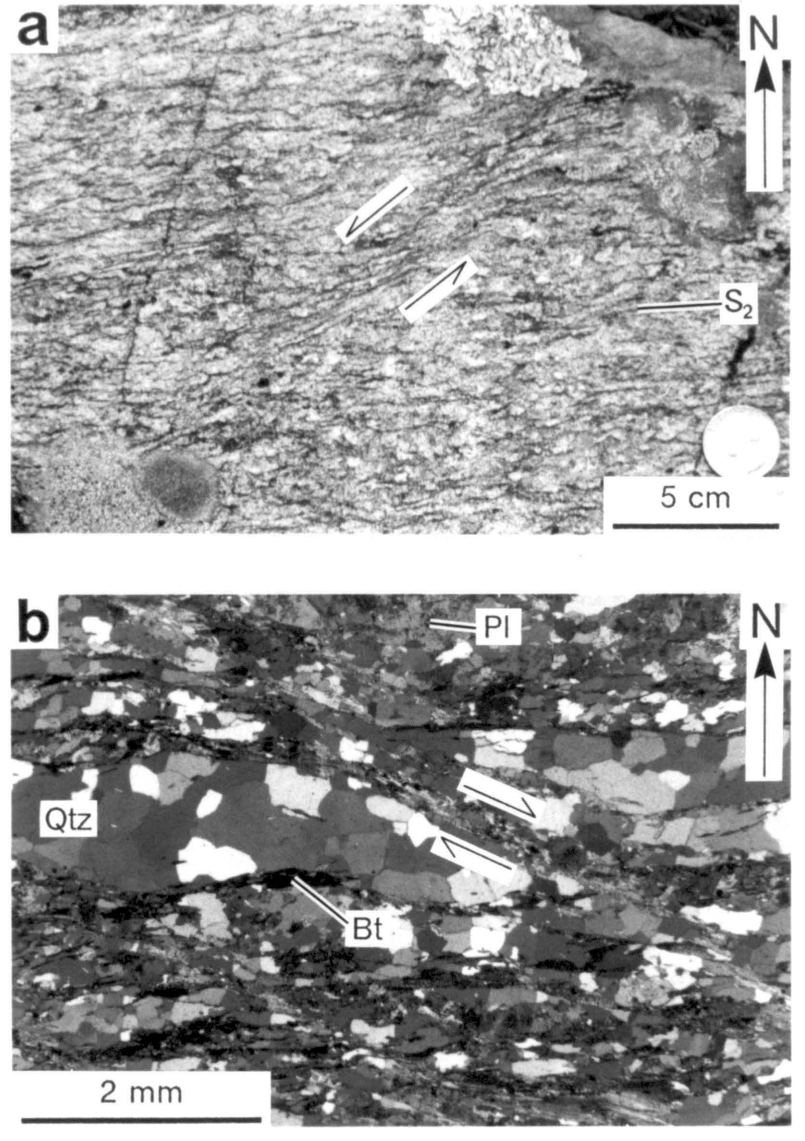
a
N
$S_2$
5 cm
b
Pl
N
Qtz
Bt
2 mm
c
N
N
Northern Domain
n = 10
Southern Domain
n = 30

Garnet porphyroblasts are common in many of the felsic lithologies of unit 1. In the northern domain, they are wrapped around by $S_2$ and contain straight trails of quartz inclusions ($S_1$) that are either oblique or parallel to $S_2$. Garnets from unit 1 south of Coal Bank Pass either contain curved inclusion trails that are continuous with the external $S_1$ foliation (Fig. 2-9a) or enclose $F_2$ crenulations (Fig. 2-9b) and are wrapped around by $S_2$. Many of these garnets are partially altered to randomly oriented biotite (felsic gneisses, Fig. 2-9a) or corroded and surrounded by polycrystalline plagioclase (mafic gneisses). Rocks of unit 1d commonly contain large ($\leq$1.5 cm) garnets with an internal $S_1$ foliation surrounded by a matrix comprised of non-aligned, strain-free grains of biotite, low-Ca amphibole, plagioclase, quartz, and small euhedral garnets.

$S_3$ in the Tenmile and Whitehead Granites is defined by the dimensional alignment of tabular feldspar crystals, a weak preferred orientation of biotite flakes, and quartz lenses comprised either of polygonal, equant grains with planar boundaries or irregularly shaped grains with serrated margins, subgrains and deformation bands. In strongly foliated examples, plagioclase contains bent twins and potassium feldspar is marginally altered to myrmekite and recrystallized to 0.01-0.03 mm equant grains that define ribbons along $S_3$. Microcline, biotite, and muscovite occur as $\sigma$-type porphyroclasts (Passchier and Simpson, 1986) in mylonites derived from the Tenmile Granite.

## CHRONOLOGY OF DEFORMATION AND METAMORPHISM

Deformation in the northwestern Needle Mountains may be considered in terms of two polyphase deformational events, $D_B$ and $D_{BC}$, which were temporally separated by emplacement of the ca. 1690 Ma granitoids and deposition of the

Figure 2-9: Metamorphic textures in the gneisses.

a) rotated garnet porphyroblast with internal foliation continuous with external $S_1$ in unit 1a; note alteration of garnet to randomly oriented biotite (Bt); plane light;

b) garnet porphyroblast with crenulated internal $S_1$; plane light.

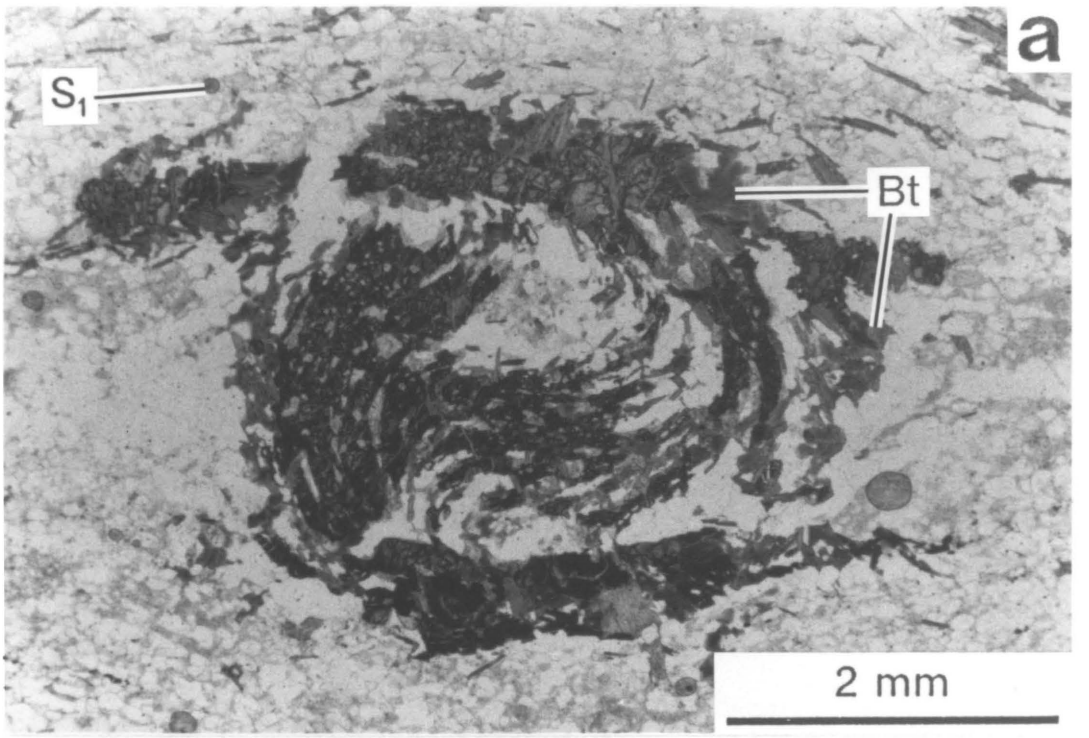
a
S1
Bt
2 mm

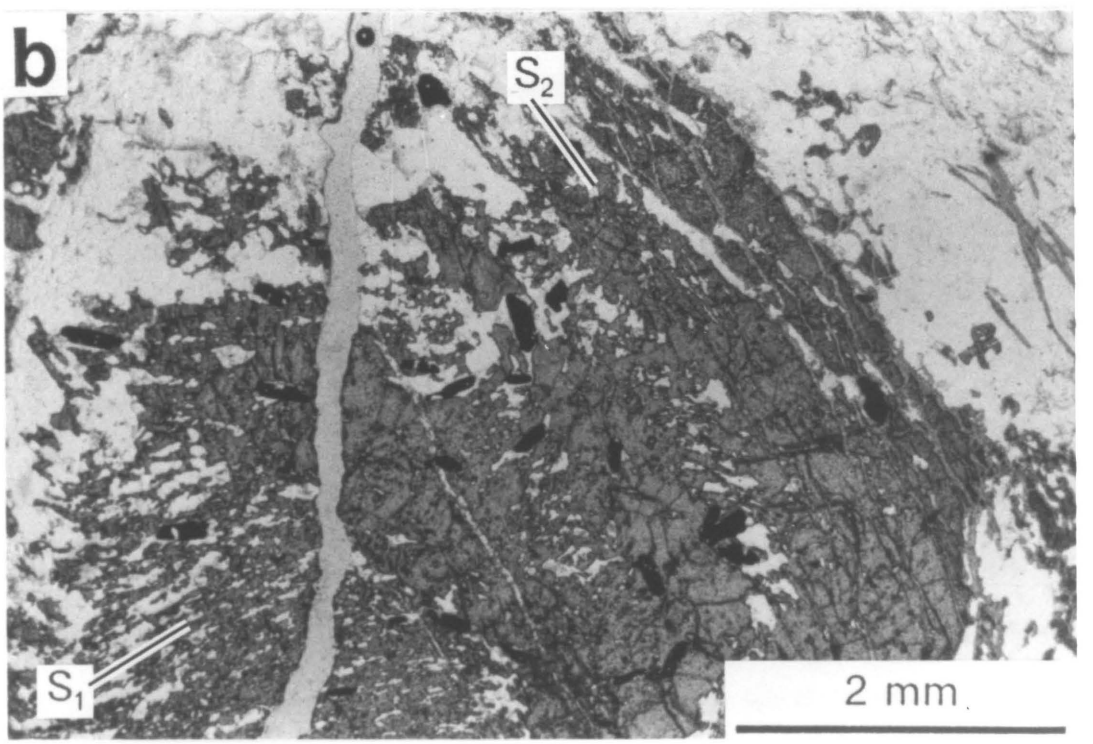
b
S2
S1
2 mm

Uncompahgre Group (Harris et al., in press). $F_1$ and $F_2$ folds, and their associated $S_1$ and $S_2$ foliations, are cut by the granitoids and are, therefore, attributed to the pre-1690 Ma $D_B$ event. In addition, these fabrics are truncated along contacts with the Uncompahgre Group (e.g. south of Snowdon Peak - Fig. 2-2b) and overprinted by fabrics related to shearing along these contacts (Gibson and Simpson, 1986). Porphyroblast textures, especially in unit 1 of the southern domain, indicate that garnet growth overlapped in time with both $S_1$ development and $F_2$ folding (Fig. 2-9). This continuity of garnet growth with respect to deformation suggests that $F_1$ and $F_2$ formed during a single progressive $D_B$ deformational episode. Metamorphism coincident with $D_B$ is called $M_B$.

Deformation of the ca. 1690 Ma granitoids and reorientation of $S_2$ is interpreted to have occurred during $D_{BC}$, which also affected the Uncompahgre Group. $F_3$ folds are the oldest structures that deform the granitoids. Major macroscopic structures in the Uncompahgre Group include upright folds (second generation of Tewksbury, 1985; $F_{2C}$ of Harris et al., in press) with east to east-southeast trending, gently plunging axes and half-wavelengths of 0.5-1.5 km. The similarity in orientation and scale of $F_3$ folds in the basement with macroscopic folds in the cover suggests that these structures are temporally equivalent. The youngest folding to affect the Uncompahgre Group is represented by a nearly vertical fold with a north-striking axial surface that refolds an east-trending syncline in the vicinity of Lime Creek ($F_{3C}$ of Harris et al., in press). The steeply plunging axial orientation of this fold compares favorably with that of $F_4$ folds, found only in the basement rocks of the same area. The macroscopic sigmoidal pattern of $S_2$ (Fig. 2-6a) is interpreted to have developed during $D_{BC}$ because of the subparallelism of bedding in the Uncompahgre Group and $S_2$. This feature is most obvious in the southern domain east of Lime Creek where

$S_2$, the basement-Uncompahgre Group contact, and bedding in the Uncompahgre Group all gradually change in strike from east-west to nearly north-south (Fig. 2-6a).

Dynamic recrystallization textures in potassium feldspars from the granitoids and crystal-plastic strain effects in clinoamphiboles from mesoscopic strike-slip shear zones suggest that $D_{BC}$ occurred under upper-greenschist to amphibolite-grade conditions (cf. Voll, 1976; Simpson, 1985). The absence of crystal-plastic strain features in other mineral grains and the apparent post-kinematic growth of non-aligned porphyroblasts in some gneisses indicate that the peak of metamorphism outlasted $D_{BC}$. This second metamorphic episode, $M_{BC}$, was probably also responsible for the post-$D_{BC}$ growth of porphyroblasts in rocks of the Uncompahgre Group (Harris et al., in press). The age of $M_{BC}$ is poorly constrained although Barker (1969) showed that metamorphic grade in the Uncompahgre Group increases toward the post-kinematic, ca. 1430 Ma Eolus Granite. Therefore, 1430 Ma is considered the minimum age for the peak of $M_{BC}$.

## ANALYSIS OF $D_{BC}$ STRUCTURES

### Relationships Between Folds and Lineations

The northern basement domain, like many gneiss terranes (e.g. Simpson, 1982; Grocott, 1984), is characterized by a colinearity of mineral lineations and axes of successive fold generations. Models proposed to explain this relationship include 1) all linear structures were rotated into parallelism with the maximum finite stretching direction (X) during the closing phases of deformation (Bryant and Reed, 1969); 2) the mineral lineation is "apparent" and does not represent the long axis of the finite

strain ellipsoid (Sanderson, 1974); or 3) folds nucleated with their axes parallel to the stretching lineation (Watkinson, 1975; Cobbold and Watkinson, 1981).

Folds that undergo rotation of axes toward the X-direction also tighten during reorientation and commonly are strongly non-cylindrical (Bryant and Reed, 1969; Cobbold and Quinquis, 1980). In the northwestern Needle Mountains, the absence of $F_3$ sheath folds and the parallelism of all $F_1$, $F_2$, and $F_3$ folds, regardless of their tightness, to the mineral lineation argue against reorientation during $F_3$ folding as a cause for colinearity.

Sanderson (1974) proposed that many mineral lineations on folded surfaces represent the maximum finite extension direction within the two-dimensional section of the strain ellipsoid on that surface and may not correspond to the X-direction of the three-dimensional strain ellipsoid. "Apparent" stretching lineations parallel to fold axes may form within fold hinges for a variety of strain states but deviate from this axis-parallel orientation on fold limbs (Stainforth, 1978). No such deviation is observed in rocks of the northern basement domain where lineations define a strong point maximum (Fig. 2-4c).

The parallelism of $F_3$ axes with the mineral lineation is, therefore, most consistent with fold nucleation parallel to the lineation. If the mineral lineation represents the X-direction of the strain ellipsoid responsible for $F_3$ folding, the development of $F_3$ folds by buckling is possible if the intermediate finite strain axis (Y) was oriented at a high angle to layering and X was close to the layering prior to folding (Watkinson, 1975). An alternative possibility is that the mineral lineation was present prior to $F_3$ folding and exerted a mechanical control on the orientation of later structures. Folds in layered rock sequences containing a strong pre-existing linear anisotropy will tend to develop with axes subparallel to the linear fabric (Cobbold and Watkinson, 1981). Evidence supporting the possibility that the mineral lineation pre-dated $F_3$ includes

1) the lineation is strongly developed on $S_2$ and is truncated along contacts with the granitoids that only locally contain a weak lineation on $S_3$; 2) in some areas, the lineation is most pronounced in $F_2$ fold hinges; and 3) a predominantly linear fabric in parts of unit 3 is modified to a planar fabric upon entering mesoscopic strike-slip shear zones.

In contrast to the northern domain, the portion of the southern domain west of Lime Creek is characterized by a wide range of lineation plunges (Fig. 2-4a) and non-coaxial superposition of $F_4$ folds onto older structures (Fig. 2-7). Two possible interpretations of this pattern are that 1) it is a relict of an early stage in the deformation history and escaped transformation into the more typical point-maximum-type pattern and 2) it is a late-stage modification of a point-maximum distribution. Rare folded lineations, the occurrence of variably oriented lineations in the only area affected by $F_4$ folding (cf. Clifford et al., 1957), and the absence of a continuous transition between girdle and point-maxima patterns, suggest that the lineations in the area west of Lime Creek were modified during $F_4$ folding. Detailed outcrop-scale analysis necessary to fully understand the geometrical relationships and significance of structures in this area has not been undertaken.

**Quartz Preferred Crystallographic Orientations**

In order to place constraints on the symmetry and kinematics of $D_{BC}$ deformation, quartz *c*-axis preferred orientations were measured with a universal stage on ten gneiss samples with prominent quartz ribbons or deformed quartz veins, and two samples each of foliated Tenmile and Whitehead Granite. Measurements were made on surfaces orthogonal to the foliation and parallel to the mineral lineation. Except for sample 55, collected from gneisses with a subhorizontal $S_2$ fabric in the hinge of

an $F_3$ antiform, all measurement surfaces were within 25° of the horizontal. Photographs were used as guides in order to avoid duplicating measurements made along transects perpendicular to the foliation in each thin section.

Measured *c*-axis patterns are illustrated in Figure 2-10. Most of the fabrics from the gneiss samples are transitional between single girdle (55, 228) and type I (Lister, 1977) crossed girdle patterns (26, 83, 118, 166, 213, 334). Fabrics from sample 141 and 355 resemble type II (Lister, 1977) crossed girdles in that they appear to consist of two partially developed girdles that intersect at the foliation trace. Quartz *c*-axes in sample 165A (Tenmile Granite) define a crossed girdle whereas those in sample 381 (Whitehead Granite) define a partial girdle orthogonal to the foliation with a maximum near the foliation trace. Other granitoid samples have very weak *c*-axis preferred orientations with a clustering near the lineation in sample 233 and possible incipient crossed girdle development in sample 165.

Maximum concentrations of *c*-axes within several of the samples are near the pole to the foliation (141, 55, 213) and are consistent with deformation of quartz predominantly by basal slip in the <a> crystallographic direction (Tullis, 1977). Other maxima, which either coincide with the foliation trace (26, 141, 381) or occur at positions between the foliation and foliation normal (26, 83, 228, 334), may represent components of slip on the prism and rhomb planes in the <a> direction (Wilson, 1975; Tullis, 1977). The asymmetric distribution of data about the foliation within the girdles (83, 165A, 166, 355) could be the result of modifying a strong pre-existing crystallographic preferred orientation (e.g. Lister and Price, 1978) or unequal activity of the positive and negative rhomb planes during slip (Schmid and Casey, 1986). Weak preferred crystallographic orientations in the granitoid samples may reflect either low strain (Lister and Hobbs, 1980) or low modal quartz content (Starkey and Cutforth, 1978).

Figure 2-10: Quartz *c* -axis preferred orientation patterns referred to sample localities. Contoured at 1, 3 (stippled), and 5 (black) points per (100/n)% area on lower hemisphere, equal-area projection. Inset shows orientation of all projections except 55; inferred flow planes and shear senses indicated by split arrows; precise sample localities are given in Appendix D.

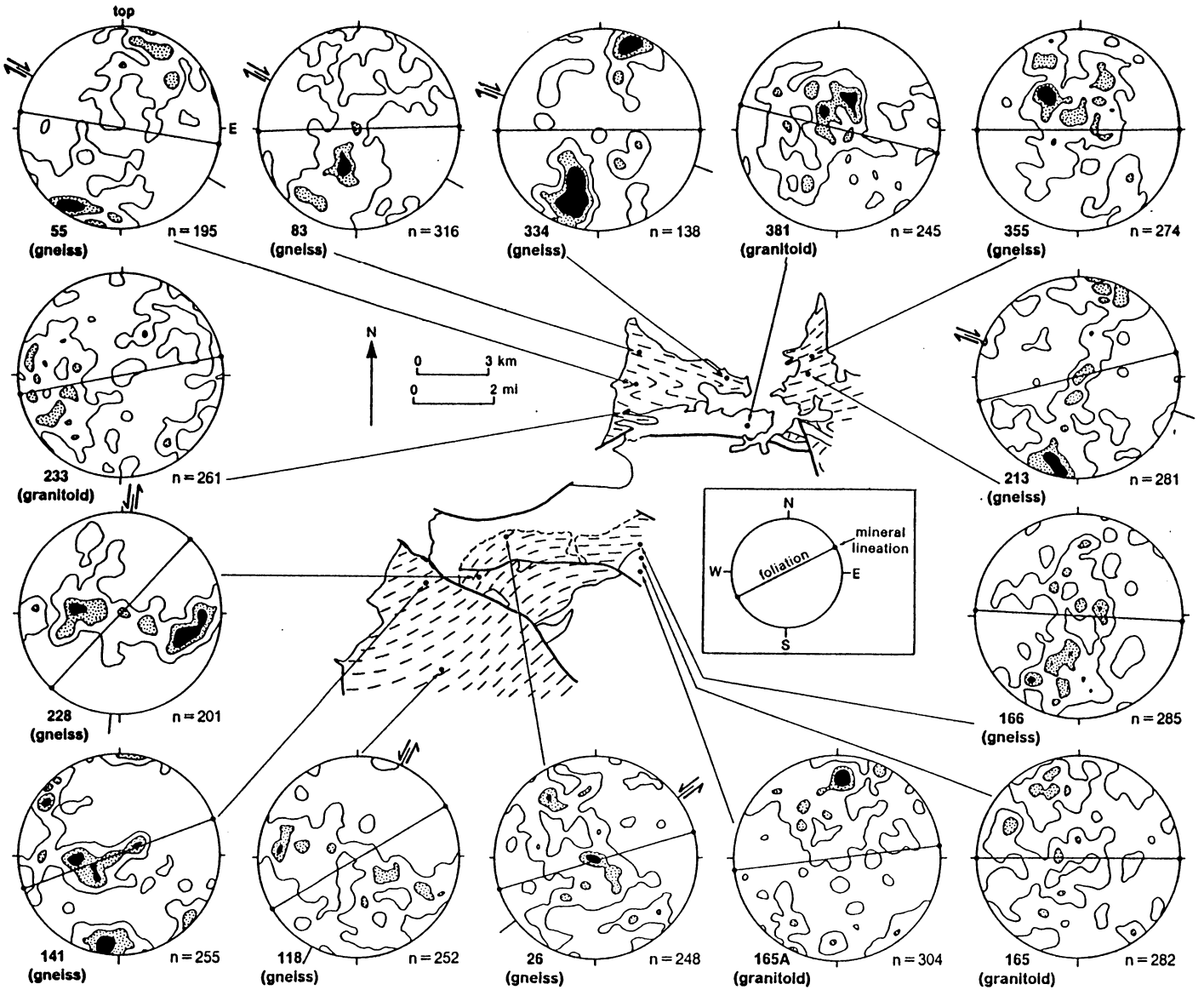
top
E
55
(gneiss)
n = 195
83
(gneiss)
n = 316
334
(gneiss)
n = 138
381
(granitoid)
n = 245
355
(gneiss)
n = 274
233
(granitoid)
n = 261
213
(gneiss)
n = 281
228
(gneiss)
n = 201
166
(gneiss)
n = 285
141
(gneiss)
n = 255
118
(gneiss)
n = 252
26
(gneiss)
n = 248
165A
(granitoid)
n = 304
165
(granitoid)
n = 282
N
0 3 km
0 2 mi
N
mineral lineation
W
foliation
E
S

Computer simulations of crystal-plastic flow (Lister and Hobbs, 1980) and complete fabric analysis of naturally deformed specimens (Schmid and Casey, 1986) indicate that the central segment of a quartz *c*-axis girdle forms perpendicular to the maximum finite stretching direction during coaxial deformation or the shear direction in simple shear. Assuming this to be the case, the fabrics illustrated in Figure 2-10 are interpreted to record either subhorizontal coaxial extension or shear. The approximate parallelism of inferred flow directions in both the gneisses and granitoids suggests that the crystallographic fabrics in both units developed during $D_{BC}$. This is consistent with the findings of Lister and Price (1978) and Lister and Williams (1979) who suggested that *c*-axis fabrics record the kinematic framework of the final stages of crystal-plastic deformation.

The asymmetry of quartz *c*-axis fabrics with respect to the foliation indicates the sense of shear during non-coaxial deformation (e.g. Berthe et al., 1979; Simpson and Schmid, 1983). Quartz *c*-axis fabrics from gneisses of the northern basement domain (83, 213, 334) are asymmetric with respect to the foliation trace in a sense consistent with dextral shear along subvertical flow planes striking 108° to 120° (Fig. 2-10). Fabric asymmetry in sample 55, collected in the core of an $F_3$ antiform, indicates top-to-the-east shear parallel to the gently east-plunging fold axis. Asymmetric quartz fabrics in gneiss samples from the southern domain (26, 118, 228) record sinistral shear along flow planes striking 006° to 058° (Fig. 2-10). Approximately symmetrical quartz fabrics in the granitoid samples (165, 381) and three of the gneiss samples (141, 166, 355) imply either a coaxial strain history or late-stage coaxial overprint (Lister and Williams, 1979; Lister and Hobbs, 1980).

## Deformation Model for $D_{BC}$

Alternating domains of east-striking and northeast-striking structural fabrics (Fig. 2-6a) in the northwestern Needle Mountains combine to yield a sigmoidal map pattern similar to that of a large-scale ductile shear zone (cf. Ramsay and Graham, 1970; Ramsay, 1980). Domains of east-trending structures are interpreted to be the product of $D_{BC}$ deformation superimposed onto older northeast structural trends because 1) the ca. 1690 Ma granitoids contain an east-striking foliation (Fig. 2-4b, 4c); 2) the plunge of the mineral lineation is most uniform on foliation surfaces striking 100° to 125° (e.g. Fig. 2-4c); and 3) east-striking domains are more laterally continuous than northeast-striking domains (Fig. 2-6a). Although sigmoidal foliation patterns are commonly considered indicative of simple shear deformation, identical geometries may be produced by a variety of coaxial and non-coaxial strain paths (Ramsay, 1980). Two end-member models for the development of this pattern in the northwestern Needle Mountains are 1) east-striking domains were produced during north-south coaxial shortening (pure shear) and 2) east-striking domains represent zones of dextral simple shear.

The pure shear hypothesis for the generation of east-west trending structures is attractive because it accounts for 1) the scarcity of asymmetric fabric elements in both the gneisses and ca. 1690 Ma granitoids and 2) the subequal occurrence of mesoscopic dextral and sinistral shear zones in the northern domain (Fig. 2-8c). Because the granitoids were not subjected to $D_B$ deformation, the orientation of $S_3$ and the mineral lineation on it should represent the XY plane and X-axis direction, respectively, of the $D_{BC}$ strain ellipsoid. An XY plane of 090°, 90° and X-axis plunging 25° toward 090° are assumed based on fabric orientations in the Whitehead Granite. Superposition of a strain with these principal axis orientations onto an area with an

older northeast structural grain results in reorientation of planar fabrics toward parallelism with the XY plane and linear fabrics toward the X-axis. Beginning with a population of lineations representative of those found on northeast-striking $S_2$ surfaces in the northeastern corner of the map area and along the east side of Lime Creek, the reorientation of lineations was calculated using equations from Ramsay (1967, pp. 129-130). For a coaxial, plane-strain deformation, lineations rotate toward X but do not concentrate into a well-defined point maximum at strains up to $\lambda = 64$ (Fig. 2-11a). In addition to not producing a strong point maximum, this pure shear mechanism cannot lead to the observed 100° trend of lineations (Fig. 2-11a) as this would necessitate rotation through the XY plane of the strain ellipsoid. Because this is not possible during a coaxial strain history (Lister and Williams, 1983), the pure shear model is considered unreasonable.

The alternative simple shear hypothesis is supported by the predominantly dextral asymmetry of quartz *c*-axis patterns from the northern basement domain (Fig. 2-10). If this model is appropriate, the magnitude of the shear strain ($\gamma$) necessary to reorient foliations striking 040° (e.g. northeastern corner of map area, Fig. 2-2b) to strikes of 100° (e.g. along Animas River in northern domain, Fig. 2-2b) may be estimated if the orientation of the shear plane is known (Ramsay, 1967, pp. 83-91). Assuming a shear plane strike of 115° based on the inferred flow planes from quartz *c*-axis fabrics in the gneisses (83, 213, 335; Fig. 2-10), $\gamma$ approximately equals 3.5. The degree of reorientation of lineations during such a simple shear deformation has been calculated using equations from Skjernaa (1980, p. 108) for a variety of lineations representative of those found on northeast-striking $S_2$ surfaces. Figure 2-11b illustrates the results of these calculations and clearly shows that a shear strain of 3.5 is capable of reorienting the lineations toward the subhorizontal, 090°-110° orientation typical of the northern basement domain (cf. Fig. 2-4c). If $F_3$ folding occurred by

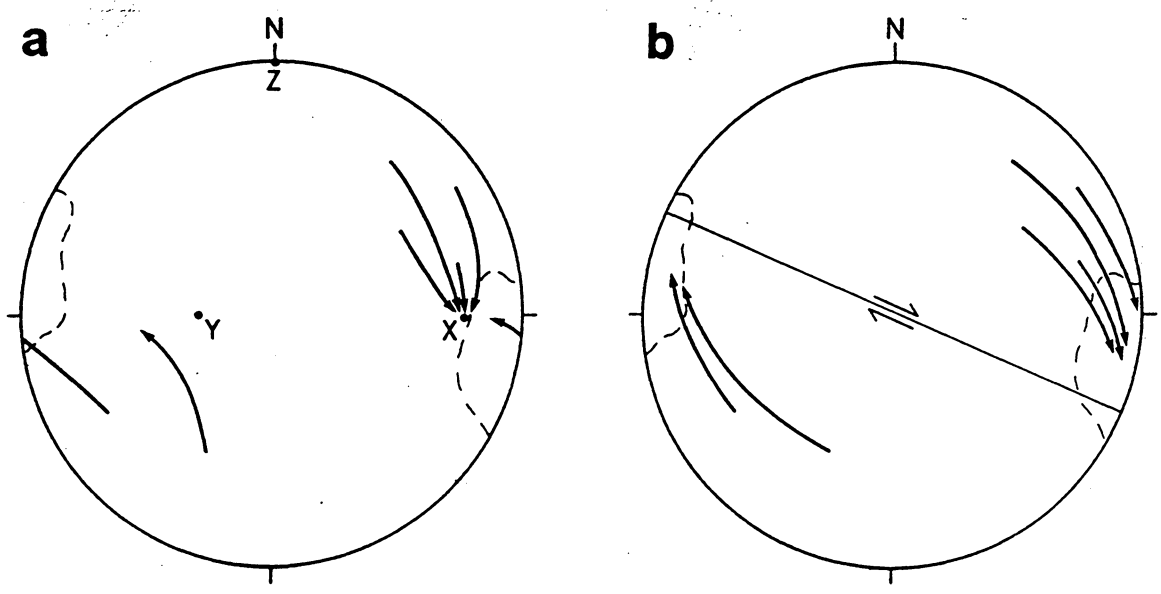


Figure 2-11: Reorientation of pre-existing lineations during deformation. Tails of arrows are original orientations and heads are final positions. a) pure shear, plane strain, $\lambda = 64$ at arrowheads; b) simple shear, $\gamma = 3.5$ at arrowheads. Dashed line is 4 points per 0.5% area contour of lineations from Figure 2-4c.

buckling during dextral shearing, a minimum shortening value ( $\lambda$ = (final length/initial length)$^2$) may be arrived at by unfolding the $F_3$ folds shown in Figure 2-4c. The derived value of $\lambda = 0.49$ deviates considerably from the predicted value of 0.05 for $= 3.5$ (Ramsay, 1967, p. 85). This large deviation is not surprising considering the uncertainty in fold geometry above and below the erosional surface and the possibility that the lengths of layers were not preserved during folding. It may be possible to duplicate the observed fabric patterns equally well or better by a more general (pure shear + simple shear), non-coaxial strain history. Quantitative strain data from the granitoids, which are not presently available, are necessary to constrain these more complex models.

Although a dextral shearing model appears to favorably account for the map pattern, fabric orientations, and quartz *c*-axis asymmetry in the northern domain, the ca. 1690 Ma granitoids do not display asymmetric fabrics typical of granitoids deformed in simple shear regimes (e.g. Berthe et al., 1979). The apparent orthorhombic symmetry of $S_3$ and the quartz *c*-axis fabrics in the granitoids imply that deformation within them was largely non-rotational. This apparent anomaly may be explained by the partitioning (Lister and Williams, 1983) of $D_{BC}$ deformation into subparallel zones of coaxial and non-coaxial strain. Similar phenomena have been observed in several major ductile thrust zones (Law et al., 1984; Platt and Behrmann, 1986). The cause of this strain partitioning in the Needle Mountains may be related to lithology because a strong linear anisotropy, such as was present in the gneisses prior to $D_{BC}$, tends to enhance the ability of that material to deform by shear parallel to the anisotropy (Cobbold and Watkinson, 1981). The pre-existing foliation and lineation within the gneisses may have helped to localize non-coaxial deformation.

The dextral shear zone model presented above is based largely on data from the northern basement domain and the southern domain east of Lime Creek. How-

ever, a considerable body of evidence, including mesoscopic shear fabrics (Fig. 2-8c) and quartz *c*-axis fabric asymmetry (Fig. 2-10), suggests that sinistral shear along a northeast-striking zone was also important in the evolution of the western portion of the southern domain. Most of the evidence for sinistral shearing comes from rocks along and west of Lime Creek where $F_4$ folds have reoriented fabrics around steeply plunging axes. The spatial association of $F_4$ folds and sinistral shear fabrics suggests a genetic relationship between these structures. In addition, the vertical fold that refolds earlier east-trending subhorizontal folds in the Uncompahgre Group at Lime Creek is associated with the sinistral offset of stratigraphic units within the cover sequence (Harris et al., in press). It is suggested, therefore, that sinistral shearing along a northeast-striking zone in the vicinity of Lime Creek may account for the northeast strike of fabric elements and the anomalous steeply plunging folds in this area.

The relative timing relationships between dextral and sinistral shearing are difficult to constrain. The superposition of steeply plunging folds related to sinistral shearing onto east-trending, upright folds in the Uncompahgre Group near Lime Creek suggests that dextral shearing preceded sinistral movement. If the orientations of mesoscopic shear fabrics are representative of large-scale shear zones of the same movement sense, this sequence of events also accounts for the variable orientations of dextral shear fabrics in the southern domain (Fig. 2-8c) where they could have been reoriented during sinistral shearing. In the absence of radiometric age constraints on the timing of these shearing events, they are both considered part of the $D_{BC}$ deformational episode. A schematic model for the deformation of the basement rocks during $D_{BC}$ in the northwestern Needle Mountains is illustrated in Figure 2-12. $F_3$ folding and coeval dextral shearing occurred synchronous with infolding of the Uncompahgre Group as a cuspate synclinorium (Harris et al., in press)

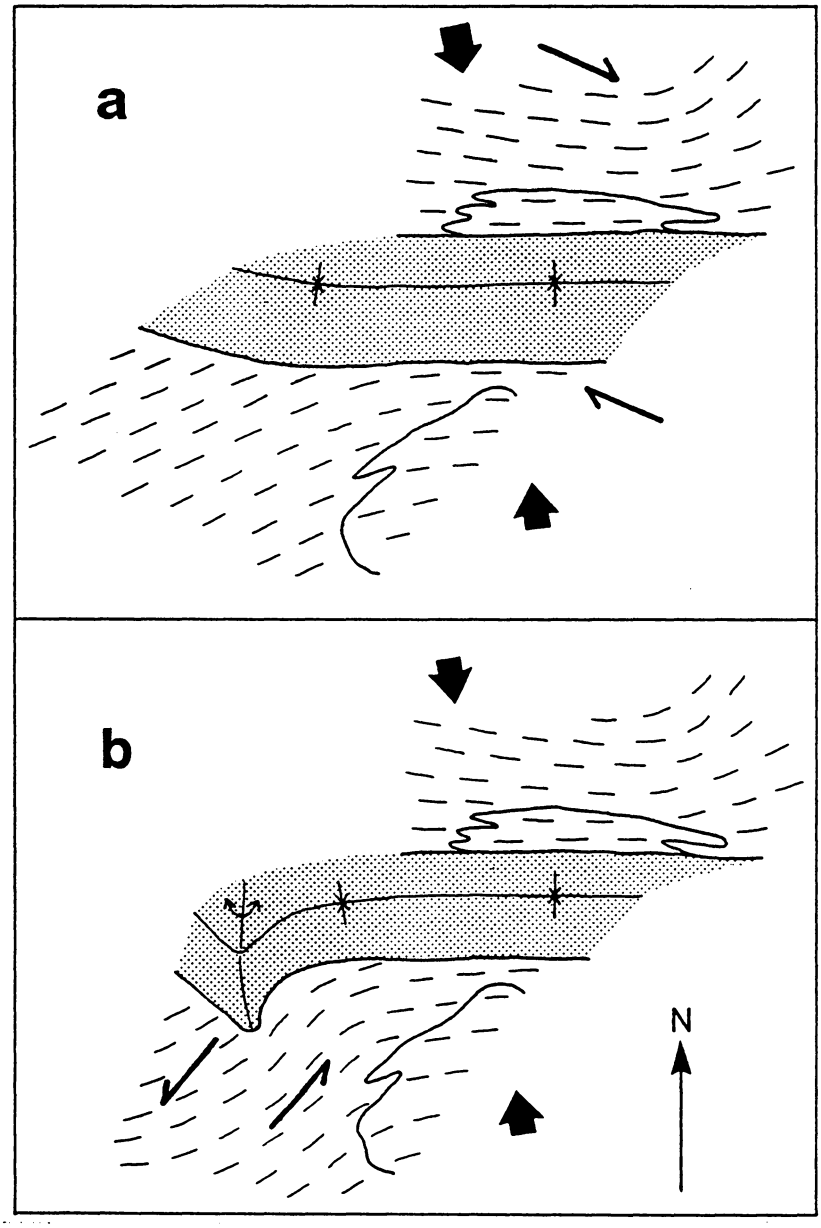


Figure 2-12: Proposed conjugate shear zone model for evolution of sigmoidal map pattern in northwestern Needle Mountains. Dashed lines signify general orientations of structural fabrics in basement; stippled area is Uncompahgre Group; bold arrows indicate interpreted shortening direction.

into the basement (Fig. 2-12a). Subsequent sinistral shearing caused local curvature of east-striking fabrics into northeasterly orientations and resulted in the formation of steeply plunging $F_4$ folds in the vicinity of the sinistral movement zone (Fig. 2-12b).

The geometric relationship between an east-southeast striking dextral shear zone and a northeast-striking sinistral shear zone resembles that of conjugate shear zones observed on the mesoscopic scale in many crystalline terranes (Ramsay, 1980). Observations of natural conjugate shear zones (e.g. Choukroune and Gapais, 1983) and experimental production of similar features (Cobbold et al., 1971) indicate that bulk shortening occurs along the obtuse bisector and extension along the acute bisector of the angle between conjugate ductile shear zones. If the dextral and sinistral shear zones in the Needle Mountains developed in response to the same overall bulk strain, this implies north-northwest/south-southeast shortening during $D_{BC}$ (Fig. 2-12). However, due to the domainal nature of deformation in crystalline terranes, the scale of observation is critical to the evaluation of bulk strain over large areas (e.g. Choukroune and Gapais, 1983). For this reason, it remains uncertain whether the structures preserved in the Needle Mountains are the product of heterogeneous coaxial shortening (Bell, 1981) or non-coaxial deformation (e.g. simple shear) on the crustal scale.

## REGIONAL IMPLICATIONS

In the preceeding section, it was demonstrated that structures within basement rocks of the northwestern Needle Mountains developed during two deformational events, $D_B$ between 1750 and 1690 Ma and $D_{BC}$ between approximately 1690 and 1430 Ma. This section reviews the chronology of deformation in other well-studied

parts of the Colorado Province and bounding areas and attempts to integrate the Needle Mountains data with that from other localities.

Reed et al. (1987) compiled U-Pb radiometric data from the Colorado Province and concluded that, although there is a general tendency for deformation to become younger toward the south, systematic trends in the ages of deformation in adjacent areas are obscure. They suggested that much of the polyphase deformation in the region was related to multiple phases of pluton emplacement rather than regional crustal shortening or shearing. However, Figure 2-13, constructed using a similar procedure and much of the same data as that of Reed et al. (1987), shows a surprisingly uniform history for the entire region consisting of 1) sedimentation or volcanism and plutonism, 2) deformation, 3) emplacement of 1730-1610 Ma plutons and siliciclastic sedimentation, 4) deformation, and 5) emplacement of ca. 1400-1500 Ma plutons. Intrusive rocks that pre-date the earliest deformation are generally potassium feldspar-poor (gabbros, diorites, tonalites, granodiorites) and have locally been interpreted to be cogenetic with the metavolcanic rocks that they intrude (e.g. Condie and Shadel, 1984). Younger plutons of the 1730-1610 Ma group are typically quartz monzonite, granodiorite, or granite (Tweto, 1980). Generally undeformed, potassic, 1400-1500 Ma granites comprise part of an anorogenic intrusive and extrusive suite found along a trend extending from eastern Canada to southern California (Anderson, 1983).

Two deformational events are evident in most of the studied areas (Fig. 2-13). The term "event" is used here to designate a period of single-phase or polyphase deformation bracketed in age by dated plutons with known cross-cutting relationships to tectonic fabrics in their country rocks. Pre-1700 Ma deformation occurred earliest (approximately 1760 Ma) in the Cheyenne Belt and became progressively younger toward the south. It culminated during the 1700-1720 Ma interval in northern New

Figure 2-13: Summary of radiometric age constraints on deformation in the Colorado Province and adjacent areas: short dashed lines - periods of supracrustal deposition (unit names given where appropriate), long dashed lines - ages of plutonism, solid lines - maximum time span for deformational event. Numbers at top of columns indicate sources of data: 1. Anderson et al. (1971), 2. Barker (1969), 3. Barovich (1986), 4. Bickford (1986), 5. Bickford and Boardman (1984), 6. Bowring et al. (1984), 7. Cullers and Wobus (1986), 8. Duebendorfer and Houston (1987), 9. Hansen and Peterman (1968), 10. Harris et al. (in press), 11. Hutchinson (1981), 12. Karlstrom and Conway (1986) and references therein, 13. Karlstrom and Houston (1984) and references therein, 14. Peterman et al. (1968), 15. Premo (1984), 16. Reed (1984), 17. Silver and Barker (1968), 18. Soegaard and Eriksson (1986), 19. Williams et al. (1980), 20. Wobus and Hedge (1982).

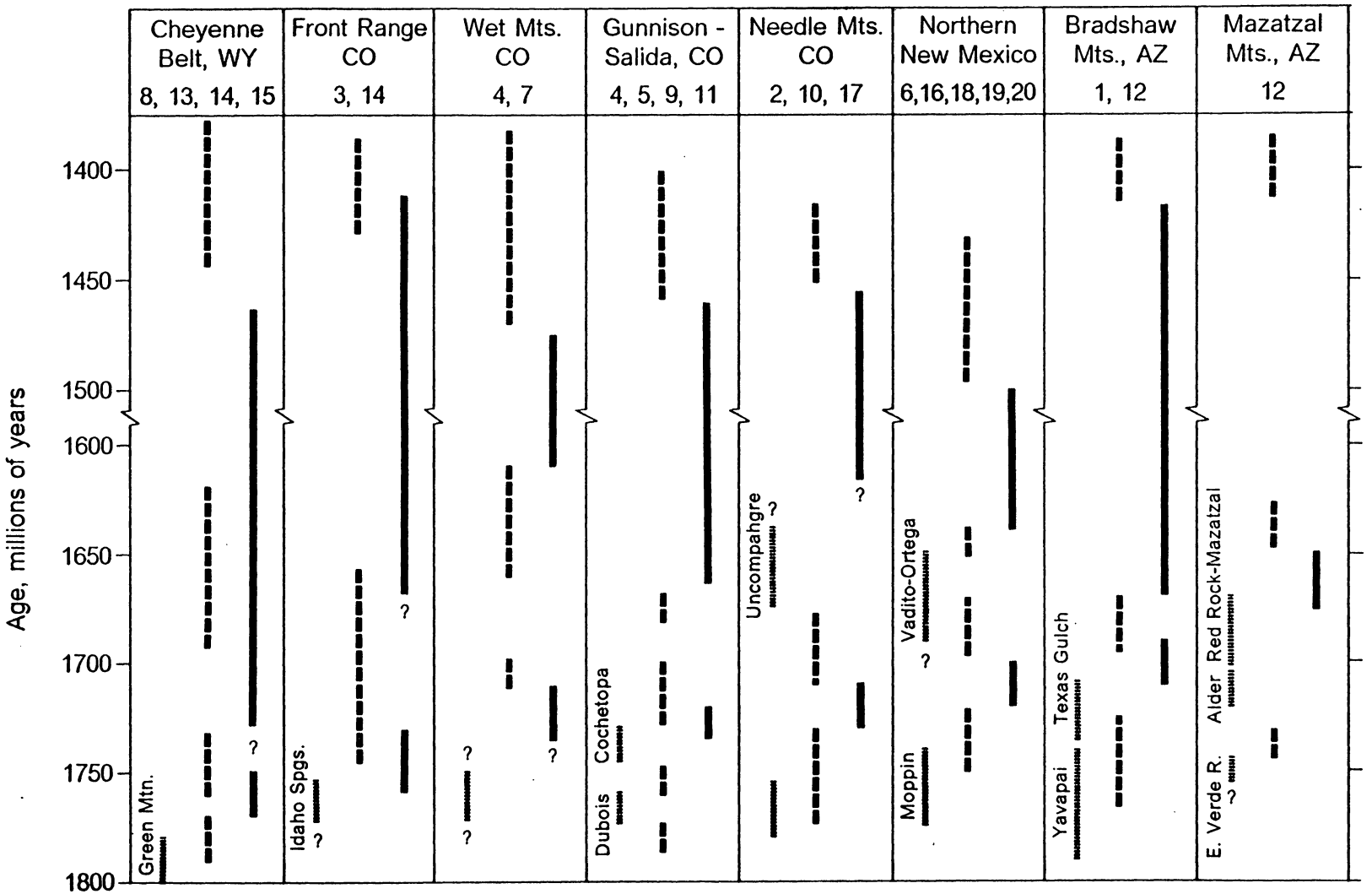
Cheyenne Belt, WY
8, 13, 14, 15
Front Range CO
3, 14
Wet Mts. CO
4, 7
Gunnison - Salida, CO
4, 5, 9, 11
Needle Mts. CO
2, 10, 17
Northern New Mexico
6,16,18,19,20
Bradshaw Mts., AZ
1, 12
Mazatzal Mts., AZ
12
Age, millions of years
1400
1450
1500
1600
1650
1700
1750
1800
Green Mtn.
Idaho Spgs.
Dubois
Cochetopa
Uncompahgre
Vadito-Ortega
Moppin
Yavapai
Texas Gulch
E. Verde R.
Alder
Red Rock-Mazatzal

Mexico where it is recorded solely as foliated inclusions within 1670-1700 Ma plutons in the Taos Range (Reed, 1984; Bowring et al., 1984). Plutons, ranging in age from 1730 to 1610 Ma, cross-cut fabrics related to this early deformation (Silver and Barker, 1968; Bowring et al., 1984; Bickford and Boardman, 1984; Barovich, 1986).

The 1730-1610 Ma plutons and post-1700 Ma siliciclastic sedimentary sequences (Uncompahgre Group, Ortega Group, and Mazatzal Group) were deformed during a younger (post-1700 Ma) deformation. Quartz monzonite plutons of this age group in the Cheyenne Belt are apparently undeformed (Duebendorfer and Houston, 1987) whereas a 1644 Ma pluton in northern New Mexico contains a strong tectonic fabric (Reed, 1984). Throughout the central part of the Colorado Province, the degree of deformation of the 1730-1610 Ma plutons is highly variable, ranging from a weak to non-existent foliation in the 1720-1730 Ma granite of South Beaver Creek near Gunnison (Bickford and Boardman, 1984) to plutons with margins foliated concordantly with their country rocks (e.g. 1676 Ma Cochetopa pluton, Hutchinson, 1981; Bickford and Boardman, 1984) to strongly foliated, concordant 1652-1610 Ma tonalite and granite bodies in the Wet Mountains (Bickford, 1986). Undeformed 1360-1500 Ma granites place a minimum age on this younger deformation.

Isotopic studies (Stacey and Hedlund, 1983; Nelson and DePaolo, 1985) indicate that the oldest igneous rocks in the Colorado Province were derived from the mantle without interaction with Archean crustal material. Considered along with the chemistry of the metavolcanic rocks (e.g. Condie and Shadel, 1984; Condie and Knoper, 1986), this observation has led to the interpretation of the Colorado Province as one or more volcanic arc/back-arc basin complex(es). Accretion of part of this terrane to the Wyoming Craton probably occurred by northward thrusting along the Cheyenne Belt prior to or during intrusion of the 1744-1763 Ma Sierra Madre Granite into the inferred suture zone (Hills and Houston, 1979; Karlstrom and Houston, 1984;

Duebendorfer and Houston, 1987). Because of the smoothly diachronous nature of the pre-1700 Ma deformation across the Colorado Province (Fig. 2-13), it is tempting to attribute all pre-1700 Ma deformation to accretion along the Cheyenne Belt. However, most of the metavolcanic and plutonic rocks exposed in the Salida-Gunnison area and southward are equivalent in age to or younger than the end of thrusting along the Cheyenne Belt (Fig. 2-13). This suggests that pre-1700 Ma deformation may have resulted from a more complex set of tectonic interactions involving both accretion along the Cheyenne Belt and assembly of pre-1700 Ma volcanogenic terranes farther south (Reed et al., 1987).

The paucity of plutons in the 1500-1650 Ma age range precludes precise determination of the timing of post-1700 Ma deformation in the areas summarized in Figure 2-13. However, existing age constraints allow the post-1700 Ma deformational episode to be correlated throughout the Colorado Province and adjacent areas in Wyoming, Colorado, and New Mexico. A period of quartzite-pelite sedimentation, beginning approximately 1700 Ma, and subsequent deformation is recorded in the Mazatzal Mountains of Arizona (Mazatzal Group), northern New Mexico (Ortega Group), and the Needle Mountains (Uncompahgre Group). The effects of post-1700 Ma deformation are most pervasive near the boundary with the Southwestern Province (Fig. 2-1) in New Mexico and vary in intensity throughout the central part of the province. In northern New Mexico, structures related to this event developed during north-northwest directed translation of fold and thrust nappes and subsequent upright folding (Grambling and Codding, 1982; Grambling and Ward, 1987). Similarly, rocks of the Mazatzal Group in central Arizona were thrust northwestward in a thin-skinned fashion (Puls and Karlstrom, 1985). Post-1690 Ma conjugate strike-slip shearing in the Needle Mountains also accommodated north-northwest/south-southeast shortening. Because of the consistent north to northwest shortening direction in these three

widely separated areas, it is suggested that post-1700 Ma deformation in the southern part of the Colorado Province is related to regional crustal shortening. This shortening may have been the result of tectonic interactions along the boundary between the Colorado and Southwestern Provinces (Fig. 2-1) where post-1700 Ma deformation was most pronounced. Along-strike diachroneity may account for the apparently earlier deformation in Arizona than in areas farther east (Fig. 2-13).

Much of the Colorado Province, especially north of the Needle Mountains, is characterized by irregular foliation orientations that do not conform in a straightforward manner to the pattern expected during regional crustal shortening (Reed et al., 1987). Considerably more data on the geometric and age relationships among structural fabrics and rock units are necessary to understand the significance of these patterns. Because of the highly inhomogeneous nature of post-1700 Ma deformation throughout this region, it is critical to differentiate between those tectonic fabrics that are cross-cut by, and those which deform, rocks of the 1730-1610 Ma intrusive suite(s). In addition, it is necessary to evaluate the possible control of pre-existing structural fabrics on the orientations of structures developed during a subsequent deformation. Inhomogeneous deformation such as that found in much of the Colorado Province is characteristic of basement terranes which have accommodated crustal shortening by deformation concentrated in narrow shear belts (e.g. Proterozoic of Greenland, Watterson, 1978; Archean of southern Africa, Coward et al., 1976).

## CONCLUSIONS

Structures in ca. 1750+ Ma metavolcanic and metaplutonic rocks of the northwestern Needle Mountains preserve evidence for two distinct polyphase defor-

mational events, $D_B$ and $D_{BC}$, separated by pluton emplacement at approximately 1690 Ma. Polyphase folding and syn-tectonic metamorphism during $D_B$ produced strong planar and linear fabrics. $D_{BC}$ deformation involved folding and reorientation of these fabrics into a sigmoidal pattern comprised of northeast- and east-striking structural domains. Fabric orientations, kinematic data, and structural superposition are best explained by a sequence of dextral followed by sinistral strike-slip shearing during $D_{BC}$. Movement senses and orientations of these shear zones conform to the geometry of a conjugate system and indicate that $D_{BC}$ accommodated north-northwest/south-southeast shortening.

Field and radiometric age data from throughout the Colorado Province show that $D_B$ and $D_{BC}$ in the Needle Mountains are representative of two regionally extensive deformational episodes. Deformation during the 1770-1700 Ma time interval probably occurred during one or more events leading to the assembly of the Colorado Province and its accretion onto the Archean Wyoming Craton along the Cheyenne Belt. Post-1700 Ma deformation is interpreted to be the result of north-northwest/south-southeast crustal shortening induced by tectonic interactions along the southern terrane boundary. These results support tectonic models which explain the southward-younging Proterozoic age provinces in southwestern North America as the product of sequential terrane accretion onto an Archean cratonic nucleus (e.g. Condie, 1982; Reed et al., 1987).

# Chapter 3: Contact Relationships Between Gneissic Basement and Metasedimentary Cover in the Needle Mountains

## INTRODUCTION

In deformed and metamorphosed geologic terranes, understanding the nature and significance of contacts between supracrustal sequences and adjacent metamorphic complexes is necessary to evaluate the geologic history. The recognition of erosional features, basal conglomerates, and/or clasts of the metamorphic complex within the supracrustal sequence supports the interpretation of such contacts as unconformities. However, where locally intense or complex deformation is present along such boundaries (e.g. Gee, 1980; Gratier and Vialon, 1980; Coney, 1980; Jacob et al., 1983; Lambert and van Staal, 1987), it is important to distinguish between deformation zones that signify zones of major displacement and disrupt original stratigraphic relationships and those of minor displacement across which stratigraphic relationships are preserved.

Early to Middle Proterozoic rocks in the northwestern Needle Mountains of southwestern Colorado (Fig. 3-1) comprise two contrasting lithologic suites, a volcano-plutonic basement complex and a siliciclastic sedimentary cover sequence. The presence of localized penetrative deformation along the basement-cover contacts in this area has hindered interpretation of the original contact relationships and, thus, the relative ages of these suites. Previous workers have interpreted the contacts as either unconformities (Cross et al., 1905; Barker,, 1969) or Proterozoic thrust faults (Tewksbury, 1985). In this paper, field, microstructural, and geochemical fea-

tures are described as a basis for evaluation of the origin and significance of these deformed basement-cover contacts. Available evidence supports interpretation of them as segments of an unconformity with an underlying regolith that localized ductile deformation.

## GEOLOGIC SETTING OF THE NEEDLE MOUNTAINS

The area of interest is located in the northwestern part of the Needle Mountains (Fig. 3-1a), a 1100 $km^2$ exposure of Proterozoic rocks surrounded by Paleozoic sedimentary rocks and Tertiary volcanogenic rocks in southwestern Colorado. Proterozoic basement rocks in the study area (Fig. 3-1b) consist of a layered gneiss complex intruded by granite to quartz monzonite plutons. The gneiss complex is composed predominantly of pl + qtz + bt ± ksp ± ep ± ms ± hb ± grt gneiss and hb + pl ± ep ± bt ± qtz gneiss with rare primary features indicative of felsic and mafic volcanogenic and plutonic protoliths (Barker, 1969; Chapter 2). U-Pb zircon and Rb-Sr whole-rock dating yield ages of approximately 1750 Ma for part of the gneiss complex and about 1690 Ma for the granitoid plutons (ages recalculated from Silver and Barker, 1968; Barker et al. 1969; Bickford et al., 1969). Proterozoic cover rocks of the Uncompahgre Group occupy an east-west trending outcrop belt bounded on both the north and south by basement (Fig. 3-1b). The Uncompahgre Group is a 3 + km-thick sequence with an internal stratigraphy consisting of four quartzite and four pelite units with well-preserved primary sedimentary structures (Harris and Eriksson, 1987). Most of the Uncompahgre Group is thought to have been deposited in a shallow marine setting although the lowest part of the basal quartzite unit ($Q_1$) is probably alluvial in origin (Harris and Eriksson, 1987).

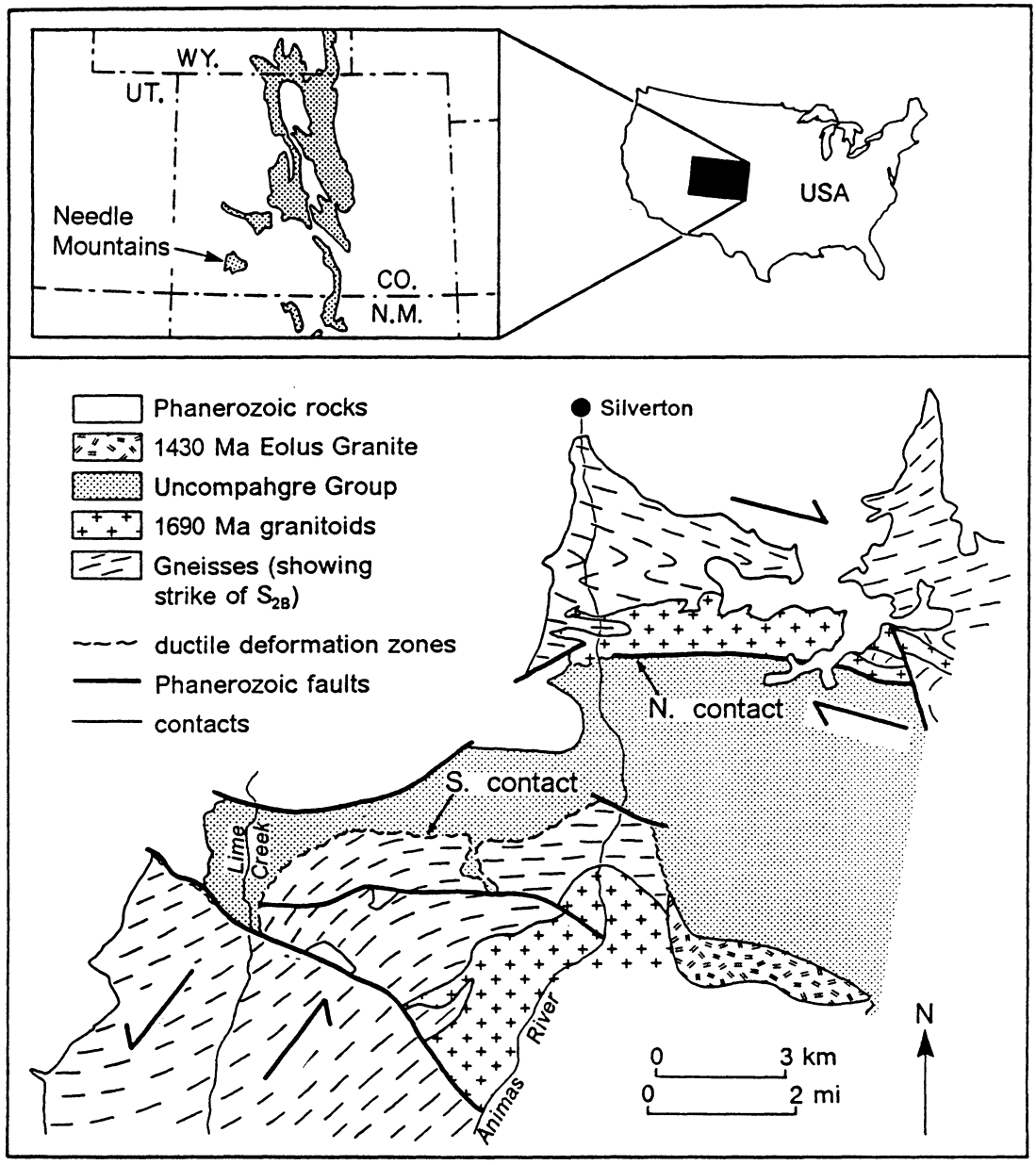


Figure 3-1:

a) Location of Needle Mountains; stippled areas are regions of Early to Middle Proterozoic outcrop.

b) Geologic map of northwestern Needle Mountains simplified from Harris et al. (in press); split arrows indicate areas of dextral and sinistral shearing defined in Chapter 2.

The polyphase structural evolution of this area is described in Chapter 2 and Harris et al. (in press). Rocks of the gneiss complex were polydeformed ($D_B$) and metamorphosed ($M_B$) prior to intrusion of the ca. 1690 Ma granitoids. $D_B$ deformation culminated with the production of a penetrative $S_{2B}$ foliation and mineral lineation defined by quartz and feldspar ribbons and aligned biotite or amphibole in rocks of the gneiss complex. Subsequent $D_{BC}$ deformation affected the gneiss complex, granitoids, and Uncompahgre Group. An initial phase of north-directed thrusting within the Uncompahgre Group was followed by folding of both the cover rocks and basement gneisses about subhorizontal, east-west trending axes ($F_{3B}$ and $F_{2C}$) and development of an east-striking, subvertical foliation ($S_{3B}$) in the granitoids (Harris et al. in press). Mapping within the Uncompahgre Group has shown that its outcrop belt is a synclinorium (Barker, 1969) that has been interpreted as a cuspate structure formed during contemporaneous folding of the basement and cover (Harris et al. in press). North-northwest shortening during $D_{BC}$ was partly accommodated by movement along east-southeast-striking dextral and northeast-striking sinistral conjugate strike-slip shear zones (Chapter 2). Zones of major dextral and sinistral shearing within the basement, as delineated by the regionally sigmoidal geometry of $S_{2B}$, mesoscopic shear indicators, and quartz petrofabrics, are shown in Figure 3-1b. Steeply-plunging cross-folds in both the basement ($F_{4B}$) and cover ($F_{3C}$) near Lime Creek (Fig. 3-1b) are attributed to sinistral shearing in this area. A second metamorphic episode, $M_{BC}$, caused syn- to post-$D_{BC}$ porphyroblast growth and annealling of minerals in both the basement and cover rocks. The minimum ages of $D_{BC}$ and $M_{BC}$ are constrained by emplacement of the undeformed ca 1430 Ma Eolus Granite exposed to the south and east of the study area (Fig. 3-1b).

## BASEMENT-COVER CONTACTS

Previous workers in the Needle Mountains have documented that the Uncompahgre Group is typically in contact with the basement gneisses and granitoids along a zone of foliated micaceous rock (phyllonite of Barker, 1969; Tewksbury, 1985). Cross et al. (1905) and Barker (1969) concluded that these contacts are part of an unconformity at the base of the Uncompahgre Group although Barker (1969) recognized that portions of the southern contact may be a thrust fault. Tewksbury (1985) examined the microstructures in rocks along the contacts and concluded that they resemble those found in ductile shear zones; she interpreted the contacts as fault zones and argued that the relative ages of rocks on either side could not be constrained. On the basis of the fault zone interpretation, Tewksbury (1985) proposed a fold-thrust belt model for the evolution of this area, in which both the northern and southern basement-cover contacts are south-verging, listric thrust faults (Fig. 3-2a). Harris et al. (in press) have questioned this interpretation and suggested that the contacts are unconformities that localized deformation during infolding of cover rocks into basement during $D_{BC}$ (Fig. 3-2b).

The northern contact zone is vertical in the bottom of the Animas River canyon (Fig. 3-3a) and dips steeply northward at higher elevations on the western canyon walls; this defines a slight convex upward and northward shape for the contact surface. The steeply dipping micaceous zone along this contact is unconformably overlain by quartzite-cobble conglomerate of the Late Cambrian Ignacio Formation (Baars and See, 1968) at location I (Fig. 3-3a) and is, therefore, of Proterozoic origin. The southern contact is horizontal at high elevations south of Snowdon Peak (Fig. 3-3b) and steepens in dip toward the north so that it is also convex upward and northward. East of Snowdon Peak, the contact dips gently to moderately northward

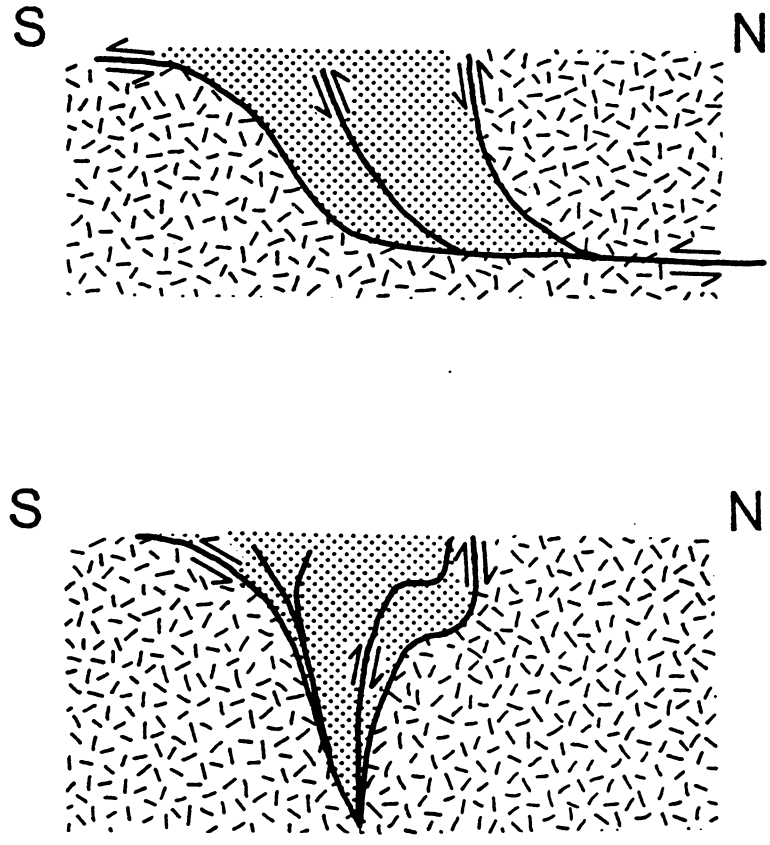


Figure 3-2: Possible interpretations of basement-cover relationships in the north-western Needle Mountains displayed in schematic north-south cross-sections along the Animas River: a) fold-thrust belt model after Tewksbury (1985); b) cuspate fold model after Harris et al. (in press).

whereas, west of Snowdon Peak, it becomes vertical to steeply south-dipping (Fig. 3-3b). The southern contact also varies in strike from east-west near Snowdon Peak to north-south near Lime Creek (Fig. 3-3b). East of the Animas River, the micaceous zone forming the southern boundary of the Uncompahgre Group is cross-cut by the ca. 1430 Ma Eolus Granite (Barker, 1969; Tewksbury, 1985).

Detailed mapping of the basement-cover contacts in the northwestern Needle Mountains indicates that, although some segments are characterized by a zone of foliated micaceous rock, others lack this zone. Contacts lacking the micaceous zone are characterized by fracturing, iron staining, and local cataclasis that overprint older penetrative tectonic fabrics in the adjacent rocks. These contacts are interpreted as fault zones. Late Paleozoic or younger movement along some of the faults in the area is implied by the juxtaposition of Proterozoic basement with Pennsylvanian sedimentary rocks along the Coal Bank Pass and Andrews Lake faults (Fig. 3-3). On the basis of facies and thickness variations in the Paleozoic sedimentary rocks, Baars and See (1968) and Spoelhof (1976) demonstrated that these faults underwent episodic movement throughout much of the Paleozoic and, possibly, into the Tertiary. Ages of last movement on other faults that modify the Proterozoic basement-cover contacts are not constrained by cross-cutting relationships with the Paleozoic sequence. However, post-Proterozoic and pre-Oligocene movement along these faults is implied by 1) the parallelism of the northeast-striking fault that offsets the northern contact with the Andrews Lake fault and 2) the overlapping of Oligocene volcanogenic rocks across the east-striking fault along the northern contact (Fig. 3-3a). Because the aim of this study was to evaluate the pre-deformational relationships along the Proterozoic basement-cover contacts and the nature of Proterozoic deformation along these boundaries, portions of the contacts that have been modified by Phanerozoic faulting are not discussed further.

Figure 3-3: Strip maps and cross-sections of (a) northern and (b) southern basement-cover contacts; Roman numerals denote outcrop locations cited in text and numbers in parentheses indicate locations of samples analyzed for quartz *c* -axis fabrics; precise outcrop and sample locations are given in Appendix D.

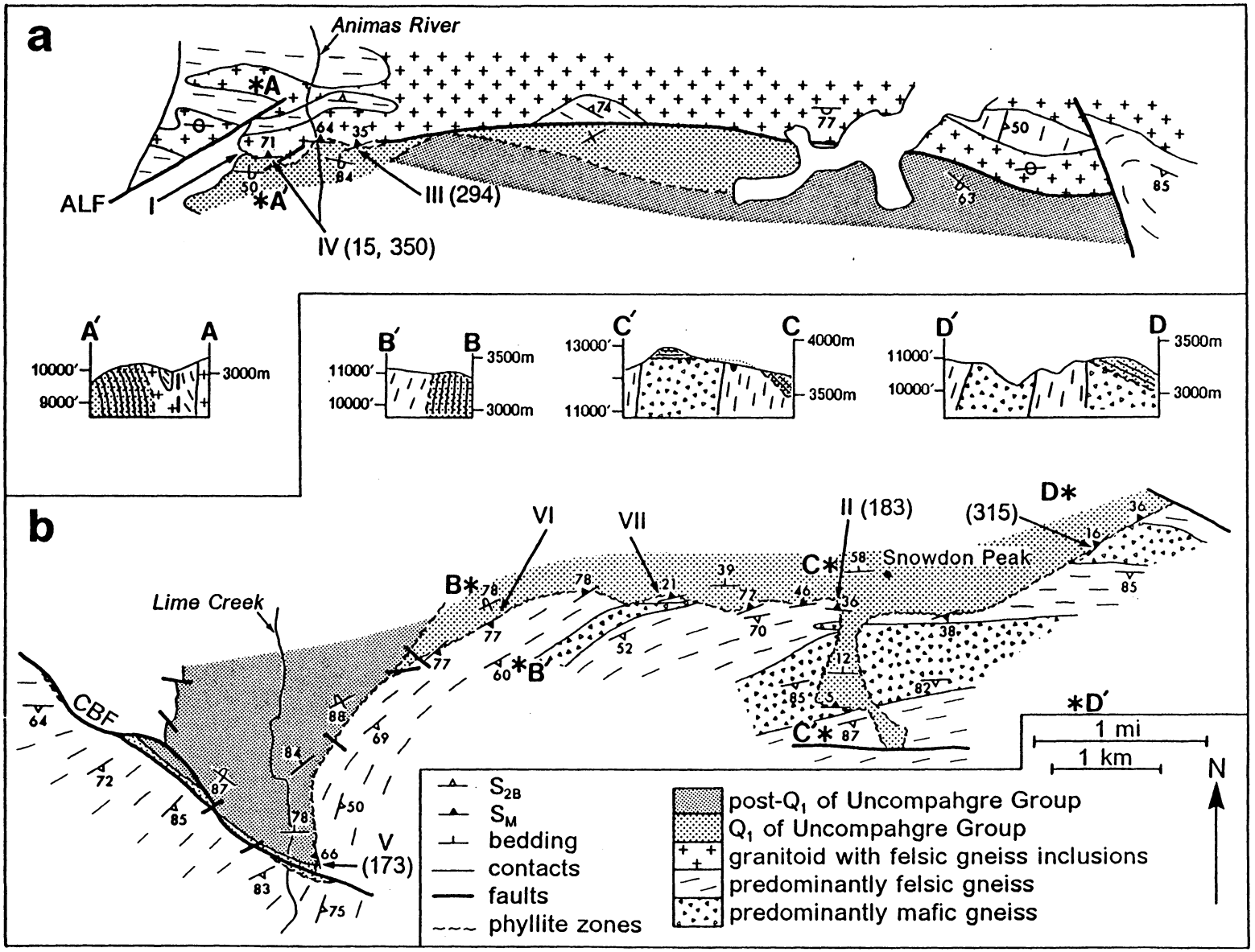
a
Animas River
*A
*A'
ALF
I
III (294)
IV (15, 350)
A'
A
10000'
9000'
3000m
B'
B
11000'
10000'
3500m
3000m
C'
C
13000'
11000'
4000m
3500m
D'
D
11000'
10000'
3500m
3000m
b
VI
VII
II (183)
(315)
D*
Snowdon Peak
B*
C*
Lime Creek
CBF
*B'
*D'
C*
V
(173)
1 mi
1 km
N
S2B
SM
bedding
contacts
faults
phyllite zones
post-Q1 of Uncompahgre Group
Q1 of Uncompahgre Group
granitoid with felsic gneiss inclusions
predominantly felsic gneiss
predominantly mafic gneiss

Away from the Phanerozoic faults, the basement and cover are everywhere separated from one another by a zone of quartz + muscovite + Fe/Ti-oxide ± chloritoid ± andalusite ± chlorite rock that attains a maximum thickness of approximately 12 m southwest of Snowdon Peak (Fig. 3-3b) but is more typically less than 6 m thick. This zone is parallel to bedding in the adjacent Uncompahgre Group but is generally oblique to $S_{2B}$ in the basement gneisses (Fig. 3-3). Cross-bedding in the Uncompahgre Group invariably indicates facing away from the basement (Harris et al. in press). At locations II and IV (Figs. 3-3a-b), the boundary between the Uncompahgre Group conglomerates and micaceous zone is highly irregular (Figs. 3-4a, 3-4b). The basal stratigraphic unit ($Q_1$) of the Uncompahgre Group is everywhere in contact with basement except along the north- to northeast-striking segment of the contact immediately east of Lime Creek (Fig. 3-3b) where younger quartzites and pelites of the Uncompahgre Group are juxtaposed with basement (Harris et al. in press).

**Fabric Elements**

Micaceous rocks exposed along the contacts typically contain a prominent muscovite foliation, $S_m$. Where $S_m$ is present, these rocks are best described as phyllites. The term "phyllite" is used here, instead of "phyllonite" (Barker, 1969; Tewksbury, 1985), as a non-genetic term to denote these fine-grained, muscovite-bearing rocks because 1) their protoliths are not always determinable and 2) their fine grain size may not be entirely due to mechanical grain size reduction of their protoliths (cf. definitions in American Geological Institute, 1980). Along the northern contact, $S_m$ dips moderately to steeply northward and locally contains a faint down-dip muscovite lineation, $L_m$ (Fig. 3-5a). Along the southern contact, the dip of $S_m$ varies

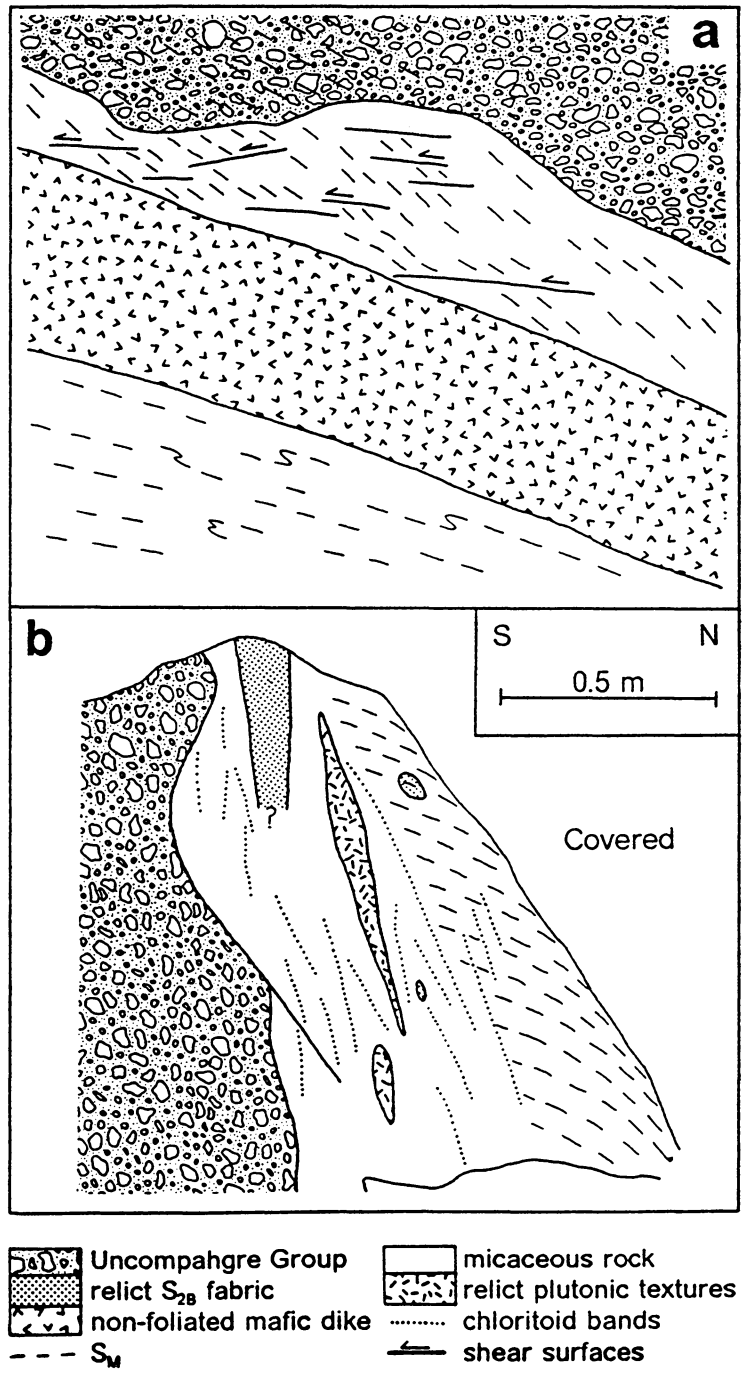


Figure 3-4: Sketches from photographs of mesoscopic basement-cover relationships at locations II (a) and IV (b) (Fig. 3-3). See text for discussion.

sympathetic with the change in orientation of the contact along its length; poles to $S_m$ define a girdle distribution with the majority of $S_m$ surfaces dipping northward (Fig. 3-5b). Gentle southward dips for $S_m$ were observed in one area southeast of Snowdon Peak (Fig. 3-3b). $L_m$ pitches steeply to the west on $S_m$ (Fig. 3-5b).

Conglomerates at the base of the Uncompahgre Group grade into the contact zone phyllites over a distance of less than 1 m and locally acquire a deep red staining. Clasts in these basal conglomerate layers commonly display a strong bedding-parallel alignment. On the basement side of the contact zones, $S_m$ is axial planar to crenulations that deform $S_{2B}$ in the basement gneisses (Figs. 3-5b, 3-6a). $S_{2B}$ is commonly not apparent in rocks exposed within 1 m of the Uncompahgre Group. Granitoids along the northern contact at location III (Fig. 3-3a) also grade into the phyllite, within which lenses of less deformed granite are locally preserved.

$S_m$ is defined by a continuous (Powell, 1979) alignment of $\leq$0.1 mm long muscovite grains that define beards adjacent to and wrap around equant to elongate quartz aggregates (Fig. 3-6b). Where it overprints $S_{2B}$ (Figs. 3-6c, 3-7a), $S_m$ sometimes consists of both a continuous muscovite alignment and anastomosing domains with concentrations of very fine-grained ilmenite that wrap around quartz grains. In some samples, fine-grained muscovite in the lithons between spaced $S_m$ cleavage domains is not consistently aligned and contacts between the cleavage domains and terminations of $S_{2B}$ quartz ribbons have a scalloped or wavy morphology (Fig. 3-7a). Aggregates of euhedral ilmenite $\pm$ quartz $\pm$ chlorite are aligned in tabular arrays subparallel to $S_{2B}$ (Fig. 3-6c) that mimic the morphology of biotite grains in the protolith felsic gneisses. No feldspar is present in rocks that preserve $S_{2B}$ although irregularly shaped muscovite aggregates and interstitial muscovite between quartz grains are interpreted as pseudomorphs after feldspar. Feldspar grains that are lo-

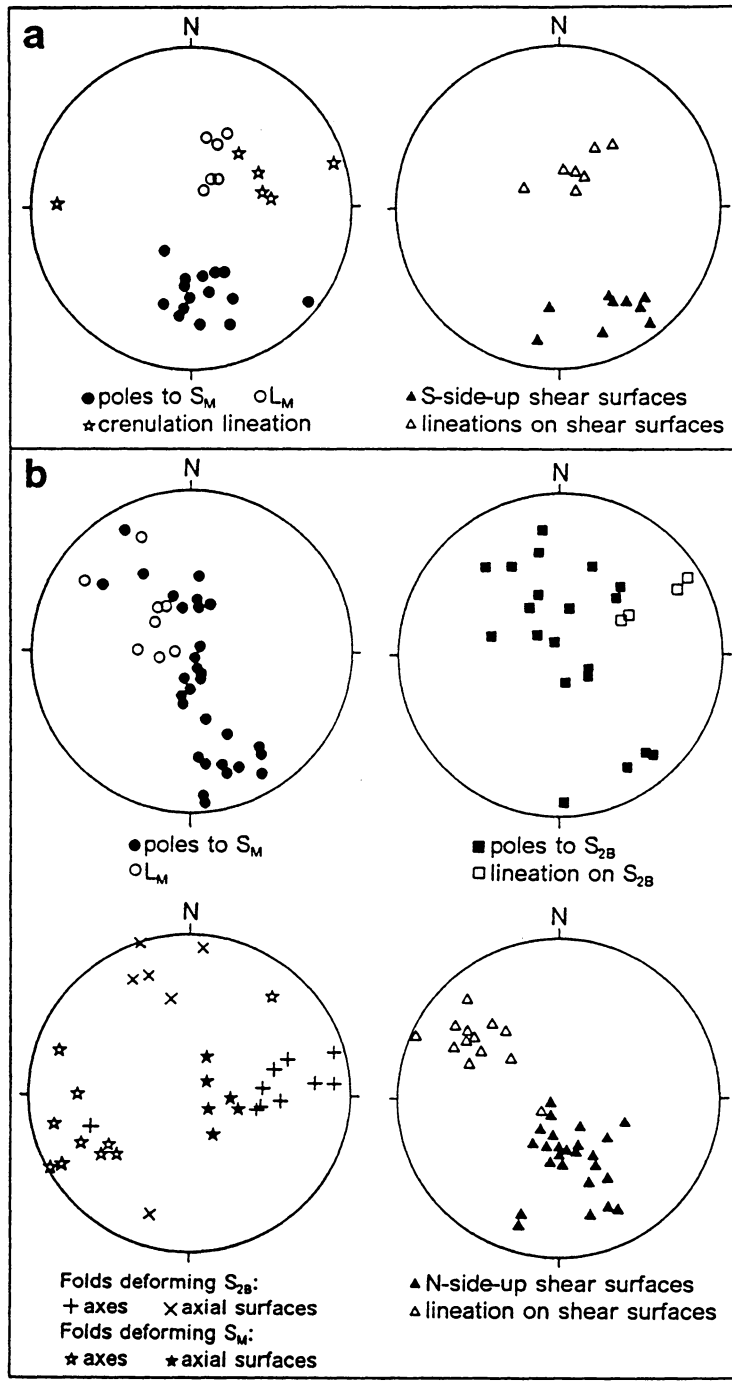


Figure 3-5: Orientation data for fabric elements in rocks along northern (a) and southern (b) basement-cover contacts; lower hemisphere equal-angle projections.

Figure 3-6: Fabric elements along basement-cover contacts.

a) $S_m$ overprinting $S_{2B}$ in outcrop of retrograded felsic basement gneiss;

b) continuous $S_m$ fabric defined by muscovite wrapping around equant quartz aggregates; plane light;

c) spaced, anastomosing $S_m$ domains oblique to relict $S_{2B}$ in retrograded felsic gneiss; note ilmenite + chlorite pseudomorphs (Bt) after biotite; plane light.

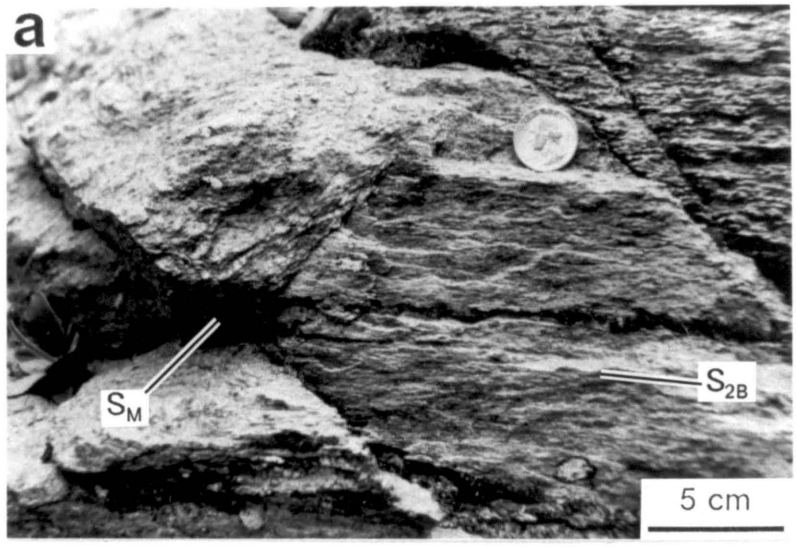
a
$S_M$
$S_{2B}$
5 cm

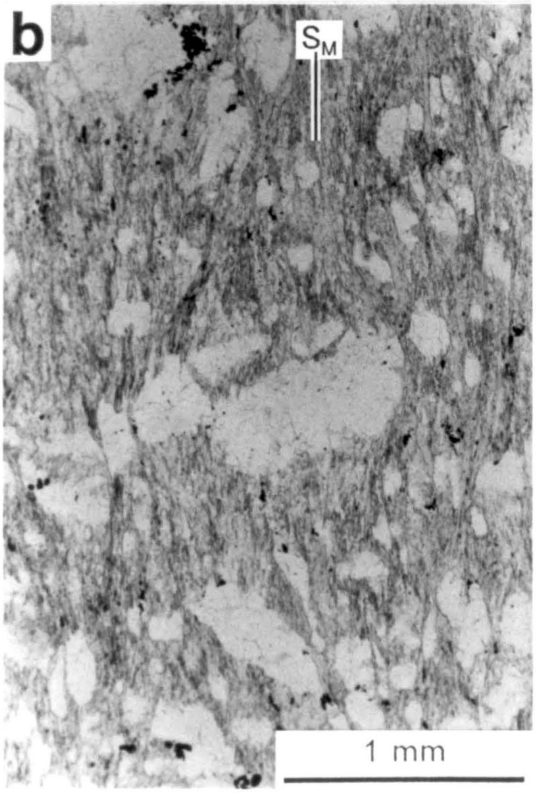
b
$S_M$
1 mm

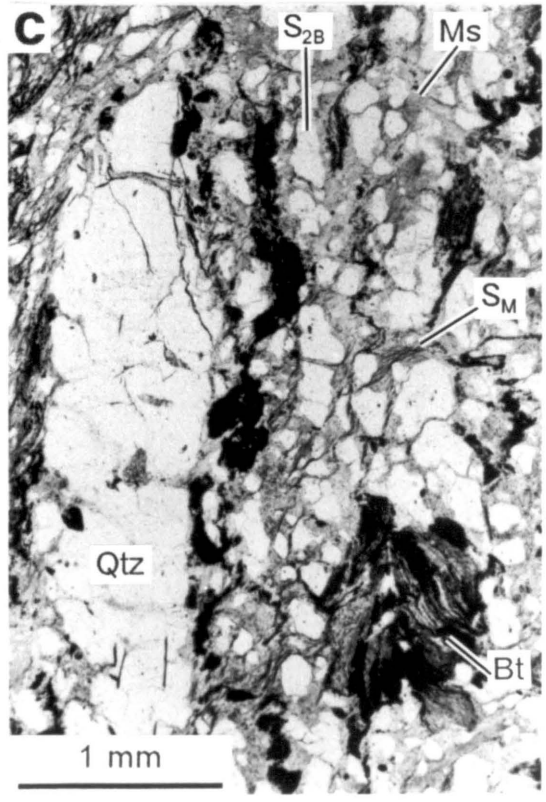
c
$S_{2B}$
Ms
$S_M$
Qtz
Bt
1 mm

Figure 3-7: Microfabrics from the northern basement-cover contact.

a) spaced $S_m$ domains cross-cutting $S_{2B}$; muscovite-rich areas between quartz ribbons show no preferential mineral alignment; note euhedral Fe-oxide porphyroblasts and scalloped terminations of quartz ribbons (arrow); plane light.

b) fractured and altered feldspar porphyroclast in phyllite derived from granitoid; arrows indicate inferred sense of shear; crossed nicols;

c) relict crystal outlines of original feldspar grains preserved by muscovite grain size variation in retrograded granitoid; dark chloritoid grains (ctd) occur intergrown with muscovite; crossed nicols;

d) porphyroblasts of chloritoid (ctd), chlorite (chl), and Fe-oxide (black) in sample with relict gneissic compositional layering and $S_{2B}$ defined by quartz ribbons; plane light.

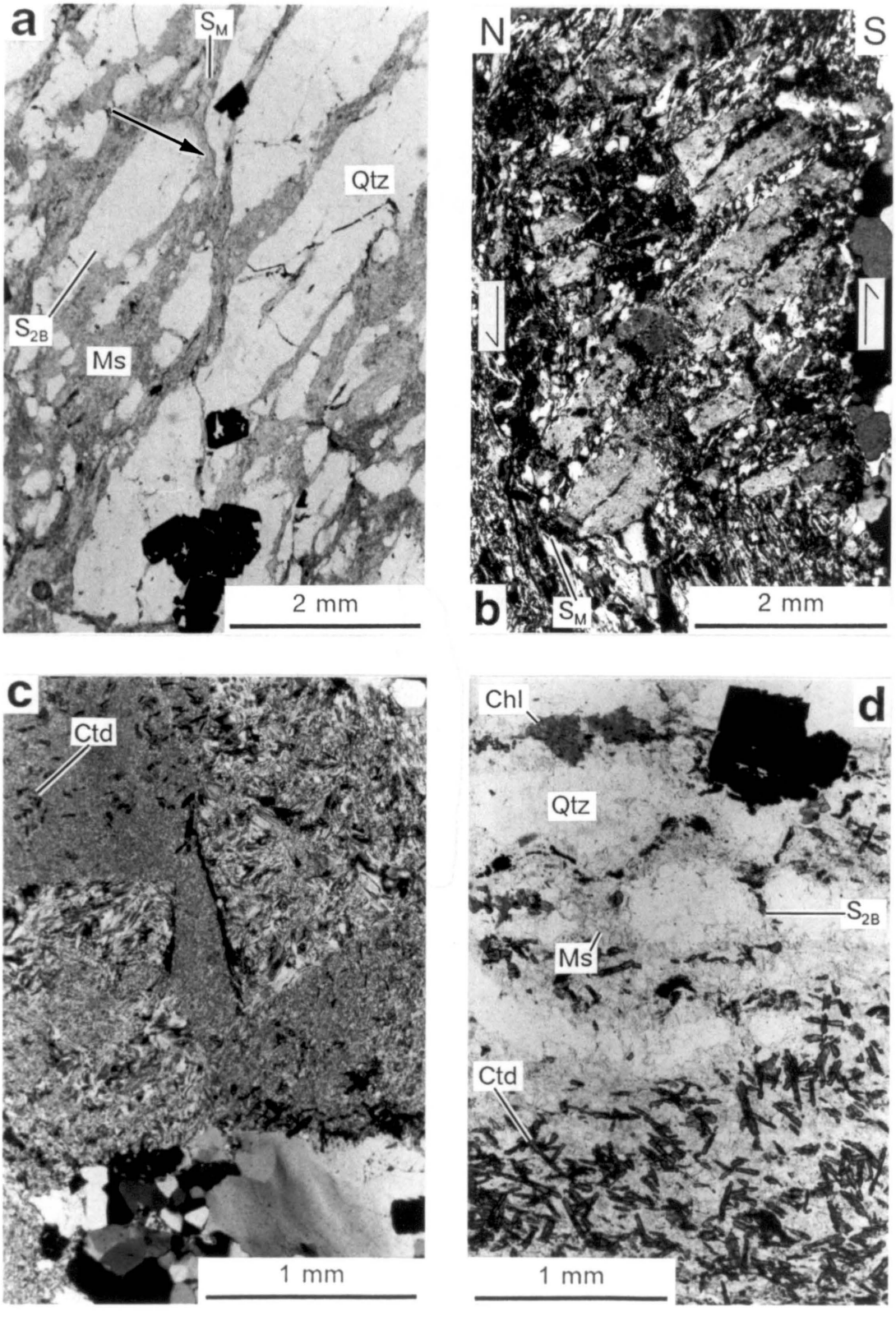
a
$S_M$
Qtz
$S_{2B}$
Ms
2 mm
N
S
b
$S_M$
2 mm
c
Ctd
1 mm
Chl
d
Qtz
$S_{2B}$
Ms
Ctd
1 mm

cally preserved in phyllites derived from granitoids at location III (Fig. 3-3a) are fractured and heavily altered to fine-grained muscovite (Fig. 3-7b).

Although the micaceous lithology along the basement-cover contacts typically contains $S_m$, this fabric is not always present along the northern contact. At location IV (Fig. 3-3a), a basal conglomerate of the Uncompahgre Group is in contact along an irregular, subvertical surface with a weakly to non-foliated, tan, micaceous rock that contains patches of relict $S_{2B}$ and lenses of coarse-grained granitoid (Fig. 3-4b). This lithology consists of equant polycrystalline aggregates of polygonal quartz surrounded by a matrix of randomly oriented, fine-grained muscovite. Despite this secondary mineralogy, outlines of primary plutonic textures are preserved within the granitoid lenses (Fig. 3-7c). Diffuse, $\leq$5 mm thick, dark gray bands occur subparallel to the contact with the conglomerate and are defined by concentrations of chloritoid grains. Approximately 0.5 m north of the contact, $S_m$ appears as a gently north-dipping foliation that intensifies and steepens in dip toward a covered interval that separates this outcrop from basement rocks exposed several meters farther north (Fig. 3-4b). Compositional banding, which is defined by varying proportions of muscovite, chlorite, and chloritoid (Fig. 3-7d) and is comparable in scale to layering in the adjacent gneiss complex, occurs in other weakly foliated micaceous lithologies along the contact in this area.

Small folds and crenulations locally deform $S_m$ (Fig. 3-8a). Along the southern contact, subhorizontal to east-plunging, tight crenulations are present along gently dipping segments of the contact. They have subhorizontal axial surfaces and contain an axial planar crenulation cleavage (Fig. 3-5b). Along the northern contact, $S_m$ is locally a crenulation of an older mica fabric although mica-rich laminae within the phyllite are more typically deformed by $\leq$0.3 mm wavelength, open crenulations with axial surfaces oriented at high angles to $S_m$. Fold trains cannot be traced for signif-

Figure 3-8: Metamorphic textures in contact zone phyllites.

a) folded $S_m$ defined by polygonal quartz ribbons and muscovite overgrown by andalusite porphyroblasts (and); crossed nicols;

b) muscovite porphyroblasts overgrowing $S_m$; crossed nicols;

c) nearly straight, fibrous quartz pressure fringes adjacent to Fe-oxide porphyroblasts; crossed nicols.

d) possible south-side-up shear bands (vertical dark areas with split arrows) deflecting $S_m$ in phyllite from northern contact zone; crossed nicols.

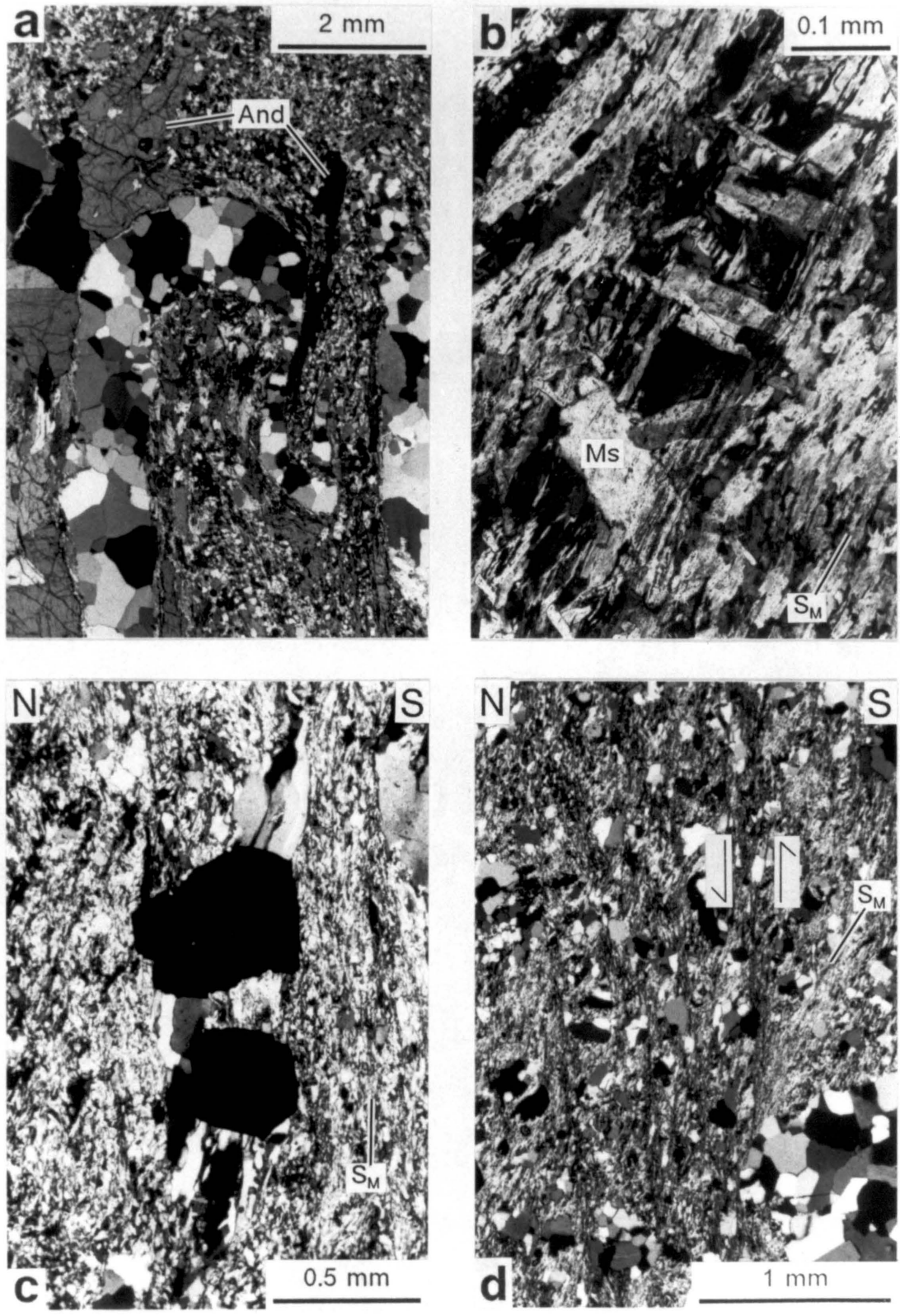
a
2 mm
And
b
0.1 mm
Ms
$S_M$
N
S
$S_M$
c
0.5 mm
N
S
$S_M$
d
1 mm

icant distances within the phyllite and are not present in the adjacent basement or cover rocks. In some instances, muscovite grains are aligned parallel to crenulation axial surfaces.

Quartzites adjacent to the contacts generally do not contain a penetrative foliation that is visible in outcrop. In thin section, however, they commonly display an anastomosing foliation defined by fine-grained muscovite grains along the boundaries and as symmetrical beards adjacent to detrital quartz grains.

The north- to northeast-striking segment of the southern contact east of Lime Creek (Fig. 3-3b) is unique because Uncompahgre Group rocks younger than $Q_1$ are adjacent to basement (Harris et al. in press). Poor exposure allowed examination of only one outcrop along this segment. At location V (Fig. 3-3b), $S_m$ in retrograded gneisses is vertical to west-dipping and contains a mineral lineation plunging approximately 40° toward, 195°.

Equant and ribbon-shaped quartz aggregates within the phyllites are generally polycrystalline and polygonal with little optically visible, non-recovered crystal-plastic strain, even in the hinges of crenulation folds (Fig. 3-8a). The degree of polygonization is generally greater in rocks along the northern contact than in those from the southern contact, within which deformation bands, subgrains, and core-and-mantle textures (White, 1976) are locally preserved. Blocky quartz grains commonly enclose trails of muscovite or ilmenite that are aligned parallel to $S_m$. Undeformed, randomly oriented porphyroblasts of muscovite, chloritoid, andalusite, and Fe-oxide cross cut all of the deformation fabrics in many phyllite samples (Figs. 3-7d, 3-8a, 3-8b). Mineral assemblages consisting of andalusite + chlorite + muscovite, chloritoid + chlorite + muscovite, andalusite + chloritoid + muscovite, andalusite + muscovite, chloritoid + muscovite, and chlorite + muscovite in addition to quartz and Fe-oxides have been observed in samples either lacking or con-

taining the relict $S_{2B}$ basement fabric. In some specimens from the northern contact, Fe-oxide porphyroblasts up to 2 mm across are bounded by short, recrystallized quartz pressure shadows elongate parallel to $S_m$ (Fig. 3-8c). Although these porphyroblasts are hematite, they have an octahedral crystal form (Fig. 3-8c) and are interpreted as pseudomorphs after magnetite. Locally, andalusite is pseudomorphed by kaolinite (?) and chloritoid is replaced by fine-grained hematite.

**Quartz Petrofabrics**

Universal stage measurements of quartz c-axis fabrics in polycrystalline ribbons that define $S_m$ (samples 183 and 294) and 0.5-2 cm thick quartz lenses (15, 173, 315, 350) within the phyllites are shown in Figure 3-9. Only sample 183, a deformed Uncompahgre Group conglomerate from near location II (Fig. 3-3b), displays a well-developed crossed girdle pattern similar to those found in other plastically deformed quartzites (e.g. Lister, 1977, Tullis, 1977, Law, 1986). The fabric of sample 173 is a partially developed crossed-girdle whereas the remainder of the samples (15, 294, 315, 350) do not yield preferred orientations that are clearly related to $S_m$ and $L_m$ (Fig. 3-9).

**Kinematic Analysis**

Consistent asymmetric sense-of-shear indicators (Simpson and Schmid, 1983) are generally absent from phyllites in the northern contact zone. In phyllites exposed west of the Animas River (Fig. 3-3a), the superposition of $S_m$ onto $S_{2B}$ produced a fabric that can be mistaken for shear bands in outcrop but does not show a consistent sense of asymmetry or the sigmoidal geometry of shear bands when examined in thin

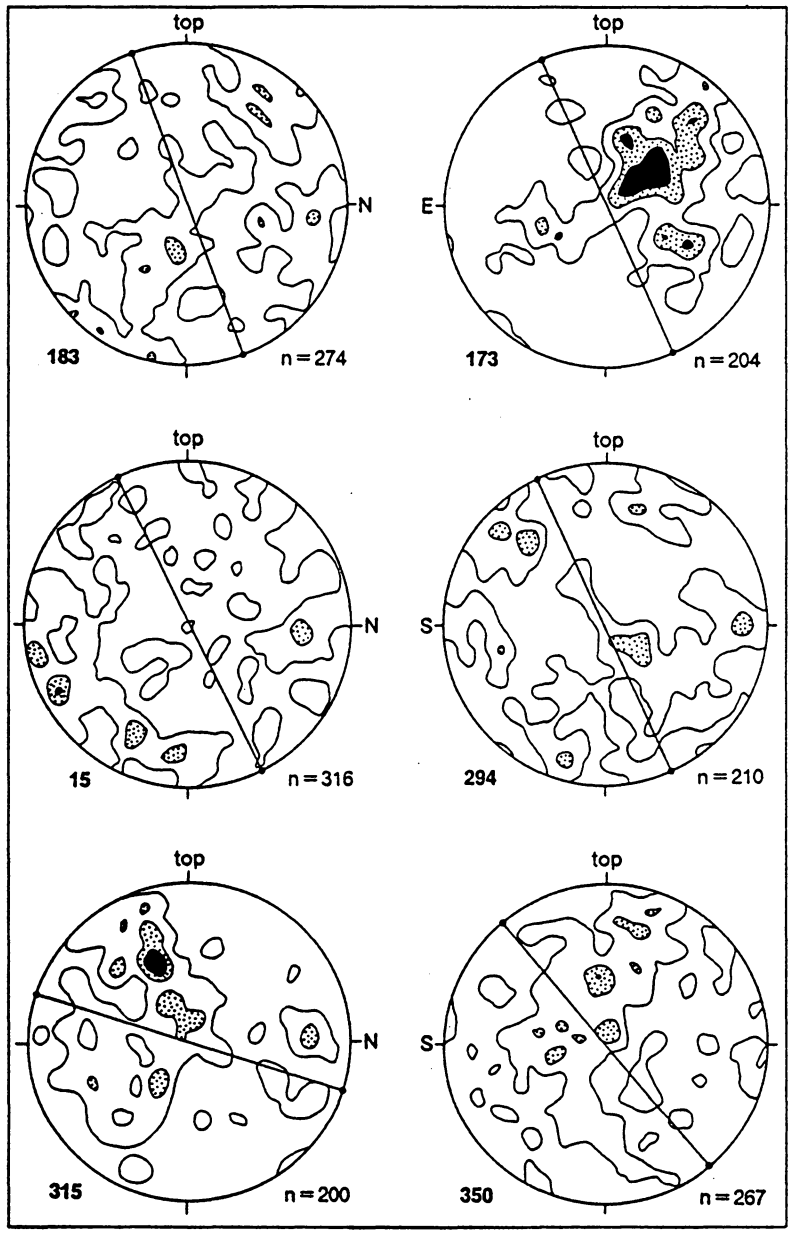


Figure 3-9: Quartz *c* -axis preferred orientations contoured at 1, 3 (stippled), and 5 (black) points per (100/n)% area on lower hemisphere equal area projection; $S_m$ shown as solid line with $L_m$ at edge of projection; sample numbers at lower left of each projection corrspond to those in Figure 3-3; sample localities are given in Appendix D.

section. Mica beards developed adjacent to equant quartz aggregates generally have orthorhombic symmetry in sections cut normal to $S_m$ and parallel to $L_m$ (Fig. 3-6b). However, the sense of foliation deflection into the phyllite zone at locations III and IV (Figs. 3-3a, 3-4b) suggests a south-side-up component of shearing during phyllite formation. This sense of shear is verified by fractured feldspar porphyroclasts in deformed granitoids (Fig. 3-7b) and poorly developed shear bands that locally deform $S_m$ (Fig. 3-8d).

Within 20 m of the northern contact, steeply south-dipping shear zones up to 10 cm thick and slickensided surfaces with down-dip mineral lineations occur within the Uncompahgre Group (Fig. 3-5a). The shear zones contain an internally sigmoidal foliation defined by quartz ribbons and muscovite that merges asymptotically into bedding that defines the shear zone boundaries (Fig. 3-10a). The foliation dips more gently northward than the shear zone margin, indicating south-side-up movement. Steps on discrete slip surfaces that locally transect bedding at a low angle also indicate south-side-up displacement. Both the shear zones and slickensided surfaces display polygonal quartz fabrics and andalusite overgrowing the foliation.

Rocks along the southern contact only display abundant asymmetric kinematic indicators at high elevations around Snowdon Peak where the contact is subhorizontal to gently north dipping (Fig. 3-4a). Shear bands and retort-shaped quartz aggregates, (Fig. 3-10b) having the geometry of σ-type porphyroclasts (Passchier and Simpson, 1986), consistently indicate north-side-up movement within the phyllite zones. This sense of movement is substantiated by the sense of asymmetry of the central segment of the quartz *c*-axis fabric pattern for sample 183 (Fig. 3-9). Along the steeply-dipping, northeast- to east-striking section of the contact, $S_m$ is typically a crenulation of $S_{2B}$ and asymmetric kinematic indicators are largely absent. At location VI (Fig. 3-3b), conjugate shear bands offset $S_{2B}$ although gently north-dipping, south-

Figure 3-10: Kinematic indicators near basement-cover contacts.

a) south-side-up bedding-parallel shear zone in Uncompahgre Group near northern contact along Animas River; black line highlights foliation orientation within zone;

b) north-side-up shear bands and σ-type quartz porphyroclasts in deformed Uncompahgre Group conglomerate along southern contact at location II (Fig. 3-3b); crossed nicols;

c) north-side-up quartz + chlorite shear zones cross-cutting compositional layering in retrograded gneiss along southern contact at location VI (Fig. 3-3b);

d) sinistral shear zone in retrograded gneiss at location V (Fig. 3-3b); plane light.

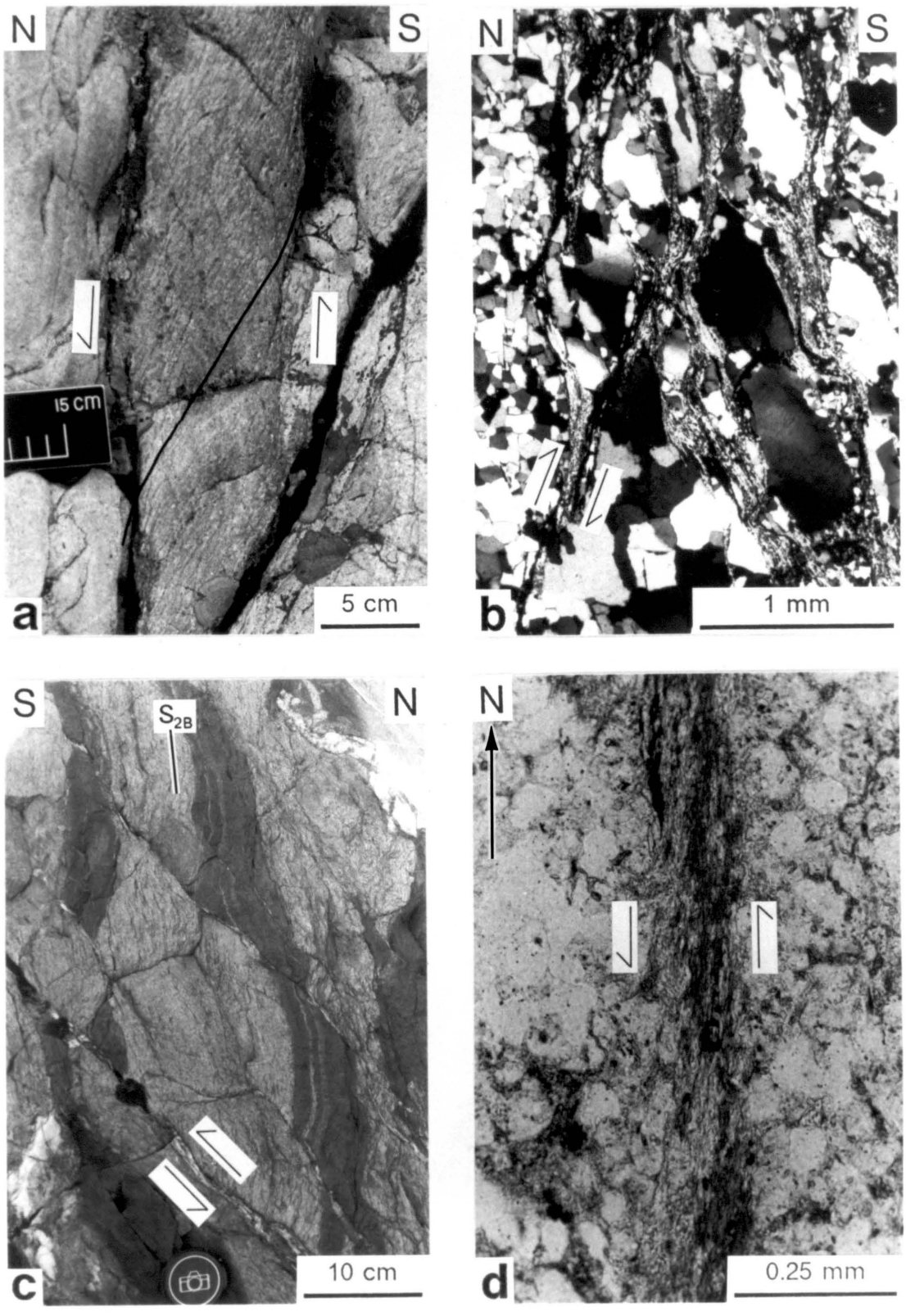
N
S
15 cm
5 cm
a
N
S
1 mm
b
S
N
$S_{2B}$
10 cm
c
N
0.25 mm
d

directed, ≤ 1 cm wide shear zones are most prominent (Fig. 3-10c). Along the north-striking segment of the contact at location V (Fig. 3-3b), ≤ 1 mm thick, muscovite- and chlorite-rich, sinistral shear zones occur within the retrogaded gneisses (Fig. 3-10d).

Numerous shear zones, similar to those near the northern contact but typically lacking andalusite, occur in the Uncompahgre Group within 10 m of the southern contact. The majority of these zones dip northward, subparallel to bedding, and contain moderately northwest-plunging mineral lineations (Fig. 3-5b). Foliation asymmetry and slickenside steps indicate oblique north-side-up and dextral motion. Subvertical, east-striking, south-side-up shear zones are also present but are much less common.

## DISCUSSION

### Deformation History

The preservation of some crystal-plastic strain features in quartz (Fig. 3-10b) and the development of preferred quartz *c*-axis orientations in some samples (183; Fig. 3-9) indicate that dislocation creep was an important deformation mechanism during formation of $S_m$. However, the weakness of the quartz fabrics in most samples (15, 294, 315, 350; Fig. 3-9) implies that much of the strain along the contact zones was accommodated by other deformation mechanisms. Concentrations of Fe-oxides along spaced cleavage domains, scalloped terminations of quartz aggregates adjacent to the cleavage domains, and quartz pressure fringes on Fe-oxide porphyroblasts suggest that solution transfer (Durney, 1972) was important. In addi-

tion, the abundance of phyllosilicates in these rocks may have permitted strain accommodation by grain boundary sliding along micaceous layers (Borradaile, 1981).

The formation of $S_m$ and subsequent folding of this fabric are interpreted to have occurred progressively because the folds 1) are restricted to the contact zones and do not occur in either the adjacent basement or cover rocks, 2) contain an axial planar foliation similar to $S_m$, and 3) are tight to isoclinal where their axial surfaces are subparallel to the margins of the deformation zones and open where they are oriented at higher angles (cf. Platt, 1983). Progressive refolding of foliations within ductile deformation zones requires that material surfaces move from the extension to shortening fields of the infinitesimal strain ellipsoid (Platt, 1983). This can only happen when the finite and infinitesimal strain ellipsoid axes are non-parallel and, thus, when the strain history is non-coaxial (Ramsay, 1967). The presence of shear bands, asymmetric recrystallized porphyroclast tails, and fractured porphyroclasts in the phyllites along some parts of the contacts also indicates a non-coaxial component to the deformation. However, steeply dipping segments of the contacts display predominantly symmetrical kinematic indicators, including mica beards (Fig. 3-6b), conjugate shear bands, and nearly straight quartz pressure fringes (Fig. 3-8c), that suggest either a coaxial strain history or late-stage coaxial overprint.

Kinematic indicators in the contact zones and immediately adjacent rocks record upward movement of the Uncompahgre Group relative to basement in opposite directions on the northern and southern contacts. If it is assumed that deformation along both contacts occurred approximately synchronously, the opposed movement senses imply that the basal part of the Uncompahgre Group is parautochthonous upon basement and has not been tectonically transported a significant distance from its site of deposition. This interpretation is substantiated by observations from location IV (Fig. 3-3a) where the contact between conglomerates of the Uncompahgre

Group and basement rocks is not tectonized (Fig. 3-4b). This contact is interpreted as a portion of an unconformity at the base of the Uncompahgre Group which is preserved intact either as a lens within the phyllite zone or along the margin of the phyllite zone where it deviates from its typical position along the contact surface.

The portion of the southern contact immediately east of Lime Creek (Fig. 3-3b) cannot be interpreted as an unconformity because the basal unit ($Q_1$) of the Uncompahgre Group is absent (Harris et al. in press). Obliquely plunging mineral lineations and sinistral kinematic indicators (Fig. 3-11d) at location V (Fig. 3-3b) suggest that this segment of the contact is a ductile shear zone with oblique sinistral and west-side-down displacement. This interpretation is supported by the left-lateral strike separation of $Q_1$ (Fig. 3-3b) and the occurrence of sinistral kinematic indicators in the basement rocks exposed south of this area (Fig. 3-1b) (Harris et al. in press; Gibson, 1987).

Tectonic fabrics along the basement-cover contacts were superimposed onto fabrics generated during $D_B$ in the basement rocks. They do not overprint older fabrics in the Uncompahgre Group and are, therefore, interpreted to have formed during $D_{BC}$, the only major Proterozoic deformation event to affect the cover rocks.

**Origin of Micaceous Zones**

The localization of ductile deformation along the basement-cover interface implies that this zone was a mechanically weak lithologic horizon. Textural evidence, such as spaced $S_m$ domains transecting fine-grained muscovite aggregates that otherwise display no mineral alignment (Fig. 3-7a), suggests that the basement rocks were largely altered to micaceous mineral assemblages prior to $D_{BC}$. However, syn-

Table 3-1: Modal mineral assemblages of basement rocks and samples from basement-cover contacts; counts of 1000 points per thin section; sample locations given in Appendix D.

| | Sample | Pl | Ksp | Qtz | Hb | Act[2] | Grt | Ep[3] | Bt | Ms | Chl[4] | Ctd | And | Ox |
|---|---|---|---|---|---|---|---|---|---|---|---|---|---|---|
| Basement | 28 | 43.0 | 6.6 | 35.3 | ---- | ---- | ---- | 5.8 | 5.9 | ---- | 3.0 | ---- | ---- | tr |
| | 29 | 32.9 | ---- | tr | 30.9 | 14.8 | ---- | 3.6 | 5.4 | ---- | 10.9 | ---- | ---- | 1.2 |
| | 162 | 47.4[1] | | 33.1 | 3.0 | ---- | tr | ---- | 16.2 | ---- | ---- | ---- | ---- | tr |
| | 180 | 49.0[1] | | 32.4 | ---- | ---- | ---- | ---- | 12.6 | 6.0 | ---- | ---- | ---- | tr |
| | 327 | 48.1[1] | | 35.8 | ---- | ---- | tr | 5.3 | 8.6 | ---- | 1.9 | ---- | ---- | tr |
| Contact Zone | 220A | ---- | ---- | 36.5 | ---- | ---- | ---- | ---- | ---- | 32.9 | 8.0 | 5.5 | ---- | 17.1 |
| | 220B | ---- | ---- | 2.9 | ---- | ---- | ---- | ---- | ---- | 53.5 | ---- | 41.5 | ---- | 2.1 |
| | 316 | ---- | ---- | 55.6 | ---- | ---- | ---- | ---- | ---- | 28.8 | ---- | ---- | 13.7 | 1.9 |
| | 317 | ---- | ---- | 45.0 | ---- | ---- | ---- | ---- | ---- | 38.6 | ---- | 4.6 | 6.5 | 5.3 |
| | 326 | ---- | ---- | 40.1 | ---- | ---- | ---- | ---- | ---- | 44.5 | 11.9 | ---- | ---- | 3.5 |
| | 412 | ---- | ---- | 36.9 | ---- | ---- | ---- | ---- | ---- | 50.2 | ---- | 7.5 | ---- | 5.4 |

[1] undifferentiated feldspar
[2] rims around hornblende
[3] replaces plagioclase
[4] pseudomorphs biotite in basement rocks

to post-kinematic porphyroblast textures (Figs. 3-7d, 3-8a, 3-8b, 3-8c) indicate that the present mineral assemblages are the product of syn- to post-$D_{BC}$, $M_{BC}$ metamorphism.

Rocks of the contact zones have mineral assemblages that include quartz (36-56%) and muscovite (28-50%) with common andalusite (≤14%), chloritoid (≤12%), chlorite (≤12%), and Fe/Ti-oxides (≤18%) (Table 3-1). Quartzo-feldspathic basement gneisses that typically occur adjacent to the contacts are composed predominantly of plagioclase (40-45%), biotite (9-16%), and quartz (32-36%) with variable proportions of potassium feldspar (≤8%), muscovite (≤6%), hornblende (≤4%), and garnet (≤1%) (Table 3-1). When plotted on ACF and AKF diagrams (Eskola, 1915), tie lines among these phases define ranges of bulk composition for the basement and contact zone rocks in terms of the apices of each diagram (Fig. 3-11). Basement rock bulk compositions lie within areas bounded by the compositions of plagioclase, biotite, potassium feldspar, muscovite, hornblende, epidote, and garnet (Fig. 3-11) that combine, in three dimensions, into an irregularly shaped compositional volume. Bulk compositions for the contact zone rocks, however, occur entirely within the AKF plane in an area bounded by the compositions of andalusite, muscovite, chlorite, and chloritoid (Fig. 3-11). The fact that these ranges of possible bulk compositions do not overlap implies that rocks within the contact zones have changed in bulk composition relative to their basement protoliths.

Although a detailed study of the bulk chemical changes accompanying the transition from the basement into the contact zones has not been undertaken, several major element analyses of felsic gneisses, ca. 1690 Ma granitoids, and contact zone rocks are available (Barker, 1969; Appendix C) and allow some tentative conclusions to be drawn. Graphical comparison of data from the contact zones and basement (Fig. 3-12) shows considerable change in the content of various oxides (e.g. $Na_2O$, CaO, $K_2O$, $Al_2O_3$) and implies open-system behavior during alteration. In order to fa-

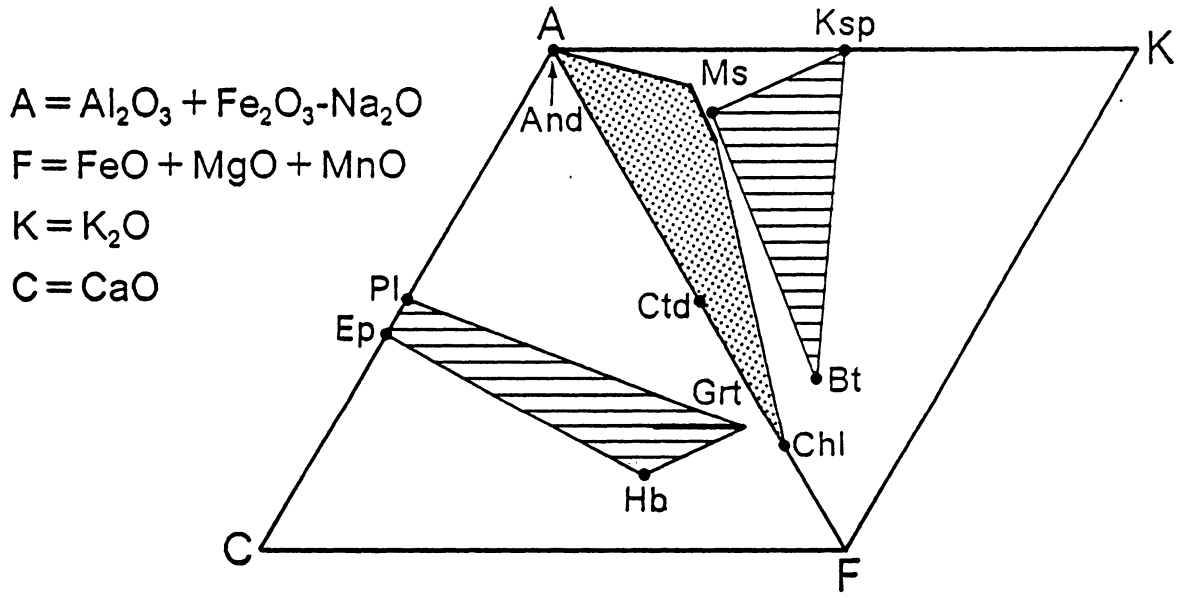


Figure 3-11: ACF and AKF diagrams showing ranges of bulk composition for basement rocks (ruled) and contact zone rocks (stippled).

cilitate discussion of oxide gains and losses, a reference frame must be established for normalizing the data. Because $Al_2O_3$ is generally considered to be relatively immobile in most geologic processes (e.g. Loughnan, 1969; Brimhall, 1979; Sinha et al., 1986), data from the contact zone samples have been normalized to 13.5 wt % $Al_2O_3$, the average value for the basement rocks (Fig. 3-12). The normalized analyses do not total to 100%, implying that volume loss occurred during alteration. Comparison of the normalized data with those from the basement samples indicates that the contact zone rocks are depleted in $SiO_2$, CaO, and $Na_2O$ and enriched in volatile components (Fig. 3-12). Two of the three contact zone samples contain less MgO than the basement rocks, although the third shows enrichment relative to a felsic gneiss collected 30 m away. This MgO-rich analysis corresponds to sample 326 (Table 3-1), which contains more chlorite than is typically present in the contact zone samples. The low MgO values, which are considered more typical of the contact zones because of the general sparcity of chlorite, also imply depletion of MgO relative to the basement. Trends in $K_2O$ and $Fe_2O_3$ cannot be accurately defined because of the wide variation of these oxides in the basement rocks. However, the redistribution of Fe from silicate minerals (e.g. biotite, amphibole) in the basement rocks into magnetite within the contact zones suggests that the rocks were oxidized during the alteration process.

Alteration of the basement rocks must have involved significant fluid influx, both as a means of hydrating pre-existing mineral assemblages and as a mechanism for the removal of $Si^{4+}$, $Ca^{2+}$, $Mg^{2+}$, and $Na^{+}$. Such fluid interaction could have resulted from a variety of processes, including interaction with magmatic fluids (e.g. Meyer and Hemley, 1967; Ferry, 1979), focussed fluid flow within a deformation zone (e.g. Beach 1980; Sinha et al., 1986), or weathering (Loughnan, 1969). A magmatic

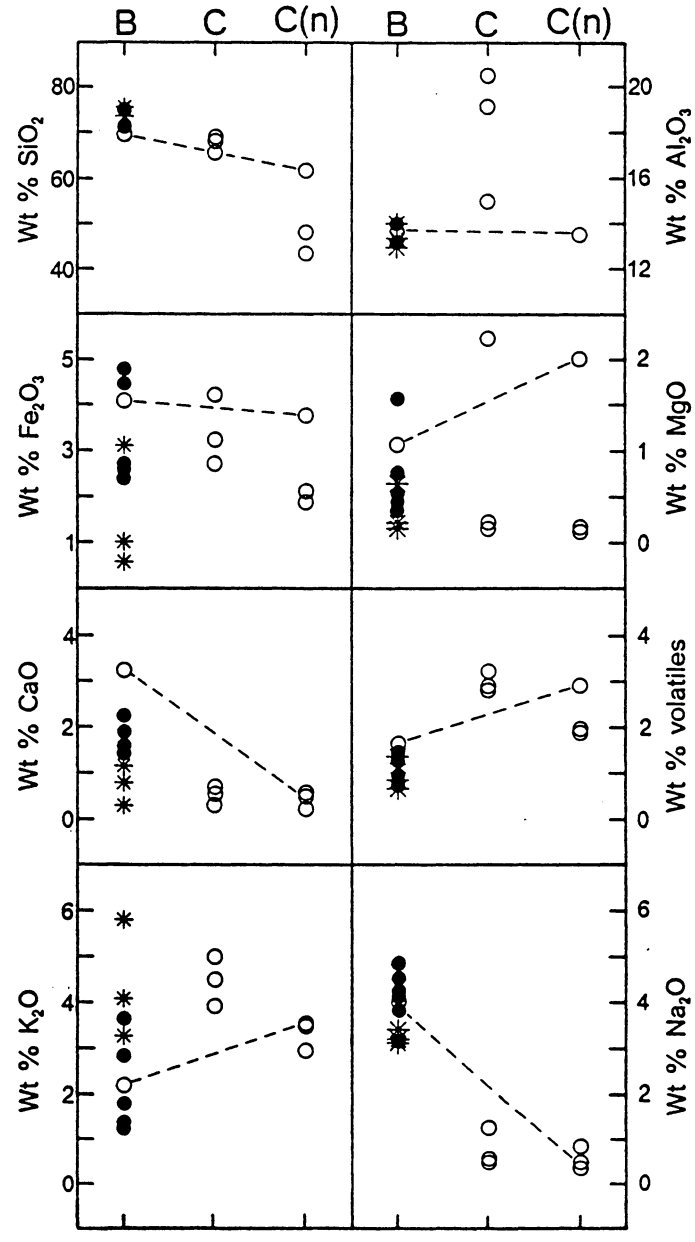


Figure 3-12: Bulk-rock compositions for basement (B), contact zone (C), and contact zone normalized to 13.5 wt % $Al_2O_3$ (C(n)); analyses of gneisses (●) and granitoids (✳) from Barker (1969); other data (o) from Appendix C; dashed lines connect values from two samples collected 30 m apart along southern contact at location VII (Fig. 3-3b).

origin for the fluids seems unlikely because the alteration is not spatially associated with intrusive bodies of either the 1690 or 1430 Ma age group.

Retrogression within shear zones typically occurs either synchronous with or subsequent to deformation and is attributed to interaction with fluids flowing along zones of relatively high permeability (e.g. Etheridge et al., 1983; Rutter and Brodie, 1985). Concurrent alteration of rocks outside the deforming zone may result in nearly complete preservation of relict fabrics (Beach and Tarney, 1978). Well-documented examples of hydrated shear zones (Beach and Tarney, 1978; Etheridge and Cooper, 1981; Sandiford, 1985; Sinha et al., 1986) display mobility of Si, Mg, Fe, Ca, Na, and K. However, specific trends for individual elements vary with the physical conditions, fluid character, protolith composition, and mineral breakdown reactions (cf. Beach and Tarney, 1978; Beach, 1980; Sinha et al., 1986) and are probably not themselves diagnostic of the hydrating shear zone mechanism.

Weathering of silicate rocks involves the breakdown of feldspar, amphibole, and biotite to clay minerals by either the exchange of $H^+$ for bonded cations or the addition of $OH^-$ to the primary minerals (Loughnan, 1969). The behavior of various cations during weathering depends on numerous factors, including the pH, redox potential, and degree of leaching by water. Under leaching conditions, $Ca^{2+}$, $Mg^{2+}$, $Na^+$, and $K^+$ are most readily lost from the system, although $K^+$ may be "fixed" within clay minerals and retained to higher degrees of weathering (Loughnan, 1969). $Si^{4+}$ is lost at a slower rate. In a reducing environment, Fe remains in the highly soluble ferrous state and may be thoroughly leached whereas, under oxidizing conditions, it is stabilized in the insoluble ferric state as oxide or hydroxide compounds (Loughnan, 1969). $Al^{3+}$ and $Ti^{4+}$ are relatively immobile and are, therefore, concentrated within the regolith. Deep weathering of felsic crystalline rocks typically results in a mixture

composed largely of quartz, kaolinite, and ferric iron/titanium compounds (Loughnan, 1969; Ollier, 1969; Pavich, 1986).

Weathering of the basement prior to deposition of the Uncompahgre Group best explains the occurrence of these micaceous zones along an inferred unconformity, the pre-deformational timing of basement alteration, and the enrichment of $Al_2O_3$ relative to numerous other oxides. The loss of $SiO_2$, MgO, CaO, and $Na_2O$, redistribution of part of the Fe into an oxide form, and hydration of basement lithologies are consistent with the processes known to occur in a wet, oxidizing weathering zone. Preserved gneissic and granitic textures in the micaceous zones imply that the regolith was, at least in part, saprolitic. Lenses with relict original textures surrounded by a structureless, micaceous rock (Fig. 3-4b) are interpreted to have originated as corestones in a more highly disaggregated matrix (cf. Ollier, 1969). Irregularities in the contact between the Uncompahgre Group and micaceous zone (Fig. 3-4) are probably the product of differential erosion into the regolith. The thickness of the micaceous zone is similar to those of other ancient regoliths, which range from tens of centimeters (Gay and Grandstaff, 1980) to in excess of 50 m (Ross and Chiaranzelli, 1985). The variable thickness of the micaceous zone may have been either inherited from original thickness variations or resulted from differential tectonic thinning. The fact that the zone is thickest where the contact is subhorizontal is not unexpected because it would have been subjected to flattening perpendicular to layering (i.e. thinning) along steeply dipping segments during north-northwest shortening associated with $D_{BC}$ (Chapter 2).

Modern regoliths from leaching environments are commonly depleted in $K^+$ and, therefore, are predominated by aluminous minerals such as kaolinite or gibbsite (Loughnan, 1969; Pavich, 1986). In contrast, K-bearing micas, not kaolinite or aluminous metamorphic minerals such as pyrophyllite or $Al_2SiO_5$ polymorphs pre-

dominate in many ancient regoliths (Matthews and Scharrer, 1968; Gay and Grandstaff, 1980; Button and Tyler, 1981; Retallick, 1986), including the contact zones in the Needle Mountains. This discrepancy between modern and ancient weathering zones has been attributed to either the incomplete leaching of $K^+$ during weathering (Weaver, 1969; Button and Tyler, 1981) or diagenetic/metamorphic alteration of primary aluminous clay minerals to more potassic compositions (Gay and Grandstaff, 1980). If the contact zone rocks were originally more depleted in $K_2O$, modification of phyllosilicate compositions could have occurred by diagenetic mineral reactions (e.g. Hower et al., 1976) during dewatering of the Uncompahgre Group. Similarly, marked depletion of the contact zones in $SiO_2$ (Fig. 3-12) could have been due to both weathering processes and silica dissolution during $D_{BC}$ deformation.

**Metamorphism**

Minerals present in the contact zone rocks are not those produced during the formation of the regolith but are the product of subsequent $M_{BC}$ metamorphism. Randomly oriented, undeformed porphyroblasts of muscovite, chloritoid, and andalusite indicate that peak $M_{BC}$ metamorphic conditions were attained after the end of $D_{BC}$ deformation. However, the alignment of muscovite within the foliation and the presence of pressure fringes adjacent to magnetite porphyroblasts imply that the earlier stages of $M_{BC}$ temporally overlapped with $D_{BC}$. The generally polygonal texture of quartz aggregates is attributed to post-kinematic recovery and grain boundary migration recrystallization.

An approximate estimate of the pressure-temperature conditions at the peak of $M_{BC}$ may be made on the basis of experimentally determined mineral reaction curves (Fig. 3-13). Pressures are limited to below the aluminosilicate triple point at

approximately 3.5 kbar by the stability of andalusite (Holdaway, 1971) and above 1 kbar by the preserved 3 km thickness of the Uncompahgre Group (Harris and Eriksson, 1987). The presence of andalusite + quartz instead of pyrophyllite implies temperatures above 400-430°C, the position of the pyrophyllite = andalusite + quartz + $H_2O$ reaction curve (Kerrick, 1968). A maximum temperature limit is imposed by the reactions muscovite + chlorite + quartz = cordierite + biotite + andalusite + $H_2O$ and Fe-chloritoid + andalusite = Fe-staurolite + quartz + $H_2O$, both of which occur within the temperature range of 520-545°C at pressures of 2-5 kbar (Richardson, 1968; Hirschberg and Winkler, 1968). The stability field for mineral assemblages in rocks of the contact zones is outlined in Figure 3-13. Replacement of magnetite and chloritoid by hematite, and andalusite by kaolinite are considered the result of later-stage alteration.

## IMPLICATIONS

The recognition of basement-cover contacts in the Needle Mountains as segments of an unconformity with a preserved regolith indicates that the Uncompahgre Group is younger than the 1694 ± 20 Ma granitoids that are truncated along the unconformity surface. This result substantiates the interpretations of Cross et al. (1905), Barker (1969), and Harris et al. (in press) (Fig. 3-2a) but is inconsistent with the model proposed by Tewksbury (1985) that the basement and cover rocks were brought in contact by south-directed thrusting (Fig. 3-2b). Instead, deformation along the basement-cover contacts probably resulted from relative movement of the basement and its parautochthonous cover while they were being folded together during $D_{BC}$. The senses of displacement along the contact zones are consistent with upward and outward movement of the Uncompahgre Group during cuspate infolding into the

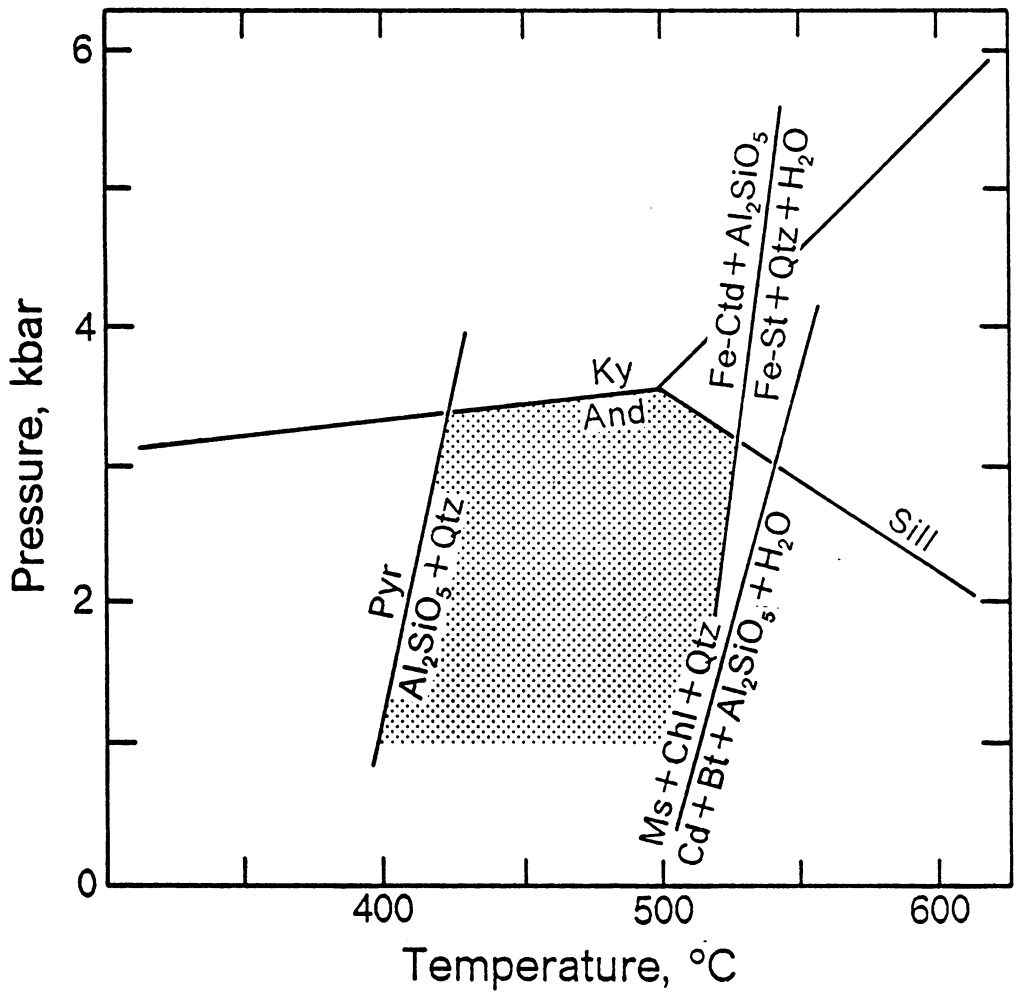


Figure 3-13: Petrogenetic grid of mineral reactions that constrain pressure-temperature conditions of peak $M_{BC}$ metamorphism; inferred conditions stippled; reaction curves from Kerrick (1968), Richardson (1968), Hirschberg and Winkler (1968), and Holdaway (1971).

basement (Harris et al. in press). A close analogy may be made between the deformation along basement-cover contacts in the Needle Mountains and the development of bedding-parallel detachments in mechanically weak stratigraphic horizons during concentric folding (Dahlstrom, 1977).

The results of this study illustrate that detailed examination of contacts between contrasting lithologic suites in deformed terranes is necessary to understand the relationships between adjacent rock units. Deformed regoliths may be preserved as zones of muscovite-rich rock along major lithologic boundaries (see also Barrientos and Selverstone, 1987). The inherent mechanical weakness of these micaceous rocks can localize deformation and lead to complex deformation histories even though the contacts are fundamentally stratigraphic in origin. Therefore, the presence of deformation zones along basement-cover contacts does not necessarily imply that the adjacent lithologies were tectonically juxtaposed. Petrographic and kinematic analysis of these zones may be necessary to distinguish them from major fault boundaries and lead to a clearer understanding of their significance with respect to the stratigraphic and tectonic evolution of a region.

# References


Afifi, A.M., 1981, Stratigraphy, petrology, and structure of Precambrian metavolcanic rocks in the Iris District, Gunnison and Saguache Counties, Colorado: *New Mexico Geological Society Guidebook* 32, 287-292.

American Geological Institute, 1980, *Glossary of Geology (second edition)*: Bates, R. L. and Jackson, J. A. (eds.), American Geological Institute, Falls Church, Va.

Anderson, C.A.; Blacet, P.M.; Silver, L.T.; and Stern, T.W., 1971, Revision of the Precambrian stratigraphy in the Prescott-Jerome area, Yavapai County, Arizona: *U.S. Geological Survey Bulletin* 1324-C, 1-17.

Anderson, J.L., 1983, Proterozoic anorogenic granite plutonism of North America: in Medaris, L.G.; Mickelson, D.M.; Byers, C.W.; and Shanks, W.G. (eds.), *Proterozoic Geology: selected papers from an international Proterozoic symposium*, Geological Society of America Memoir 161, 133-154.

Baars, D.L. and See, P.D., 1968, Pre-Pennsylvanian stratigraphy and paleotectonics of the San Juan Mountains, southwestern Colorado: *Geological Society of America Bulletin* 79, 333-350.

Barker, F., 1969, Precambrian geology of the Needle Mountains, southwestern Colorado: *U.S. Geological Survey Professional Paper* 644-A, 1-33.

Barker, F.; Peterman, Z.E.; and Hildreth, R.A., 1969, A rubidium-strontium study of the Twilight Gneiss, West Needle Mountains, Colorado: *Contributions to Mineralogy and Petrology* 23, 271-282.

Barovich, K.M., 1986, Age constraints on Precambrian deformation in the northern Front Range, Colorado: *Geological Society of America Abstracts with Programs* 18, 340.

Barrietntos, X. & Selverstone, J. 1987. Metamorphosed soils as stratigraphic indicators in deformed terranes: an example from the eastern Alps. *Geology* 15, 841-844.

Beach, A., 1980, Retrogressive metamorphic processes in shear zones with special reference to the Lewisian complex: *Journal of Structural Geology* 2, 257-263.

Beach, A. and Tarney, J., 1978, Major and trace element patterns established during retrogressive metamorphism of granulite facies gneisses, NW Scotland: *Precambrian Research* 7, 325-348.

Bell, T.H., 1981, Foliation development - the contribution, geometry and significance of progressive, bulk, inhomogeneous shortening: *Tectonophysics* 75, 273-296.

Berthe, D.; Choukroune, P.; and Gapais, D., 1979, Orientations preferentielles du quartz et orthogneissification progressive en regime cisaillant: l'exemple du cisaillement sud-armoricain: *Bulletin Mineralogie* 102, 265-272.

Bickford, M.E., 1986, Geochronology of volcanic and plutonic rocks in the Gunnison, Salida, and Wet Mountain areas, central Colorado: in van Schmus, W.R. (ed.), *Proterozoic Geology and Geochemistry*, Field Guide for International Field Conference on Proterozoic Geology and Geochemistry, 17-26.

Bickford, M.E. and Boardman, S.J., 1984, A Proterozoic volcano-plutonic terrane, Gunnison and Salida areas, Colorado: *Journal of Geology* 92, 657-666.

Bickford, M.E.; Van Schmus, W.R.; and Zietz, I., 1986, Proterozoic history of the midcontinent region of North America: *Geology* 14, 492-496.

Bickford, M.E.; Wetherill, G.W.; Barker, F.; and Chin-Nan Lee-Hu, 1969, Precambrian Rb-Sr chronology in the Needle Mountains, southwestern Colorado: *Journal of Geophysical Research* 74, 1660-1676.

Bidwell, M.E. and Bauer, R.L., 1987, Ductile shearing and coeval folding during dextral transpression, central Vermillion District, NE Minnesota: *Geological Society of America Abstracts with Programs* 19, 588.

Borradaile, G.J., 1981, Particulate flow of rock and the formation of cleavage: *Tectonophysics* 72, 305-321.

Bowring, S.A.; Reed, J.C. Jr.; and Condie, K.C., 1984, U-Pb geochronology of Proterozoic volcanic and plutonic rocks, Sangre de Cristo Mtns., N.M.: *Geological Society of America Abstracts with Programs* 16, 216.

Braddock, W.A. and Cole, J.C., 1979, Precambrian structural relations, metamorphic grade, and intrusive rocks along the northeastern flank of the Front Range in the Thompson Canyon, Poudre Park and Virginia Dale areas: in Etheridge, F.G. (ed.), *Field Guide Northern Front Range and Northwest Denver Basin, Colorado*, Geological Society of America Rocky Mountain Section Guidebook, Colorado State University, 105-121.

Brimhall, G. H. Jr.,1979. Lithologic determination of mass transfer mechanisms of multiple-stage porphyry copper mineralization at Butte, Montana: vein formation by hypogene leaching and enrichment of potassium-silicate protore. *Econ. Geol.* 74, 556-589.

Bryant, B. and Reed, J.C. Jr., 1969, Significance of lineation and minor folds near major thrust faults in the southern Appalachians and the British and Norwegian Caledonides: *Geological Magazine* 106, 412-429.

Button, A. and Tyler, N., 1981, The character and economic significance of Precambrian paleoweathering and erosion surfaces in southern Africa: *Economic Geology, 75th Anniversary Volume*, 686-709.

Byrne, T., 1984, Early deformation in melange terranes of the Ghost Rocks Formation, Kodiak Islands, Alaska: in Raymond, L.A. (ed.), *Melanges: their nature, origin, and significance*, Geological Society of America Special Paper 198, 21-25.

Choukroune, P. and Gapais, D., 1983, Strain pattern in the Aar Granite (Central Alps): orthogneiss developed by bulk inhomogeneous strain: *Journal of Structural Geology* 5, 411-418.

Clifford, P.; Fleuty, M.J.; Ramsay, J.G.; Sutton, J.; and Watson, J., 1957, The development of lineation in complex fold systems: *Geological Magazine* 94, 1-24.

Cobbold, P.R. and Quinquis, H., 1980, Development of sheath folds in shear regimes: *Journal of Structural Geology* 2, 119-126.

Cobbold, P.R. and Watkinson, A.J., 1981, Bending anisotropy: a mechanical constraint on the orientation of fold axes in an anisotropic medium: *Tectonophysics* 72, T1-T10.

Cobbold, P.R.; Cosgrove, J.W.; and Summers, J.M., 1971, Development of internal structures in deformed anistropic rocks: *Tectonophysics* 12, 23-53.

Condie, K.C., 1982, Plate-tectonics model for Proterozoic continental accretion in the southwestern U.S.: *Geology 10*, 37-42.

Condie, K.C. and Shadel, C.A., 1984, An early Proterozoic volcanic arc succession in southeastern Wyoming: *Canadian Journal of Earth Sciences* 21, 415-427.

Condie, K.C. and Knoper, M.W., 1986, Geology and origin of early Proterozoic rocks from the Gunnison area, central Colorado, in van Schmus, W.R., ed., *Proterozoic Geology and Geochemistry*, Guidebook for International Field Conference on Proterozoic Geology and Geochemistry, 3-16.

Coney, P.J., 1980, Cordilleran metamorphic core complexes; an overview: in Crittenden, M.D.; Coney, P.J.; and Davis, G. H. (eds.), *Cordilleran Metamorphic Core Complexes*, Geological Society of America Memoir 153, 7-31

Coward, M.P., 1973, The structure and origin of areas of anomalously low-intensity finite deformation in the basement gneiss complex of the Outer Hebrides: *Tectonophysics* 16, 117-140.

Coward, M.P.; James, P.R.; and Wright, L., 1976, Northern margin of the Limpopo mobile belt, southern Africa: *Geological Society of America Bulletin* 87, 601-611.

Cross, W.; Howe, E.; and Ransome, F.L., 1905, Description of the Silverton Quadrangle, Colorado: *U.S. Geological Survey Atlas*, Folio 120.

Cullers, R.L. and Wobus, R.A., 1986, Proterozoic framework of the southern Front Range and Wet Mountains, Colorado: in van Schmus, W.R. (ed.), *Proterozoic Geology and Geochemistry*, Guidebook for International Field Conference on Proterozoic Geology and Geochemistry, 55-68.

Dahlstrom, C.D.A., 1969, Balanced cross sections: *Canadian Journal of Earth Sciences* 6, 743-757.

Dahlstrom, C.D.A., 1977, Structural geology in the eastern margin of the Canadian Rocky Mountains: *Wyoming Geological Association Annual Field Conference Guidebook* 29, 407-439.

DePaor, D., 1986, Orthographic analysis of geologic structures - II. practical applications: *Journal of Structural Geology* 8, 87-100.

DePaor, D., in press, $R_f/\phi_f$ strain analysis using an orientation net: Journal of Structural Geology.

Dieterich, J.H., 1970, Computer experiments on mechanics of finite amplitude folds: *Canadian Journal of Earth Sciences* 7, 467-476.

Duebendorfer, E.M. and Houston, R.S., 1987, Proterozoic accretionary tectonics at the southern margin of the Archean Wyoming craton: *Geological Society of America Bulletin* 98, 554-568.

Dunnett, D., 1969, A technique of finite strain analysis using elliptical particles: *Tectonophysics* 7, 117-136.

Durney, D.W., 1972, Solution-transfer, an important geological deformation mechanism: *Nature* 235, 315-317.

Durney, D.W. and Ramsay, J.G., 1973, Incremental strains measured by syntectonic crystal growths: in DeJong, K.A. and Scholten, R. (eds.), *Gravity and Tectonics*, John Wiley and Sons, New York, 67-96.

Eskola, P., 1915, On the relations between the chemical and mineralogical composition in the metamorphic rocks of the Orijarvi region: *Bull. Comm. geol. Finlande* 44.

Etheridge, M. A. & Cooper, J. A., 1981. Rb-Sr isotopic and geochemical evolution of a recrystallized shear (mylonite) zone at Broken Hill. *Contributions to Mineralogy and Petrology* 78, 74-84.

Etheridge, M. A., Wall, V. J. & Vernon, R. H., 1983. The role of the fluid phase during regional metamorphism and deformation. *Journal of Metamorphic Geology* 1, 205-226.

Ferry, J. M., 1985. Hydrothermal alteration of Tertiary igneous rocks from the Isle of Skye, northwest Scotland II. granites. *Contributions to Mineralogy and Petrology* 91, 283-304.

Gay, A.L. and Grandstaff, D.E., 1980, Chemistry and mineralogy of Precambrian paleosols at Elliot Lake, Ontario, Canada: *Precambrian Research* 12, 349-373.

Gee, D.G., 1980, Basement-cover relationships in the central Scandinavian Caledonides: *Geologiska Foreningens Stockholm Forhandlingar* 102, 455-474.

Gibson, R.G., 1984, Lithologic controls on tectonic breccia generation, Appalachain foreland thrust belt, SW Virginia: *Geological Society of America Abstracts with Programs* 16, 518.

Gibson, R.G. and Simpson, C., 1986, Kinematic analysis and implications of Proterozoic strike-slip shear zones, West Needle Mtns., Colorado: *Geological Society of America Abstracts with Programs* 18, 613.

Grambling, J.A. and Codding, D.B., 1982, Stratigraphic and structural relationships of multiply deformed Precambrian metamorphic rocks in the Rio Mora area, New Mexico: *Geological Society of America Bulletin* 93, 127-137.

Grambling, J.A. and Ward, D.B., 1987, Thrusting of the Pecos greenstone belt over younger supracrustal rocks, Rio Mora area, New Mexico: *Geological Society of America Abstracts with Programs* 19, 278.

Gratier, J.-P. and Vialon, P., 1980, Deformation patterns in a heterogeneous material: Folded and cleaved sedimentary cover immediately overlying a crystalline basement (Oisans, French Alps): *Tectonophysics* 65, 151-180.

Grocott, J., 1984, Geometry of superimposed colinear deformations in the Ikerasak area, Umanik district, west Greenland: *Precambrian Research* 26, 235-263.

Hansen, W.R. and Peterman, Z.E., 1968, Basement-rock geochronology of the Black Canyon of the Gunnison, Colorado: *U.S. Geological Survey Professional Paper* 600-C, 80-90.

Harris, C.W., 1987, *Sedimentological and structural analysis of the Proterozoic Uncompahgre Group*: unpublished Ph.D. dissertation, Virginia Polytechnic Institute and State University, Blacksburg, VA.

Harris, C.W. and Eriksson, K.A., 1987, Tide-, storm-, and wave-influenced shelf sedimentation in a tectonically active intracratonic basin: the Proterozoic Uncompahgre Group, southwest Colorado: *Geological Society of America Abstracts with Programs* 19, 281.

Harris, C.W.; Gibson, R.G.; Simpson, C.; and Eriksson, K.A., 1986, Early to Middle Proterozoic polyphase deformation, West Needle Mtns., SW. Colorado: preliminary results: *Geological Society of America Abstracts with Programs* 18, 360.

Harris, L.D. and Milici, R.C., 1977, Characteristics of thin-skinned style of deformation in the southern Appalachians, and potential hydrocarbon traps: *U.S. Geological Survey Professional Paper* 1018, 40 p.

Hills, F.A. and Houston, R.S., 1979, Early Proterozoic tectonics of the central Rocky Mountains, North America: *Contributions to Geology* 17, 89-109.

Hoffman, P.F.; Tirrul, R.; Grotzinger, J.P.; Lucas, S.B.; and Eriksson, K.A., 1984, The externides of Wopmay orogen, Takijuk Lake and Kikerk Lake map areas, District of Mackenzie, in *Current research, Part A: Geological Survey of Canada, Paper* 84-1A, 383-395

Holdaway, M.J., 1971, Stability of andalusite and the aluminium silicate phase diagram: *American Journal of Science* 271, 97-131.

Hower, J.; Eslinger, E. V.; Hower, M. E.; and Perry, E. A., 1976, Mechanism of burial metamorphism of argillaceous sediment: 1. mineralogical and chemical evidence: *Geological Society of America Bulletin* 87, 725-737.

Hsu, K.J., 1974, Melanges and olistostromes: in Dott, R.H. Jr. and Shaver, R.H. (eds.), *Modern and Ancient Geosynclinal Sedimentation*, Society of Economic Paleontologists and Mineralogists Special Publication 19, 321-333.

Hutchinson, R.M., 1981, Structure and petrology of the Cochetopa pluton and its metamorphic wallrocks, Saguache County, Colorado: *New Mexico Geological Society Guidebook* 32, 297-304.

Jacob, R.E.; Snowdon, P.A.; and Bunting, F.J.L., 1983, Geology and structural development of the Tumas basement dome and its cover rocks: *Geological Society of South Africa Special Publication* 11, 157-172.

Karlstrom, K.E. and Houston, R.S., 1984, The Cheyenne belt: analysis of a Proterozoic suture in southern Wyoming: *Precambrian Research* 25, 415-446.

Karlstrom, K.E. and Conway, C.M., 1986, Deformational styles and contrasting lithostratigraphic sequences within an early Proterozoic orogenic belt, central Arizona: in Nations, J.D.; Conway, C.M.; and Swann, G.A. (eds.), *Geology of central and northern Arizona*, Geological Society of America Rocky Mountain Section Guidebook, Northern Arizona Creative Printers, Flagstaff, AZ, 1-25.

Kerrick, D.M., 1968, Experiments on the upper stability limit of pyrophyllite at 1.8 kilobars and 3.9 kilobars water pressure: *American Journal of Science* 266, 204-214.

King, J.E., 1986, The metamorphic internal zone of Wopmay orogen (Early Proterozoic), Canada: 30 km of structural relief in a composite section based on plunge projection: *Tectonics* 5, 973-994.

Lambert, M.B. and van Staal, C.R., 1987, Archean granite-greenstone boundary relationships in the Beaulieu River volcanic belt, Slave Province, N. W. T. in *Current Research, Part A, Geological Survey of Canada Paper* 87-1A, 605-618.

Law, R.D., 1986, Relationships between strain and quartz crystallographic fabrics in the Roche Maurice quartzites of Plougastel, western Brittany: *Journal of Structural Geology* 8, 493-516.

Law, R.D.; Knipe, R.J.; and Dayan, H., 1984, Strain path partitioning in thrust sheets: microstructural and petrofabric evidence from the Moine Thrust zone at Loch Eriboll, northwest Scotland: *Journal of Structural Geology* 6, 477-498.

Lisle, R.J., 1985, *Geological Strain Analysis*: Pergamon Press, Oxford.

Lister, G.S., 1977, Crossed-girdle c-axis fabrics in quartzites plastically deformed by plane strain and progressive simple shear: *Tectonophysics* 39, 51-54.

Lister, G.S. and Hobbs, B.E., 1980, The simulation of fabric development during plastic deformation and its application to quartzite: the influence of deformation history: *Journal of Structural Geology* 2, 355-370.

Lister, G.S. and Price, G.P., 1978, Fabric development in a quartz-feldspar mylonite: *Tectonophysics* 49, 37-78.

Lister, G.S. and Snoke, A.W., 1984, S-C Mylonites: *Journal of Structural Geology* 6, 617-638.

Lister, G.S. and Williams, P.F., 1979, Fabric development in shear zones: theoretical controls and observed phenomena: *Journal of Structural Geology* 1, 283-297.

Lister, G.S. and Williams, P.F., 1983, The partitioning of deformation in flowing rock masses: *Tectonophysics* 92, 1-33.

Loughnan, F.C., 1969, *Chemical Weathering of the Silicate Minerals*: American Elsevier Publishing Co., New York.

Mackenzie, J.S.; Needham, D.T.; and Agar, S.M., 1987, Progressive deformation in an accretionary complex: an example from the Shimanto belt of eastern Kyushu, southwest Japan: *Geology* 15, 353-356.

Matthews, P.E. and Sharrer, R.H., 1968, A graded unconformity at the base of the Early Precambrian Pongola system: *Transactions of the Geological Association of South Africa* 71, 257-273.

Meyer, C. and Hemley, J.J., 1967, Wall Rock Alteration: in Barnes, H.L. (ed.), *Geochemistry of Hydrothermal Ore Deposits*, Holt, Rinehart and Winston, Inc., New York., 166-235.

Nelson, B.K. and DePaolo, D.J., 1985, Rapid production of continental crust 1.7 to 1.9 b. y. ago: Nd isotopic evidence fron the basement of the North American mid-continent: *Geological Society of America Bulletin* 96, 746-754.

Ollier, C., 1984, *Weathering (second edition)*: Longman, London.

Passchier, C.W. and Simpson, C., 1986, Porphyroclast systems as kinematic indicators: *Journal of Structural Geology* 8, 831-843.

Pavich, M. J. 1986. Processes and rates of saprolite production and erosion on a foliated granitic rock of the Virginia Piedmont. in Colman, S.M. and Dethier, D.P. (eds.), *Rates of Chemical Weathering of Rocks and Minerals*, Academic Press, Orlando, 552-590.

Peterman, Z.E.; Hedge, C.E.; and Braddock, W.A., 1968, Age of Precambrian events in the northeastern Front Range, Colorado: *Journal of Geophysical Research* 73, 2277-2296.

Platt, J.P., 1980, Archean greenstone belts: A structural test of tectonic hypotheses: *Tectonophysics* 65, 127-150.

Platt, J.P., 1983, Progressive refolding in ductile shear zones: *Journal of Structural Geology* 5, 619-622.

Platt, J.P. and Behrmann, J.H., 1986, Structure and fabrics in a crustal-scale shear zone, Betic Cordillera, southeast Spain: *Journal of Structural Geology* 8, 15-33.

Powell, C. McA., 1979, A morphological classification of rock cleavage: *Tectonophysics* 58, 21-34.

Premo, W.R., 1984, U-Pb zircon geochronology of early Proterozoic plutonism in N. Colorado and SE Wyoming: *Geological Society of America Abstracts with Programs* 16, 251.

Price, R.A. and Mountjoy, E.M., 1970, Geologic structure of the Canadian Rocky Mountains between Bow and Athabasca rivers - A progress report: *Geological Association of Canada Special Paper* 6, 7-26.

Puls, D.D. and Karlstrom, K.E., 1985, Proterozoic foreland thrusting in the Mazatzal Mountains of central Arizona: *Geological Society of America Abstracts with Programs* 17, 261.

Ramsay, J.G., 1967, *Folding and Fracturing of Rocks*: McGraw-Hill Book Co., New York.

Ramsay, J.G., 1980, Shear zone geometry: a review: *Journal of Structural Geology* 2, 83-99.

Ramsay, J.G. and Graham, R.H., 1970, Strain variation in shear belts: *Canadian Journal of Earth Sciences* 7, 786-813.

Ramsay, J.G. and Wood, D.S., 1973, The geometric effects of volume change during deformation processes: *Tectonophysics* 16, 263-277.

Reed, J.C. Jr., 1984, Proterozoic rocks of the Taos Range, Sangre de Cristo Mountains, New Mexico: *New Mexico Geological Society Guidebook* 35, 179-185

Reed, J.C. Jr.; Bickford, M.E.; Premo, W.R.; Aleinikoff, J.N.; and Pallister, J.S., 1987, Evolution of the Early Proterozoic Colorado Province: constraints from U-Pb geochronology: *Geology* 15, 861-865.

Retallick, G. J. 1986. The fossil record of soils. in Wright, V. P. (ed.), *Paleosols, their Recognition and Significance*, Princeton University Press, Princeton, 1-57.

Richardson, S.W., 1968, Staurolite stability in a part of the system Fe-Al-Si-O-H: *Journal of Petrology* 9, 467-488.

Robertson, J.M. and Moench, R.H., 1979, The Pecos greenstone belt: a Proterozoic volcano-sedimentary sequence in the southern Sangre de Cristo Mountains, New Mexico: *New Mexico Geological Society Guidebook* 30, 165-173.

Robin, P-Y.F., 1977, Determination of geologic strain using randomly oriented strain markers: *Tectonophysics* 42, T7-T16.

Robinson, P.; Spear, F.S.; Schumacher, J.C.; Laird, J.; Klein C.; Evans, B.W.; and Doolan, B.L., 1982, Phase relations of metamorphic amphiboles: natural occurrence and theory: in Veblan, D.R. and Ribbe, P.H. (eds.), *Amphiboles: Petrology and Experimental Phase Relations*, Reviews in Mineralogy 9B, Mineralogical Society of America, 1-227.

Ross, G.M. and Chiarenzelli, J.R., 1985, Paleoclimatic significance of widespread Proterozoic silcretes in the Bear and Churchill Provinces of the northwestern Canadian Shield: *Journal of Sedimentary Petrology* 55, 196-204.

Rutter, E.H. and Brodie, K.H., 1985, The permeation of water into hydrating shear zones: in Thompson, A.B. and Rubie, D. C. (eds.), *Metamorphic reactions, kinetics, textures and deformation*, Springer-Verlag, New York, 242-250.

Sanderson, D.J., 1974, Patterns of boudinage and apparent stretching lineation developed in folded rocks: *Journal of Geology* 82, 651-661.

Sanderson, D.J., 1982, Models of strain variation in nappes and thrust sheets: *Tectonophysics* 88, 201-233.

Sandiford, M., 1985, The origin of retrograde shear zones in the Napier Complex: implications for the tectonic evolution of Enderby Land, Antarctica: *Journal of Structural Geology* 7, 477-488.

Schmid, S.M. and Casey, M., 1986, Complete texture analysis of commonly observed quartz c-axis patterns: *The Patterson Volume, American Geophysical Union Monograph* 36, 263-286.

Schultz, A.P., 1983, *Broken-formations of the Pulaski thrust sheet near Pulaski, Virginia*: unpublished Ph.D. dissertation, Virginia Polytechnic Institute and State University, Blacksburg, Va.

Silver, L.T. and Barker, F., 1968, Geochronology of Precambrian rocks of the Needle Mountains, southwestern Colorado: part I, U-Pb zircon results: *Geological Society of America Special Paper* 115, 204-205.

Simpson, C., 1982, The structure of the northern lobe of the Maggia Nappe, Ticino, Switzerland: *Eclogae Geologicae Helvetiae* 75, 495-516.

Simpson, C., 1985, Deformation of granitic rocks across the brittle-ductile transition: *Journal of Structural Geology* 7, 503-511.

Simpson, C. and Schmid, S.M., 1983, An evaluation of criteria to deduce the sense of movement in sheared rocks: *Geological Society of America Bulletin* 94, 1281-1288.

Sinha, A.K.; Hewitt, D.A.; and Rimstidt, J.D., 1986, Fluid interaction and element mobility in the development of ultramylonites: *Geology* 14, 883-886.

Skjernaa, L., 1980, Rotation and deformation of randomly oriented planar and linear structures in progressive simple shear: *Journal of Structural Geology* 2, 101-109.

Soegaard, K. and Eriksson, K.A., 1986, Transition from arc volcanism to stable-shelf and subsequent convergent-margin sedimentation in northern New Mexico from 1.76 Ga: Journal of Geology 94, 47-66.

Spoelhof, R.W., 1976, Pennsylvanian stratigraphy and paleotectonics of the western San Juan Mountains, southwestern Colorado. in Epis, R. C. and Weimer, R. J. (eds.), *Studies in Colorado Field Geology*, Colorado School of Mines Professional Contribution 8, 159-179.

Stacey, J.S. and Hedlund, D.C., 1983, Lead-isotopic compositions of diverse igneous rocks and ore deposits from southwestern New Mexico and their implications for early Proterozoic crustal evolution in the Western United States: *Geological Society of America Bulletin* 94, 43-57.

Stainforth, J.G., 1978, A simple theory for the dispersion of real and apparent finite-strain lineations: *Tectonophysics* 48, 107-132.

Stallard, R.F., 1986, Weathering and erosion in the humid tropics, in Lerman, A.; Meybeck, M.; and Drever, J. I. (eds.), *Physical and chemical weathering in geochemical cycles*: D. Reidel, Netherlands, 1-30.

Starkey, J. and Cutforth, C., 1978, A demonstration of the interdependence of the degree of quartz preferred orientation and the quartz content of deformed rocks: *Canadian Journal of Earth Sciences* 15, 841-847.

Steiger, R.H. and Jager, E., 1977, Subcommision on geochronology: convention on the use of decay constants in geo- and cosmochronology: *Earth and Planetary Science Letters* 36, 359-362.

Taylor, R.B., 1975, Geologic map of the Black Hawk Quadrangle, Gilpin, Jefferson, and Clear Creek Counties, Colorado: *U.S. Geological Survey Map* GQ-1248.

Tewksbury, B.J., 1981, *Polyphase deformation and contact relationships of the Precambrian Uncompahgre Formation, Needle Mountains, Southwestern Colorado*: unpublished Ph.D. dissertation, University of Colorado, Boulder, CO.

Tewksbury, B.J., 1985, Revised interpretation of the age of allochthonous rocks of the Uncompahgre Formation, Needle Mountains, Colorado: *Geological Society of America Bulletin* 96, 224-232.

Tirrul, R., 1983, Structure cross-sections across Asiak foreland thrust and fold belt, Wopmay orogen, District of Mackenzie: in *Current research, Part B: Geological Survey of Canada Paper* 83-1B, 253-260.

Tricart, P. and Lemoine, M., 1986, From faulted blocks to megamullions and megaboudins: Tethyan heritage in the structure of the western Alps: *Tectonics* 5, 95-118.

Tullis, J., 1977, Preferred orientation of quartz produced by slip during plane strain: *Tectonophysics* 39, 87-102.

Tweto, O., 1979, *Geologic Map of Colorado*: U.S. Geological Survey, scale 1:500,000.

Tweto, O., 1980, Precambrian Geology of Colorado, in Kent, H.C. and Porter, K.W. (eds.), *Colorado Geology*, Rocky Mountain Association of Geologists, 37-46.

Voll, G., 1976, Recrystallization of quartz, biotite, and feldspars from Erstfeld to the Leventina Nappe, Swiss Alps, and its geological significance: *Schweizerische Mineralogische und Petrographische Mitteilungen* 56, 641-647.

Watkinson, A.J., 1975, Multilayer folds initiated in bulk plane strain, with the axis of no change perpendicular to the layering: *Tectonophysics* 28, T7-T11.

Watterson, J., 1978, Proterozoic intraplate deformation in the light of south-east Asian tectonics: *Nature* 273, 636-639.

Weaver, C. E. 1969. Potassium, illite and the ocean. *Geochimica and Cosmochimica Acta* 31, 2181-2196.

White, S.H., 1976, The effects of strain on the microstructure, fabrics and deformation mechanisms in quartz: *Philosophical Transactions of the Royal Society of London* A283, 69-86.

Williams, M.L.; Grambling, J.A.; and Bowring, S.A., 1986, Redefinition of the Vadito Group, an extensive felsic volcanic-sedimentary sequence in the Proterozoic of N.M.: *Geological Society of America Abstracts with Programs* 18, 422.

Wilson, C.J.L., 1975, Preferred orientation in quartz ribbon mylonites: *Geological Society of America Bulletin* 86, 968-974.

Wobus, R.A., 1984, An overview of the Precambrian geology of the Tusas Range, north-central New Mexico: *New Mexico Geological Society Guidebook* 35, 193-198.

Wobus, R.A. and Hedge, C.E., 1982, Redefinition of the Precambrian Tusas Mountain and Tres Piedras Granites, north-central New Mexico: *Mountain Geologist* 19, 105-114.

# Appendix A. Broken Formation Zones

The term *broken formation* has been defined as "a body of pervasively sheared strata which lacks exotic elements" (Hsu, 1974). Broken formations typically originate by the fragmentation of little-metamorphosed sedimentary sequences and are characterized by the contrasting mechanical behavior of constituent lithologies and alternate shortening and extension parallel to bedding during deformation (Hsu, 1974). Layered gneisses exposed in part of the northwestern Needle Mountains display locally intense tectonic disruption and are considered to comprise broken formation zones although they differ in several aspects from those previously documented in the literature (Hsu, 1974; Harris and Milici, 1977; Schultz, 1986). The features, origin, and possible controls on the development of these broken formation zones are discussed in this section.

The general geology of the northwestern Needle Mountains has been described in detail in Chapters 1 and 2 and is not reiterated here. The broken formation zone occurs in layered gneisses (unit 1, Table 2-1) exposed west of Lime Creek in the southern basement domain (Fig. A-1). Unit 1 in this area consists of a variety of lithologies that are interlayered on the scale of centimeters to meters. Rock types include 1) leucocratic pl + qtz + bt ± grt gneiss commonly containing garnets up to 1 cm in diameter, 2) pl + qtz + bt ± ksp ± grt gneiss with ellipsoidal quartz "eyes" up to 1.5 cm across, 3) hb + pl ± act ± grt gneiss, and 4) coarse-grained pl + bt + qtz ± ged ± cum ± grt granofels. Lithologies 1, 2, and 3 contain a prominent foliation ($S_1$) defined by

aligned biotite or amphibole grains. The granofels varies from massive to finely banded (mm-cm scale) but typically lacks an obvious mineral alignment. This lithology is unique to this part of the northwestern Needle Mountains.

## DESCRIPTION OF BROKEN FORMATION ZONES

The layered gneisses outcrop on the limbs of a macroscopic $F_2$ synform (Fig. A-1). Poles to $S_1$ in rocks of unit 2 (Table 2-1) occupying the core of this structure define a southwest-plunging $\beta$ axis that coincides with the measured axes of mesoscopic, parasitic folds (Figs. A-2a, b). A network of small faults, one of which offsets Paleozoic cover rocks, modifies the southern limb of the synform (Fig. A-1). Chloritic alteration associated with narrow slip surfaces is intense within the layered gneisses in the vicinity of these fault zones, especially in exposures along and near U.S. Route 550.

The broken formation zone occurs in unit 1, predominantly on the southeast limb of the synform (Fig. A-1), and is broadly concordant to layering in the adjacent intact layered gneisses. Its distribution generally coincides with that of the granofels lithology. Compositional layering within the broken formation zone is discontinuous on the mesoscopic scale and lithologic units cannot generally be traced between adjacent outcrops. Two textural varieties, the *fold-and-boudin* and *block-in-matrix* types, are recognized within the disrupted zones. Both types are cross-cut by granitic pegmatite dikes up to 5 m wide.

The fold-and-boudin variety of broken formation occurs in broad zones ($\leq$100 m wide) that are transitional into the intact layered gneisses. Felsic gneiss and amphibolite layers commonly have a pinch-and-swell morphology

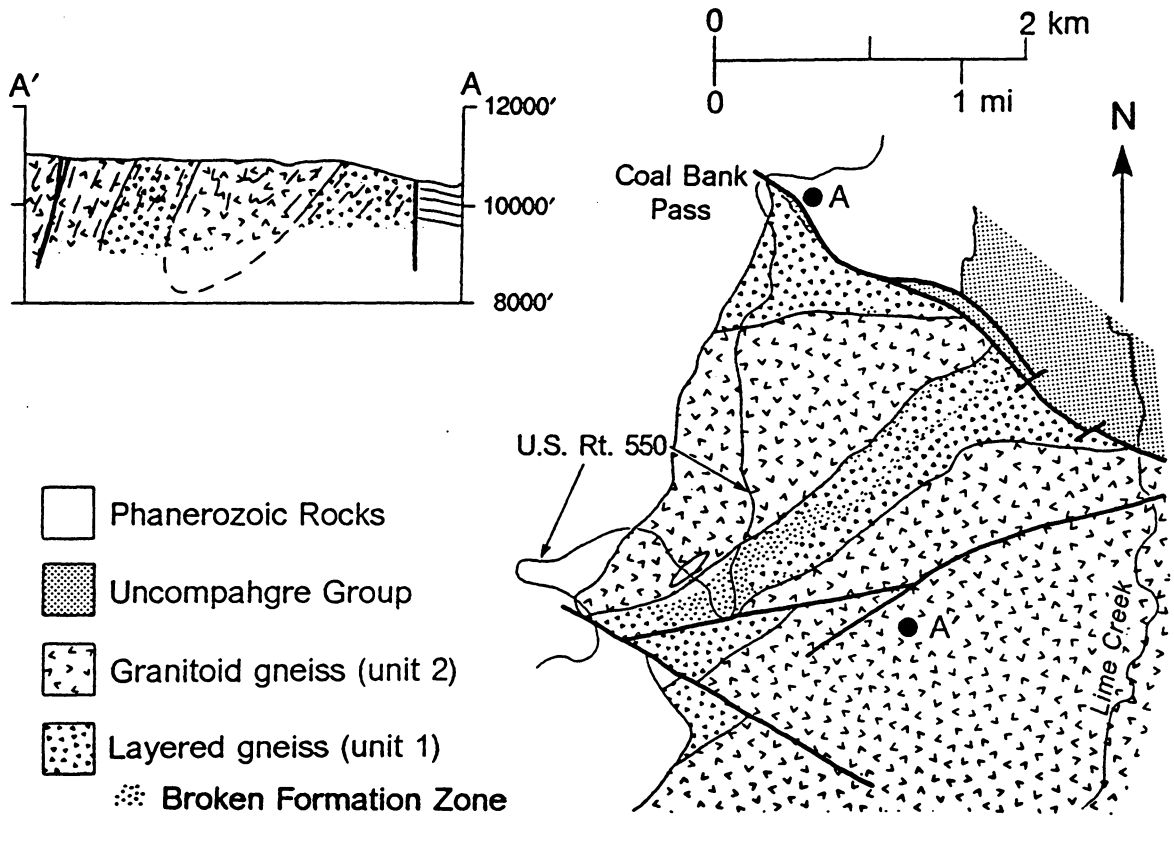


Figure A-1: Map and cross-section of western part of southern basement domain showing distribution of map units and broken formation zone.

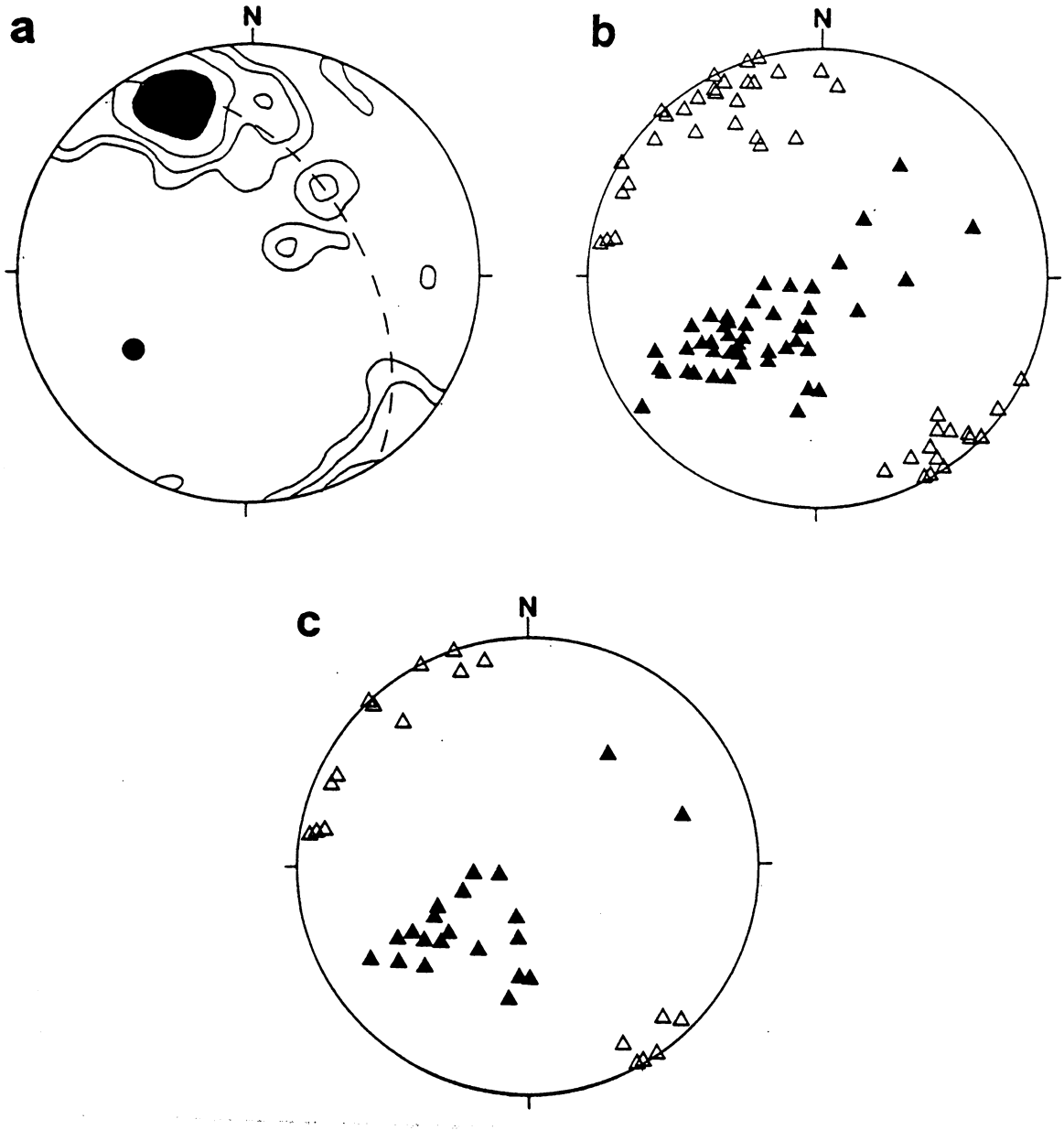


Figure A-2: Orientation data for rocks associated with broken formation: a) poles to $S_1$ in rocks of unit 2; b) $F_2$ fold axes (▲) and axial surfaces (△) in unit 2; c) $F_2$ fold axes (▲) and axial surfaces (△) in broken formation zone.

Figure A-3: Field relationships in fold-and-boudin zones.

a-b) dismembered layered gneisses folded by $F_2$ folds; three pieces of leucocratic gneiss are interpreted as boudinaged pieces of an originally continuous layer;

c-d) pinch-and-swell structure and folded boudins;

e) abrupt termination of leucocratic gneiss boudin surrounded by massive to weakly foliated granofels.

Symbols in (b), (d), and (e) are A = amphibolite, LG = leucocratic gneiss, FG = felsic gneiss, G = granofels, black = vein quartz, solid lines = lithologic contacts, dashed lines = foliation/compositional layering.

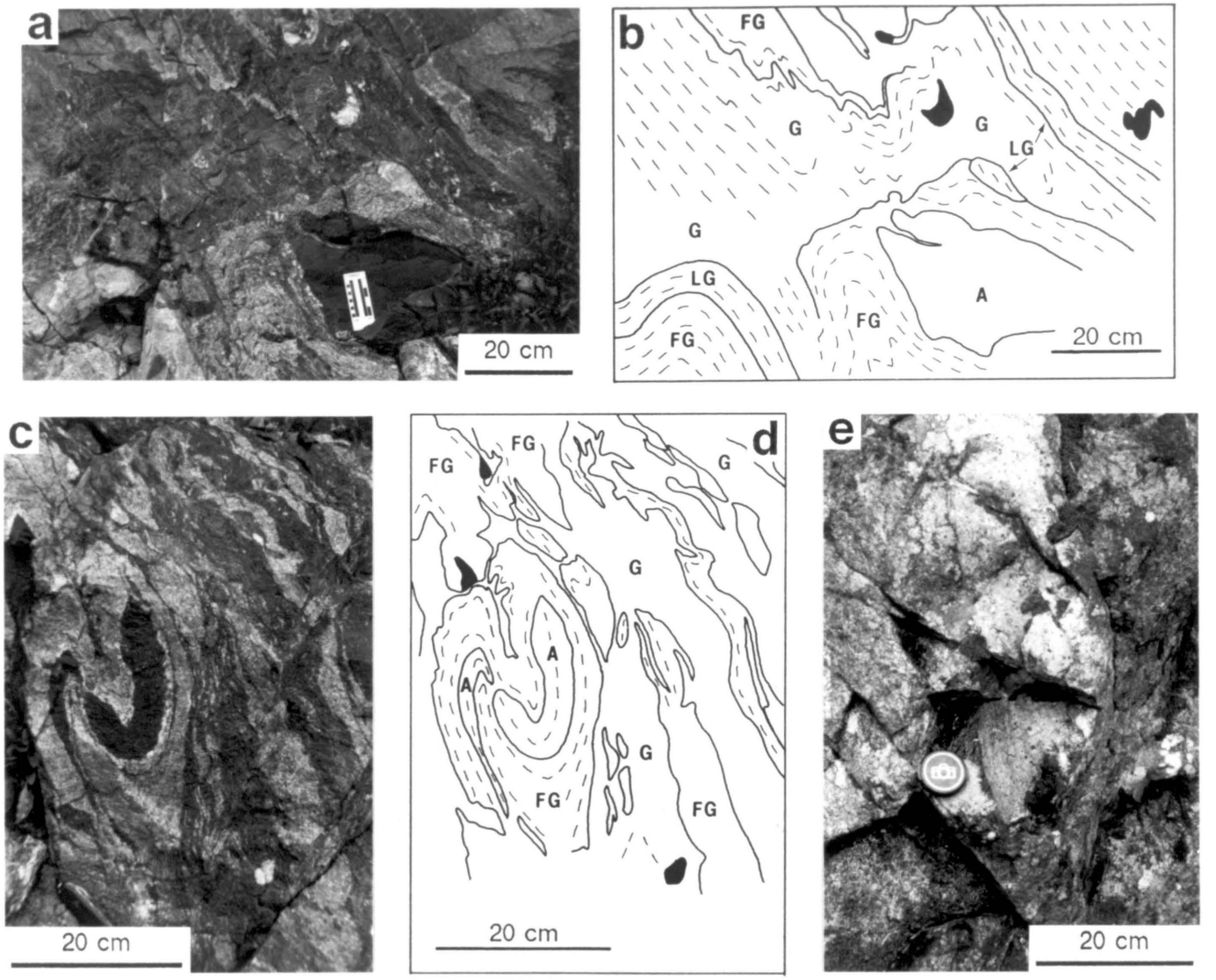
a
20 cm
b
FG
G
G
LG
G
LG
FG
A
FG
20 cm
c
20 cm
d
FG
FG
G
G
A
A
G
FG
FG
20 cm
e
20 cm

or consist of isolated, elongate fragments interpreted as boudins (Fig. A-3a-d). The boudins are elongate parallel to their internal $S_1$ foliation and commonly have abrupt terminations that cross-cut $S_1$ at angles greater than 60° (Fig. A-3e). Individual boudins, trains of boudins, and layers with pinch-and-swell morphology are folded by close to isoclinal folds (Fig. A-3a-d) with steeply dipping axial surfaces and southwest-plunging axes that define a partial girdle distribution on an equal-area projection (Fig. A-2c). Because their orientations are similar to that of folds in unit 2 (Fig. A-2b), these mesoscopic folds are interpreted as $F_2$. Locally, the $F_2$ folds are themselves isolated within boudins separated by necks filled with coarse-grained amphibole (Fig. A-4a-b).

The block-in-matrix variety of broken formation consists of felsic gneiss and amphibolite clasts in a massive to banded granofels matrix (Fig. A-4c-e). The gneiss fragments are elongate parallel to their internal $S_1$ foliation and foliation orientations vary between adjacent clasts (Fig. A-4c). Clasts are typically less than 50 cm long but locally range up to several meters in length. Folds that deform $S_1$ commonly occur isolated within individual fragments (Fig. A-4d). Clast lithologies match those in the intact layered gneisses and no exotic fragments have been identified. Lenticular fragments of white vein quartz are also abundant within these zones. Contacts between the block-in-matrix zones and intact gneisses are rarely exposed although, at one locality, the margin of a block-in-matrix zone cross-cuts compositional layering and $S_1$ in the layered gneisses (Fig. A-4e). More typically, block-in-matrix zones seem to be gradational into the fold-and-boudin type zones.

Gneissic clasts within the broken formation zone display microfabrics similar to other basement gneisses in the northwestern Needle Mountains (see Chapter 2). Quartz and feldspar aggregates are polygonal, biotite grains define decussate textures, and crystal-plastic strain features are generally absent from these minerals.

Figure A-4: Field relationships in block-in-matrix zones.

a-b) $F_2$ folds isolated within boudins separated by amphibole-rich boudin necks (dots); other symbols as in Fig. A-3;

c) felsic gneiss and vein quartz clasts in a weakly banded granofels matrix;

d) $F_2$ fold within amphibolite clast in granofels;

e) discordant contact (arrow) between block-in-matrix zone and intact layered gneisses.

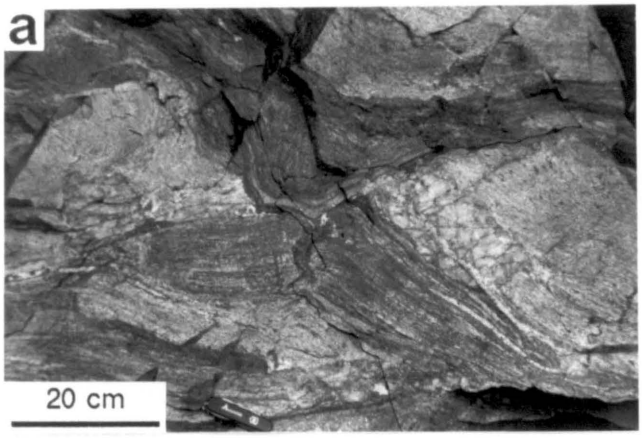
a
20 cm

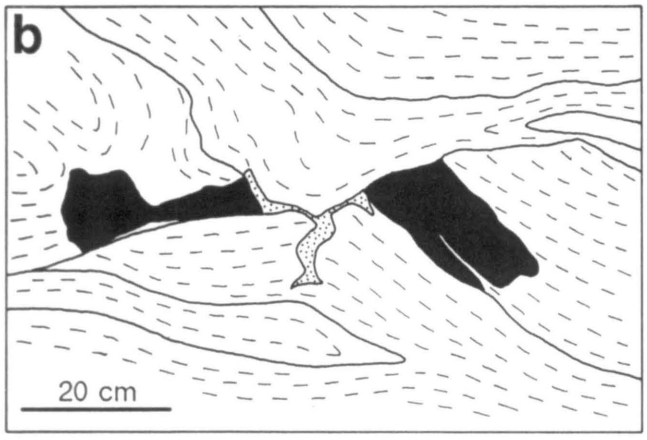
b
20 cm

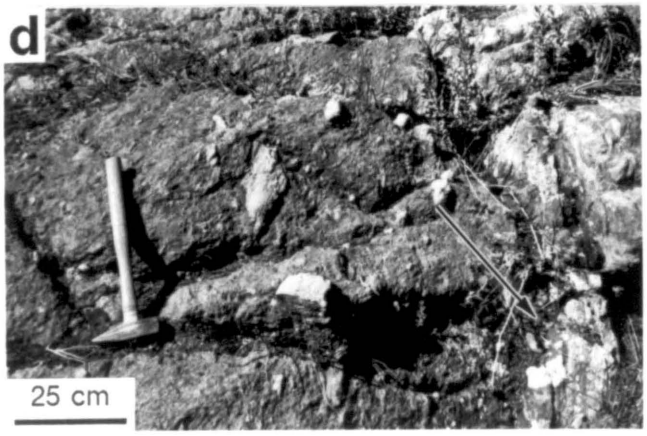
d
25 cm

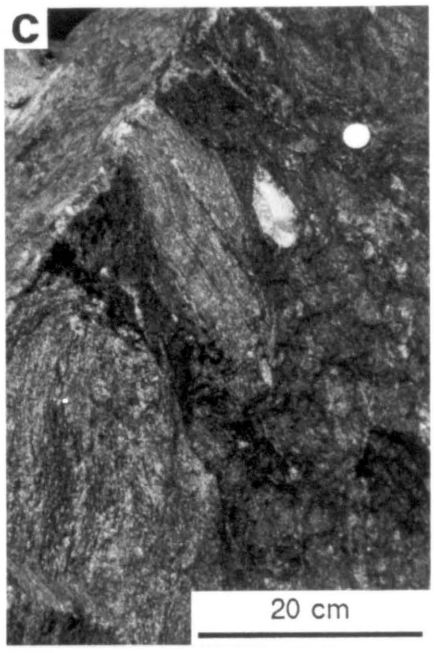
c
20 cm

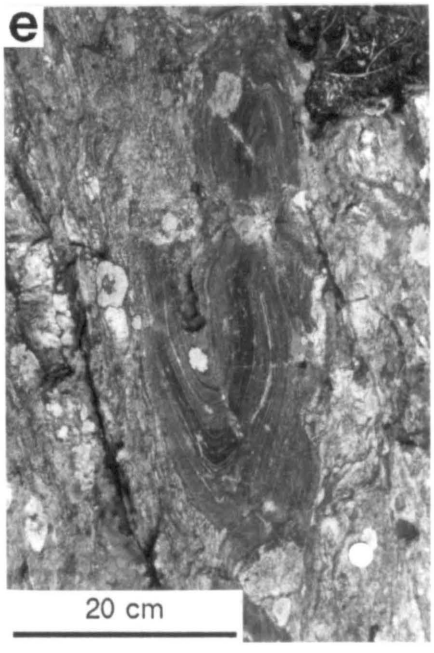
e
20 cm

Garnet porphyroblasts in felsic gneisses commonly display curved to spiral trails of quartz inclusions that are continuous with $S_1$ in the surrounding rock (Fig. A-5a). Quartz inclusions are generally finer-grained than quartz grains in the rock matrix. Pressure shadows elongate parallel to $S_1$ occur adjacent to the garnet porphyroblasts in the felsic gneisses. In rare instances, straight to gently curved inclusion trails in a garnet core become crenulated outward toward the grain margin whereas the foliation ($S_2$) in the rock matrix is parallel to the crenulation axial surfaces (Fig. A-5b). The garnets are variably altered to mats of randomly oriented biotite (Fig. A-5a).

The granofels is composed of zoned plagioclase and interstitial quartz intergrown with biotite and one or more varieties of amphibole (gedrite, cummingtonite, hornblende). Gedrite and cummingtonite are the most abundant amphiboles and commonly coexist as clusters of radiating crystals in apparent textural equilibrium (Fig. A-5c). Neither biotite nor amphibole display any tendency toward a preferred dimensional alignment although discontinuous planar quartz ribbons are present in a few samples. Garnets occur either as poikilitic porphyroblasts up to 20 mm in diameter or non-poikiloblastic, euhedral grains up to 1 mm in diameter (Fig. A-5d). Despite the general absence of a foliation in the matrix of the granofels, the large porphyroblasts contain an internal foliation defined by curved trails of quartz inclusions (Fig. A-5e), similar to those found in garnets from the felsic gneisses. Locally, the porphyroblasts are partly surrounded by inclusion-poor garnet rims (Fig. A-5e).

Metamorphic textures in the samples from the broken formation zones are interpreted to indicate that 1) garnets porphyroblasts grew during the development of $S_1$ (rotated garnets with pressure shadows), 2) porphyroblast growth locally continued during $F_2$ folding (crenulations within garnets), and 3) growth of biotite, amphibole, and garnet outlasted deformation (random orientation of grains, garnet rims and euhedral matrix grains, biotite replacing garnet).

Figure A-5: Microfabrics in broken formation zone.

a) curved inclusion trail in garnet continuous with $S_1$ in leucocratic gneiss, note biotite-poor pressure shadow and alteration of garnet to biotite (Bt);

b) crenulated $S_1$ defined by quartz inclusions in garnet in felsic gneiss; note $S_2$ in matrix parallel to crenulation axial surface.

c) coexisting cummingtonite (Cum), gedrite (Ged - partially altered to chlorite), and biotite;

d) euhedral garnets and weak biotite foliation (vertical) in granofels;

e) garnet with internal foliation and inclusion-poor rim surrounded by non-aligned biotite and gedrite (altered to chlorite).

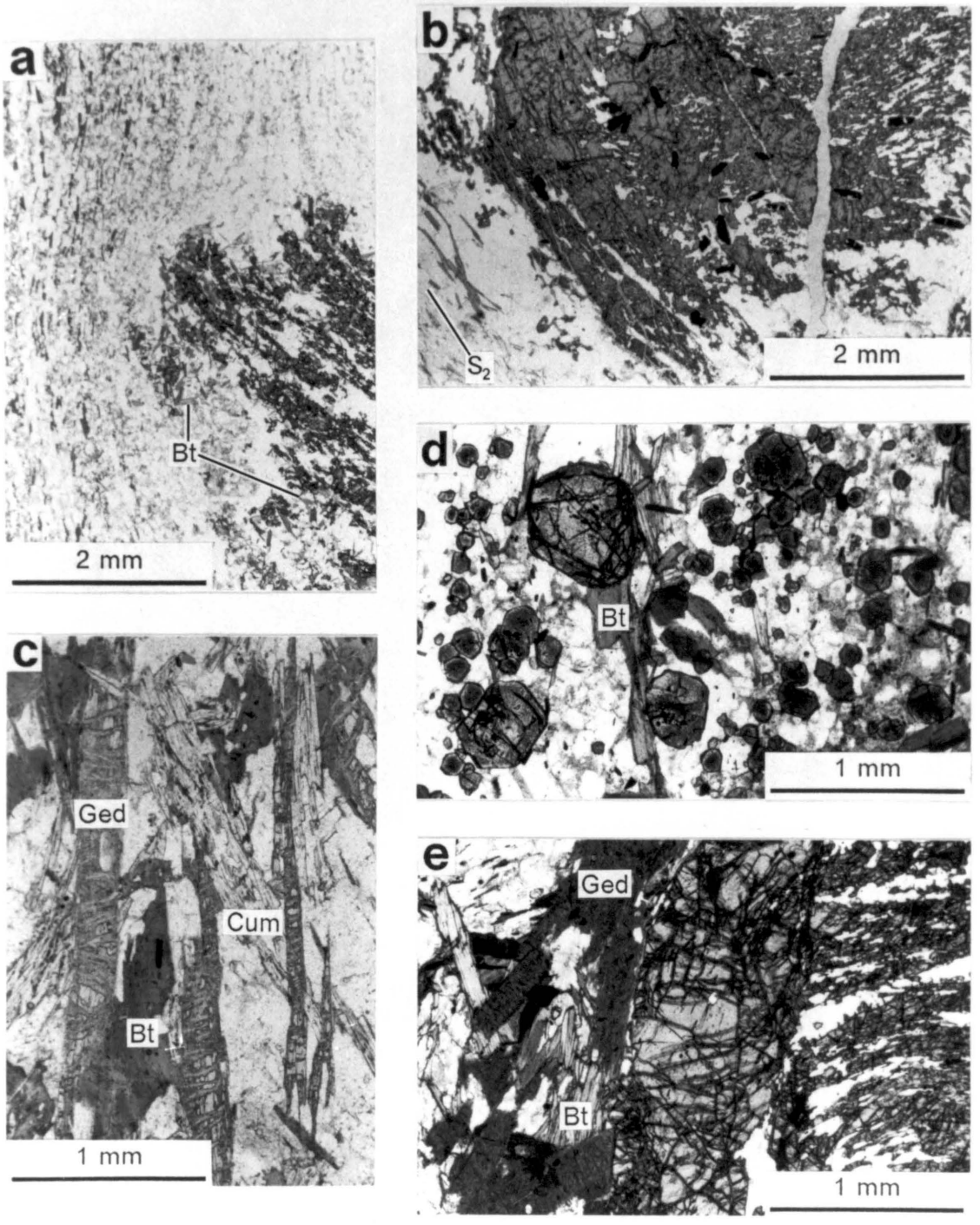
a
Bt
2 mm
b
$S_2$
2 mm
c
Ged
Cum
Bt
1 mm
d
Bt
1 mm
e
Ged
Bt
1 mm

## MECHANICAL MODEL

Because a completely exposed transition from intact layered gneisses through the fold-and-boudin type into the block-in-matrix type of broken formation has not been observed, the sequence of events involved in broken formation zone evolution must be reconstructed from isolated mesoscopic features. The proposed model is illustrated in Figure A-6. Tabular gneiss fragments are interpreted to have originated during $S_1$ development as boudins (Fig. A-6) within a highly ductile (granofels) matrix. Abrupt terminations between leucocratic gneiss boudins and the granofels indicate locally high competency contrasts whereas less dramatic contrasts are implied by pinch-and-swell structures in more biotite-rich felsic layers.

$F_2$ folding of boudins during formation of the macroscopic synform lead to development of the fold-and-boudin type zones (Fig. A-6) whereas rigid body rotation of the boudins within a flowing granofels matrix produced the block-in-matrix type zones (Fig. A-6). Minor boudinage may have accompanied these latter phases of deformation. $F_2$ folding and flowage of the granofels are illustrated as successive phases in Figure A-6 because folded gneiss fragments are common in the block-in-matrix zones. However, these processes may have overlapped in time and competed with one another such that folding predominated in domains where lithologic contrasts between the gneiss layers and granofels were not pronounced whereas rigid body rotation of boudins was the predominant process in zones of higher interlayer rheology contrast. The process(es) by which the granofels "flowed" cannot be clearly established because post-kinematic mineral growth has obliterated microtextural evidence of the deformation mechanisms. Although any macroscopically ductile process (eg. crystal-plastic flow, cataclastic flow) could achieve the necessary movement of material, the random fabric of the block-in-matrix zones and locally discordant

Figure A-6: Model for broken formation development. Dashes indicate $S_1$ in competent layers and gray areas represent granofels.

$S_1$ development and boudinage

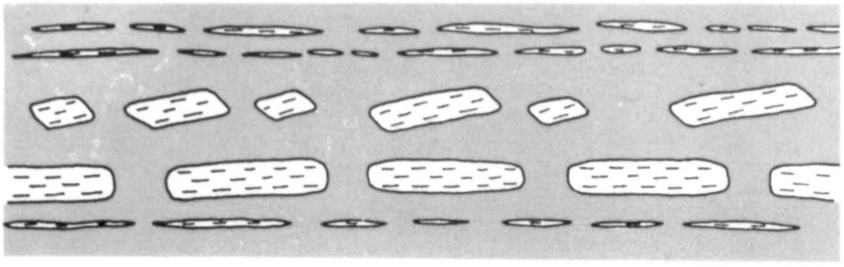

$F_2$ folding

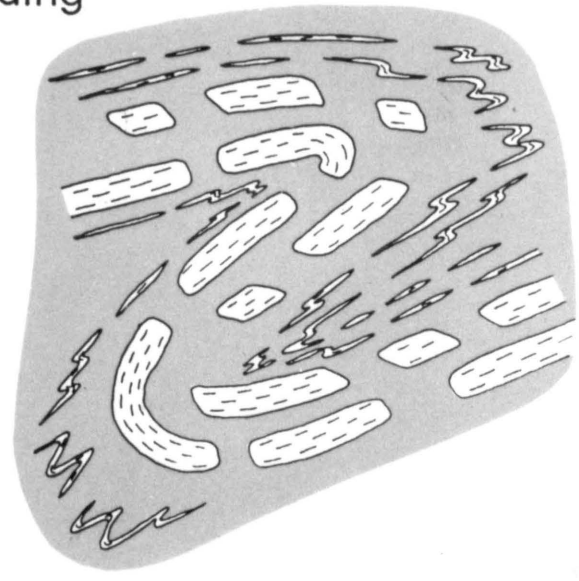

Flowage of "granofels" matrix

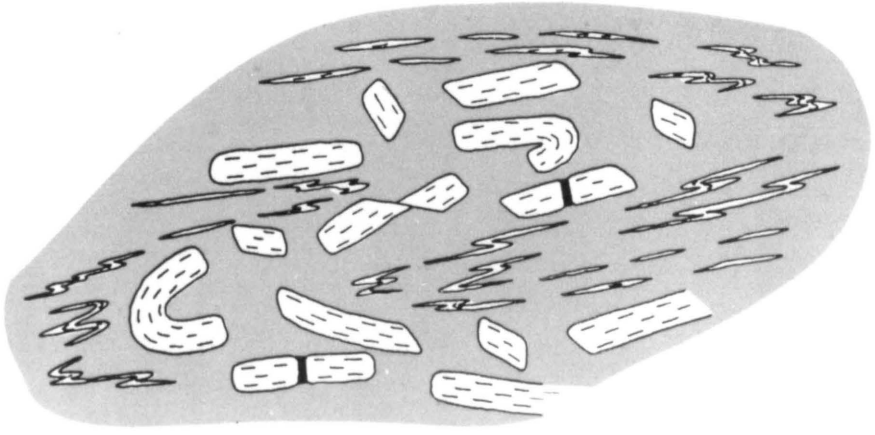

contact relationships with intact layered gneisses suggest that cataclastic flow may have been important.

The stages of broken formation zone development illustrated in Figure A-6 are interpreted as a progressive deformation sequence because 1) garnet textures indicate that both $S_1$ and $F_2$ developed during a single phase of porphyroblast growth and 2) the fold-and-boudin and block-in-matrix type zones appear entirely gradational with one another in the field. Granitic pegmatites that cross-cut the broken formation zones have been tentatively correlated with the 1690 Ma granitoids exposed farther east (chapter 2) and, thus, indicate that the broken formation zones developed during $D_B$ deformation.

Folding of previously extended layers during progressive deformation requires that layers originally within the extensional field of the finite strain ellipsoid enter the shortening field during a subsequent strain increment (Ramsay, 1967). Such a situation cannot occur during a coaxial strain history (Fig. A-7) and necessitates a non-coaxial strain path. Although folding of extensional structures is theoretically not possible in ideal simple shear (Fig. A-7), progressive refolding of foliations is common in shear zones (cf. Platt, 1983). In some cases, these folds have been interpreted to have nucleated on heterogeneities that caused perturbations in the laminar flow pattern of such zones (e.g. Lister and Williams, 1983). In the case of the broken formation zone described here, the earlier-formed boudins would represent inhomogeneities and could have induced folding in this way. Alternatively, non-coaxial deformation within the broken formation zone could have deviated significantly from simple shear (Fig. A-7), thereby allowing early-developed extensional features to undergo subsequent shortening. Shear sense criteria indicative of the sense of vorticity during non-coaxial deformation have not been recognized in the broken formation zone.

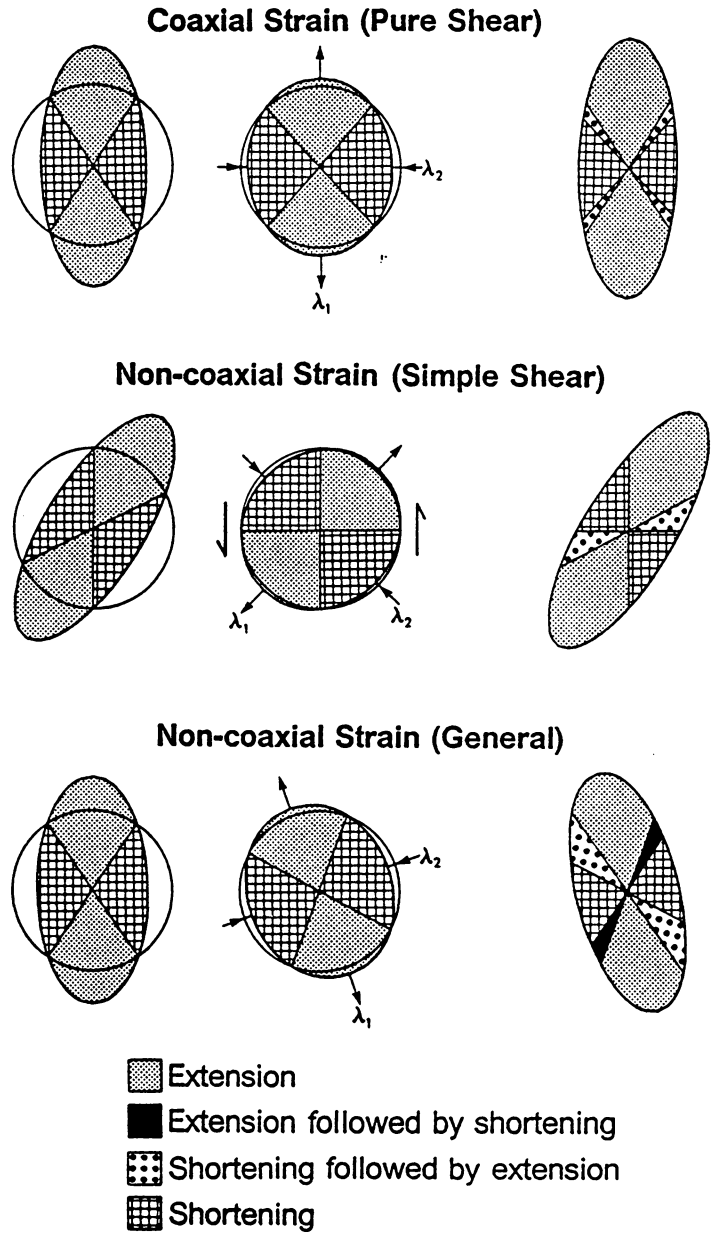


Figure A-7: Progressive deformation by a variety of strain paths. Ellipsoids on right showing shortening and extension fields constructed using the method of Ramsay (1967) by adding the strain increment represented by the middle column to the earlier strain states shown on the left.

The spatial correspondence between the broken formation zone and the distribution of the granofels suggests that the development of the broken formation zone was lithologically controlled. Field relationships indicate that the granofels was mechanically weak during deformation and its presence is, therefore, thought to have permitted the observed style of deformation. Because no primary features are preserved within the granofels, its protolith is uncertain. However, mafic and felsic gneisses with which it is interlayered are probably of volcanogenic origin (Chapter 2). The presence of Ca-poor amphiboles (gedrite and cummingtonite) suggests that these rocks have bulk compositions that are depleted in CaO and enriched in $Al_2O_3$ relative to typical metabasalts. Lithologies with such bulk compositions are commonly interpreted as altered mafic meta-igneous rocks (Spear and Schumacher, 1982), a protolith consistent with the associated lithologies. At lower metamorphic grades, rocks of such composition would have been chlorite-rich and, therefore, could have been exceedingly weak during deformation.

## CONCLUSIONS

Zones of discontinuous compositional layering and intense mesoscopic folding in layered gneisses of the southern basement domain developed by combined boudinage, folding, and flowage of a ductile matrix during progressive non-coaxial deformation associated with $D_B$. At least the early stages of deformation occurred under metamorphic conditions sufficient for garnet growth. The development of these disrupted zones was probably controlled by the presence of layers of an incompetent mafic lithology, possibly derived from altered mafic volcanic rocks. Post-kinematic metamorphic grain growth largely obliterated previously existing tectonic

fabrics in the deformed matrix of these disrupted zones, making analysis of grain-scale deformation mechanisms impossible.

The disrupted zones are considered "broken formations" (Hsu, 1974) because they 1) contain no exotic lithologies, 2) underwent progressive non-coaxial (ie. shearing) deformation, 3) were subjected to alternate shortening and extension along layering during deformation, and 4) are characterized by marked contrasts in mechanical behavior of adjacent lithologies. Major differences between these zones and other broken formations described in the literature (Harris and Milici, 1977; Byrne, 1984; Schultz, 1986) are that these evolved, at least in part, under higher grade metamorphic conditions and were subjected to a post-kinematic metamorphic overprint. The sequence of boudinage followed by folding and ductile flow of a mechanically weak matrix during formation of these zones is, however, strikingly similar to processes responsible for the disruption of layered rock sequences in other geologic settings, including fold-thrust belts (Gibson, 1984) and accretionary prisms (MacKenzie et al., 1987).

# Appendix B. Strain Analysis

In order to evaluate the geometrical relationships between fabric elements and the principle axes of the finite strain ellipsoid, data were collected at three locations where primary features are preserved in the gneisses for use in quantitative, three-dimensional strain analysis. Strain markers included volcaniclastic fragments in the layered gneisses (NA-31, HM-151) and biotite- and hornblende-rich inclusions in a tonalitic granitoid gneiss (CB-380). Sample locations are indicated in Figure B-1. Measurements used for strain analysis were collected on three non-orthogonal, planar surfaces at each location. Orientations of the foliation, mineral lineation, and measurement surfaces were recorded. At NA-31, measurements of strain marker dimensions were made in the field on a large float block that could be reliably restored to its original position and orientation in outcrop. Surfaces with strain markers at locations HM-151 and CB-380 were photographed with the camera lens orthogonal to the outcrop surface and strain marker dimensions measured on the photographs. A minimum of 18 strain markers were measured on each surface. In most cases, the foliation passes without deflection from the matrix into the markers, implying no significant rheological contrast between the materials (see Lisle, 1985). The only exceptions to this are epidote-rich clasts at NA-31 that deflect the foliation and are, therefore, interpreted to be more rigid than the amphibolitic matrix; these clasts were not utilized in the strain analysis.

Two-dimensional strain data were analyzed using 1) the $R_f$-$\phi$ technique (Dunnett, 1969; Lisle, 1985) and 2) the centroid method (Robin, 1977). Measured axial ratios and orientations of clasts used in the analyses are presented in Table B-1. For

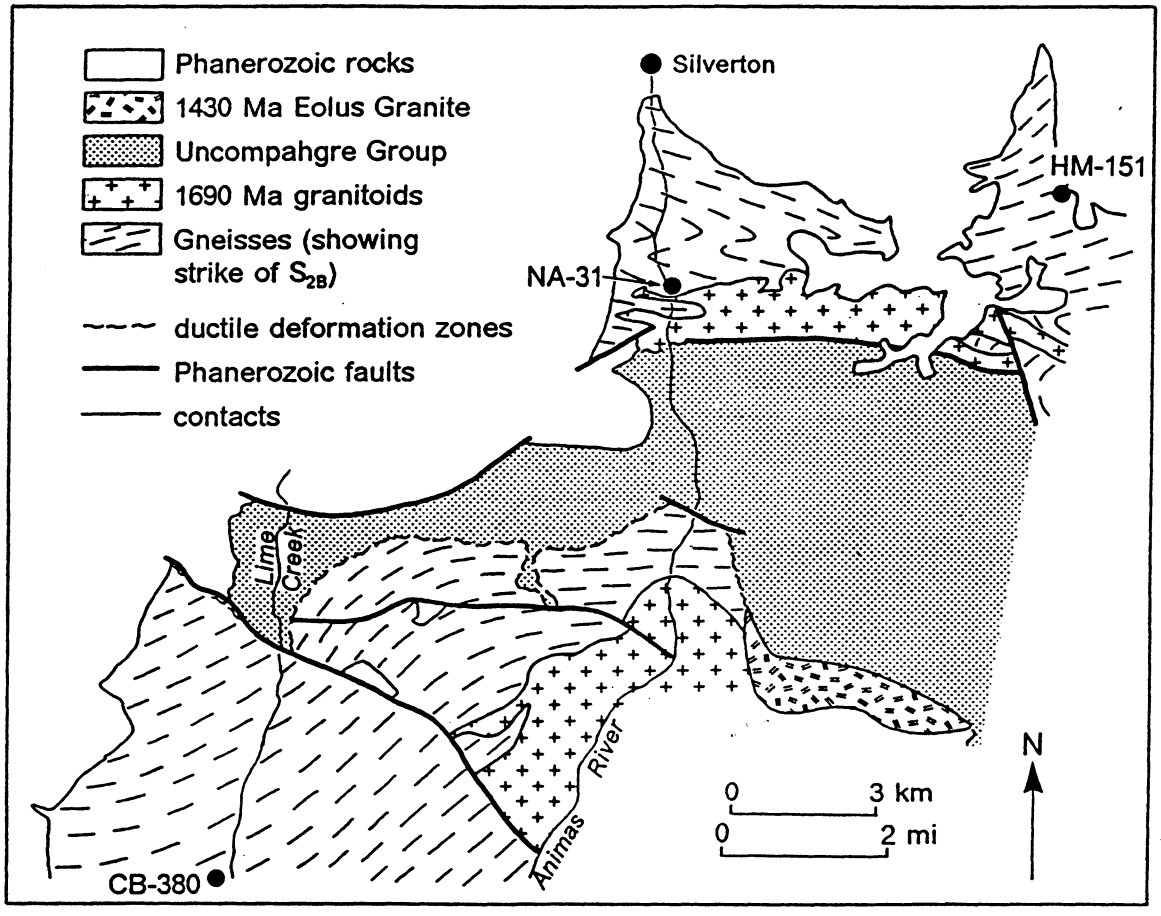


Figure B-1: Approximate locations of outcrops referred to in text; UTM coordinates for each locality given in Appendix D.

the $R_f$-$\phi$ analysis, the data were plotted on a hyperbolic net (Fig. B-2a) using a method devised by DePaor (in press). Each data population was divided into eight segments of equal area (Fig. B-2a) and subjected to a Chi-square test for symmetry (Robin, 1977) in order to detect any pre-tectonic preferred orientaion of the strain markers. All populations except that from surface HM-151b have $X^2$ values (5 degrees of freedom) that can be accounted for by sampling error at the 90% confidence level (Table B-2). Therefore, it was assumed that the markers were not preferrentially oriented prior to deformation and the populations were treated as symmetrical (see Lisle, 1985). The axial ratio (Rs) of each sectional strain ellipse was taken as the intersection of the line corresponding with the mean $\varphi$ value and the 50%-of-data curve (Fig. B-2a)(Lisle, 1985). Strain ratios greater than ten were determined by calculating the harmonic mean of the measured clast dimensions. Maximum initial shape axial ratios ($R_i$), estimated by fitting $R_i$ curves around the majority of the data points in each population, range from 1.2 to 2.0 (Table B-2).

For the centroid method (Robin, 1977), the center of gravity (centroid) of each clast was visually estimated. The trace of the foliation was assumed to be parallel to the longest axis of the sectional strain ellipse on each surface and strain marker dimensions were measured parallel (a) and orthogonal (c) to this direction. $R_f$-$\phi$ data from location NA-31 were converted to the ratio (a/c) using the mathematical relationships derived by Robin (1977) for ideal ellipsoids, which these strain markers were assumed to approximate. Once (a/c) was found for each clast, $R_s$ was calculated as the geometric mean of this ratio for all markers.

The results of the two dimensional strain analysis are summarized in Table B-2. The centroid method generally yields slightly lower $R_s$ values than the $R_f$-$\phi$ technique. In all cases, $R_s$ values determined by both methods agree within 10% of their mean value; many agree within 5%. Using the average of the two methods as

Table B-1: Axial ratios and orientations of strain markers; $\phi$ measured relative to trace of foliation on each surface; * indicates rigid, epidote-rich clasts not used in $R_s$ determination.

| Marker | $R_f$ ($R_f$-$\phi$) | $\phi$ | $R_f$ (centroid) |
|---|---|---|---|
| NA-31a | | | |
| 1* | 1.72 | 3 | 1.67 |
| 2* | 2.26 | 8 | 1.98 |
| 3* | 2.33 | 5 | 2.28 |
| 4* | 2.78 | -2 | 2.77 |
| 5* | 2.11 | -17 | 1.79 |
| 6 | 4.09 | -3 | 4.00 |
| 7 | 3.09 | -3 | 3.05 |
| 8 | 5.59 | -5 | 5.02 |
| 9 | 4.82 | 1 | 4.80 |
| 10 | 4.63 | -3 | 4.50 |
| 11 | 4.63 | -10 | 3.59 |
| 12 | 4.00 | 9 | 3.38 |
| 13 | 3.32 | -3 | 3.27 |
| 14 | 4.46 | -4 | 4.26 |
| 15 | 5.50 | 4 | 5.13 |
| 16 | 5.93 | 2 | 5.81 |
| 17 | 7.29 | 0 | 7.29 |
| 18 | 5.86 | 1 | 5.83 |
| 19 | 5.64 | 5 | 5.06 |
| 20 | 8.31 | -3 | 7.62 |
| 21 | 6.42 | 0 | 6.42 |
| 22 | 5.50 | 3 | 5.29 |
| 23 | 5.21 | 9 | 4.02 |
| 24 | 3.32 | 3 | 3.27 |
| 25 | 5.09 | 2 | 5.01 |
| 26 | 3.03 | -5 | 2.93 |
| 27 | 5.64 | 0 | 5.64 |
| 28 | 5.17 | 1 | 5.15 |
| 29 | 7.00 | 1 | 6.95 |
| 30 | 4.30 | -3 | 4.20 |
| 31 | 5.20 | -9 | 4.02 |
| 32 | 5.70 | 3 | 5.46 |
| NA-31b | | | |
| 1* | 3.70 | -1 | 3.52 |
| 2* | 5.00 | 5 | 3.59 |
| 3* | 6.14 | 3 | 4.40 |
| 4 | 13.40 | -9 | 11.00 |
| 5 | 12.50 | -6 | 12.50 |
| 6 | 12.00 | -5 | 11.80 |
| 7 | 8.40 | -10 | 7.24 |
| 8 | 5.57 | -3 | 5.35 |

Table B-1 continued:

| Marker | $R_f$ ($R_f$-$\phi$) | $\phi$ | $R_f$ (centroid) |
|---|---|---|---|
| 9 | 9.50 | -7 | 9.37 |
| 10 | 4.21 | -9 | 4.11 |
| 11 | 9.73 | -7 | 9.59 |
| 12 | 10.30 | -8 | 9.73 |
| 13 | 11.30 | -10 | 8.87 |
| 14 | 6.40 | -9 | 6.07 |
| 15 | 9.20 | -11 | 7.17 |
| 16 | 13.30 | -2 | 9.74 |
| 17 | 9.38 | -2 | 7.84 |
| 18 | 11.40 | -5 | 11.20 |
| 19 | 16.00 | -3 | 12.30 |
| 20 | 13.30 | -6 | 13.30 |
| 21 | 10.50 | -2 | 8.46 |
| 22 | 15.20 | -8 | 13.40 |
| 23 | 5.27 | -1 | 4.79 |
| 24 | 3.30 | -6 | 3.30 |
| NA-31c | | | |
| 1* | 2.71 | -10 | 2.49 |
| 2* | 3.57 | -13 | 2.85 |
| 3 | 6.91 | 2 | 6.50 |
| 4 | 6.43 | 0 | 6.39 |
| 5 | 11.60 | -1 | 11.60 |
| 6 | 8.06 | 0 | 7.89 |
| 7 | 6.76 | -1 | 6.76 |
| 8 | 5.54 | 0 | 5.51 |
| 9 | 9.47 | 0 | 9.34 |
| 10 | 9.35 | -4 | 8.40 |
| 11 | 7.37 | -3 | 7.14 |
| 12 | 11.30 | 2 | 9.73 |
| 13* | 5.84 | -10 | 4.29 |
| 14 | 9.05 | 0 | 8.94 |
| 15 | 7.95 | 1 | 7.66 |
| 16 | 9.82 | -1 | 9.82 |
| 17 | 10.30 | -4 | 9.10 |
| 18 | 6.54 | 2 | 6.19 |
| 19 | 9.72 | -4 | 8.66 |
| 20 | 6.47 | 0 | 6.43 |
| 21 | 4.44 | -1 | 4.44 |
| 22 | 9.46 | -2 | 9.33 |
| 23 | 11.40 | -3 | 10.60 |
| 24 | 6.89 | 1 | 6.70 |
| 25* | 1.74 | -5 | 1.73 |
| 26 | 12.60 | -1 | 12.60 |

Table B-1 continued:

| Marker | $R_f$ ($R_f$-$\phi$) | $\phi$ | $R_f$ (centroid) |
|---|---|---|---|
| HM-151b | | | |
| 1 | 5.45 | -8 | 4.59 |
| 2 | 7.49 | -3 | 6.81 |
| 3 | 4.93 | -1 | 6.43 |
| 4 | 6.16 | 0 | 5.81 |
| 5 | 6.15 | -1 | 6.93 |
| 6 | 17.20 | -4 | 18.60 |
| 7 | 5.54 | -7 | 5.06 |
| 8 | 5.27 | -2 | 5.24 |
| 9 | 5.79 | -1 | 4.80 |
| 10 | 3.76 | 2 | 3.88 |
| 11 | 3.85 | 3 | 2.77 |
| 12 | 4.51 | 1 | 4.76 |
| 13 | 5.04 | -1 | 4.71 |
| 14 | 5.30 | -4 | 6.70 |
| 15 | 4.88 | -2 | 5.03 |
| 16 | 6.44 | 1 | 5.56 |
| 17 | 6.61 | -2 | 6.55 |
| 18 | 5.24 | -3 | 4.82 |
| 19 | 5.06 | -3 | 4.60 |
| 20 | 4.78 | -6 | 4.30 |
| 21 | 5.63 | -4 | 4.76 |
| 22 | 8.47 | -7 | 7.39 |
| 23 | 6.67 | 1 | 6.24 |
| 24 | 6.20 | -2 | 6.22 |
| 25 | 5.31 | -3 | 4.92 |
| 26 | 4.64 | 3 | 4.50 |
| 27 | 6.72 | 1 | 5.96 |
| 28 | 4.71 | 1 | 4.18 |
| 29 | 7.32 | 1 | 6.83 |
| 30 | 5.95 | 1 | 4.85 |
| 31 | 7.65 | -3 | 8.03 |
| HM-151c | | | |
| 1 | 18.00 | 0 | 15.47 |
| 2 | 15.00 | 2 | 11.61 |
| 3 | 19.56 | 6 | 12.25 |
| 4 | 17.80 | 7 | 10.32 |
| 5 | 11.04 | 1 | 10.38 |
| 6 | 15.98 | 0 | 13.47 |
| 7 | 9.64 | -1 | 7.30 |
| 8 | 21.02 | 2 | 20.78 |
| 9 | 30.10 | 2 | 37.08 |
| 10 | 23.15 | 2 | 21.79 |
| 11 | 13.70 | 3 | 14.78 |
| 12 | 11.36 | -3 | 7.00 |
| 13 | 8.69 | -1 | 8.30 |

Table B-1 continued:

| Marker | $R_f$ ($R_f$-$\phi$) | $\phi$ | $R_f$ (centroid) |
|---|---|---|---|
| 14 | 17.04 | 0 | 18.32 |
| 15 | 21.44 | 1 | 24.35 |
| 16 | 13.40 | 2 | 13.20 |
| 17 | 12.19 | -1 | 10.13 |
| 18 | 18.88 | 2 | 23.48 |
| 19 | 12.24 | 0 | 11.19 |
| 20 | 7.60 | -1 | 6.18 |
| 21 | 30.00 | 1 | 22.40 |
| HM-151d | | | |
| 1 | 2.25 | -1 | 2.28 |
| 2 | 3.70 | 0 | 3.57 |
| 3 | 2.86 | -5 | 2.94 |
| 4 | 6.18 | -3 | 5.67 |
| 5 | 3.03 | 0 | 2.97 |
| 6 | 3.18 | 0 | 3.18 |
| 7 | 2.72 | -2 | 3.01 |
| 8 | 2.37 | 2 | 2.43 |
| 9 | 4.78 | -7 | 4.05 |
| 10 | 2.81 | -9 | 2.74 |
| 11 | 3.00 | 0 | 3.20 |
| 12 | 1.84 | 7 | 1.84 |
| 13 | 2.63 | -5 | 2.81 |
| 14 | 3.32 | -6 | 2.95 |
| 15 | 2.73 | 5 | 2.29 |
| 16 | 4.06 | -5 | 3.21 |
| 17 | 3.88 | 2 | 3.86 |
| 18 | 3.09 | -2 | 3.01 |
| 19 | 3.19 | 4 | 2.83 |
| 20 | 2.19 | 4 | 2.10 |
| 21 | 2.24 | 10 | 1.85 |
| 22 | 3.47 | 5 | 2.95 |
| 23 | 3.46 | 3 | 3.70 |
| CB-380a | | | |
| 1 | 3.80 | -24 | 3.23 |
| 2 | 3.88 | 1 | 3.47 |
| 3 | 2.93 | -9 | 3.90 |
| 4 | 4.09 | -27 | 2.23 |
| 5 | 3.86 | -26 | 1.83 |
| 6 | 3.88 | -9 | 3.53 |
| 7 | 1.88 | -10 | 1.99 |
| 8 | 1.28 | 13 | 1.05 |
| 9 | 2.48 | 1 | 2.35 |
| 10 | 2.98 | -4 | 2.97 |
| 11 | 3.40 | -8 | 3.26 |
| 12 | 9.56 | -4 | 5.17 |

Table B-1 continued:

| Marker | $R_f$ ($R_f$-$\phi$) | $\phi$ | $R_f$ (centroid) |
|---|---|---|---|
| 13 | 3.13 | -7 | 3.04 |
| 14 | 6.17 | -15 | 4.53 |
| 15 | 3.06 | -19 | 2.56 |
| 16 | 2.90 | -45 | 1.50 |
| 17 | 3.20 | -14 | 2.99 |
| 18 | 2.12 | -19 | 2.04 |
| 19 | 3.48 | -4 | 2.87 |
| 20 | 1.82 | 0 | 1.64 |
| 21 | 2.88 | -2 | 2.95 |
| 22 | 2.55 | 7 | 1.96 |
| 23 | 4.18 | -5 | 4.12 |
| 24 | 7.28 | -3 | 4.63 |
| 25 | 1.52 | -40 | .91 |
| 26 | 2.05 | -63 | .73 |
| 27 | 1.84 | -16 | 1.50 |
| 28 | 1.92 | 13 | 1.28 |
| 29 | 1.30 | +77 | .82 |
| 30 | 2.14 | -36 | 1.30 |
| 31 | 4.04 | -34 | 2.00 |
| 32 | 3.52 | -38 | 1.90 |
| 33 | 2.56 | -5 | 1.83 |
| 34 | 2.26 | -27 | 1.71 |
| 35 | 1.41 | 20 | 1.25 |
| CB-380c | | | |
| 1 | 3.67 | 10 | 3.33 |
| 2 | 2.50 | 1 | 2.41 |
| 3 | 6.31 | -6 | 3.76 |
| 4 | 4.63 | 0 | 4.81 |
| 5 | 4.71 | 1 | 3.01 |
| 6 | 10.93 | 6 | 12.17 |
| 7 | 2.75 | 4 | 2.76 |
| 8 | 3.96 | 0 | 3.00 |
| 9 | 11.39 | 0 | 7.76 |
| 10 | 6.33 | 8 | 6.35 |
| 11 | 4.90 | -2 | 3.98 |
| 12 | 8.33 | 7 | 8.38 |
| 13 | 6.88 | 12 | 6.19 |
| 14 | 7.94 | 15 | 4.50 |
| 15 | 5.88 | 3 | 5.25 |
| 16 | 3.96 | 11 | 3.75 |
| 17 | 4.14 | -1 | 3.50 |
| 18 | 4.28 | -1 | 4.70 |
| 19 | 3.82 | 4 | 3.80 |
| 20 | 6.54 | 10 | 5.58 |
| 21 | 6.58 | 2 | 5.36 |

Table B-1 continued:

| Marker | $R_f$ ($R_r$-$\phi$) | $\phi$ | $R_f$ (centroid) |
|---|---|---|---|
| CB-380d | | | |
| 1 | 4.08 | 6 | 3.76 |
| 2 | 3.52 | 2 | 3.29 |
| 3 | 3.79 | -9 | 3.37 |
| 4 | 3.44 | 4 | 3.40 |
| 5 | 8.88 | 0 | 10.76 |
| 6 | 2.61 | -2 | 2.55 |
| 7 | 4.17 | -6 | 3.92 |
| 8 | 5.42 | 1 | 4.28 |
| 9 | 5.37 | 5 | 3.99 |
| 10 | 6.39 | 8 | 5.48 |
| 11 | 3.47 | 2 | 3.45 |
| 12 | 6.92 | 0 | 7.31 |
| 13 | 2.76 | 0 | 2.60 |
| 14 | 5.15 | 5 | 4.01 |
| 15 | 3.79 | 3 | 3.41 |
| 16 | 3.21 | 5 | 3.18 |
| 17 | 3.16 | -9 | 2.89 |
| 18 | 7.04 | 2 | 7.40 |

Table B-2: Results of strain analysis: numbers in parentheses following $X^2$ values are confidence levels for acceptance of non-random initial clast orientations.

| Location | Surface orientation | Number of markers | $R_i$ | $R_s$ ($R_f$-$\phi$) | $R_s$ (centroid) | $X^2$ | |
|---|---|---|---|---|---|---|---|
| NA-31a | 132,48S | 26 | 1.5 | 5.0 | 4.7 | 7.09 | (78) |
| NA-31b | 063,44N | 21 | 1.6 | 9.2 | 8.3 | 4.34 | (50) |
| NA-31c | 176,70E | 23 | 1.5 | 8.3 | 7.9 | 4.56 | (52) |
| HM-151b | 175,39E | 31 | 1.3 | 5.4 | 5.5 | 10.94 | (95) |
| HM-151c | 106,8S | 21 | ---- | 14.5 | 13.7 | ----- | (25) |
| HM-151d | 159,86E | 23 | 1.4 | 3.0 | 2.9 | 2.65 | (59) |
| CB-380a | 065,77S | 35 | 2.0 | 2.4 | 2.2 | 4.87 | (59) |
| CB-380c | 330,16W | 35 | 1.6 | 5.1 | 4.8 | 5.67 | (65) |
| CB-380d | 130,85E | 18 | 1.5 | 3.8 | 4.1 | 5.05 | (58) |

Figure B-2: Strain analysis techniques.

a) $R_f$-$\phi$ plot for surface NA-31a; divisions along mean-$\varphi$ line are shape ratios ($R_f$ and $R_s$); table shows calculation of $X^2$;

b) stereonet construction for determination of principle stretch directions from three sectional strain ellipses for sample NA-31; dashed lines are circular sections of strain ellipsoid.

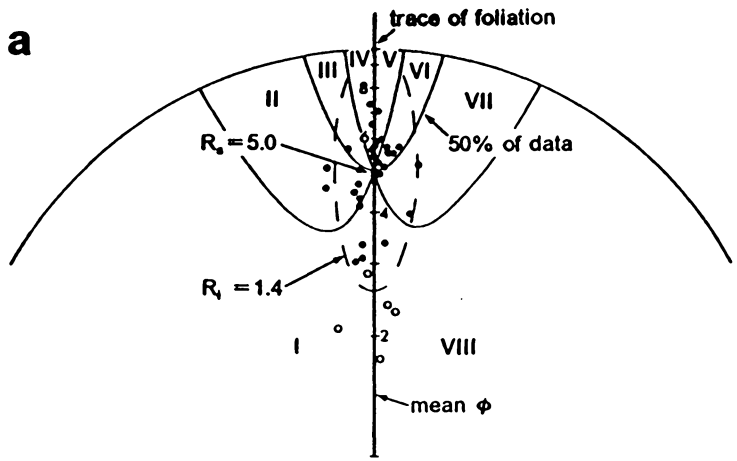


| | I | II | III | IV | V | VI | VII | VIII |
|---|---|---|---|---|---|---|---|---|
| $N_K$ | 3.5 | 5.5 | 1.0 | 3.0 | 3.0 | 6.0 | 3.0 | 1.0 |
| $(N_K-n/8)^2/(n/8)$ | 0.02 | 1.56 | 1.56 | 0.02 | 0.02 | 2.33 | 0.02 | 1.56 |

$n = 26$ $\quad X^2 = \sum(N_K-n/8)^2/(n/8) = 7.09$

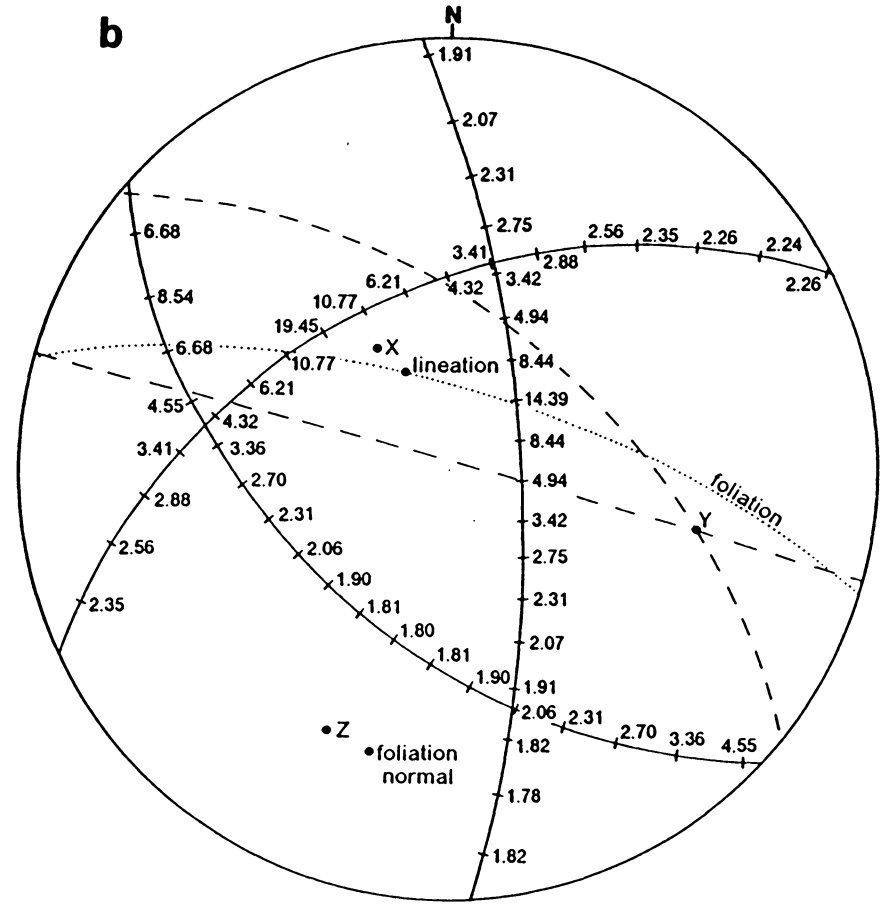

the best estimate of the actual $R_s$ values, the results from the three surfaces at each locality were combined into three-dimensional strain eliipsoids using the approach outlined by DePaor (1986). No assumptions are made with respect to the relative orientations of fabric elements and the finite strain axes using this technique. This method involves scaling and minor rotations of the axes of each determined sectional ellipse in order to minimize misfit between the ellipses in three dimensions. After scaling and rotation, the dimensions of each sectional ellipse were calculated and plotted in their proper positions on an equal angle projection (Fig. B-2b). Circular sections of the strain ellipsoid were fitted by visual inspection (Fig. B-2b). The orientations of the the principle finite strain axes ($X > Y > Z$) were determined by knowing that Y coincides with the intersection of the circular sections whereas X and Z are orthogonal to Y and bisect the angles between the circular sections (Ramsay, 1967). Because small misfits ($< 10°$) between the sectional ellipses remained in some cases after the completion of this proceedure, the orientations of the finite strain axes are considered accurate to within 10° around the determined values.

Figure B-3 illustrates the results of the three-dimensional strain analysis. Principle axes of the determined finite strain ellipsoids are systematically related to the orientations of the fabric elements; X is parallel to the mineral lineation and Z is orthogonal to the foliation (Fig. B-3a). The three localities yield a range of strain magnitudes although, in all three cases, the strain ellipsoids are oblate with values of $k < 1$ (Fig. B-3b).

Apparent oblate strains may be produced by volume loss even when the true strain is plane ($k = 1$) or prolate ($k > 1$); this is manifest on a Flinn plot by a shift of the $k = 1$ line to the right along the Y/Z axis (Ramsay and Wood, 1973). If the true strains at the three localities were actually plane strains, volume losses in excess of 60% would be necessary to account for the observed values (Fig. B-3). Because such

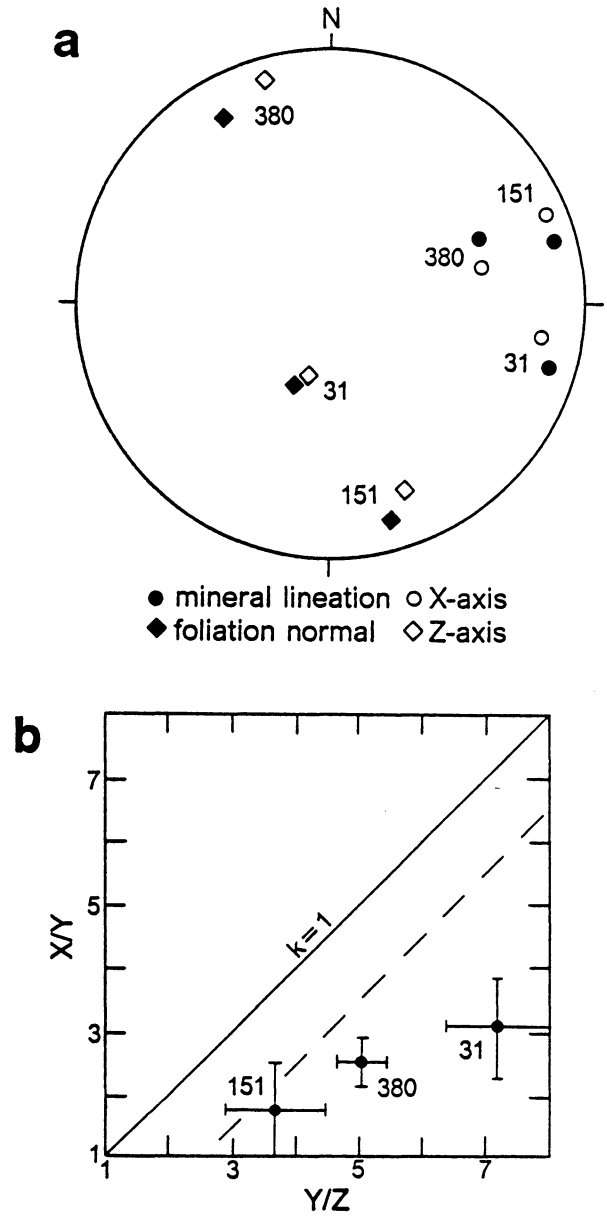


Figure B-3: Results of finite strain analysis.

a) orientations of principle stretch directions relative to fabric elements (NA-31 results rotated to coincide with orientations in outcrop);

b) Flinn plot showing strain magnitudes; dashed line is k = 1 line for 60% volume loss.

volume losses are considered unreasonable (Ramsay and Wood, 1973), these are interpreted as true oblate strains.

Models for the origin of true oblate strains include 1) the superposition of multiple strains with variable axial orientations during successive strain events (Coward, 1973), 2) differential elongation parallel to X within the foliation plane (Ramsay and Wood, 1973), 3) combined thrust and wrench shearing (Sanderson, 1980), and 4) simple shear combined with shortening across the shear plane (e.g. lateral spreading of nappes - Durney and Ramsay, 1973; transpression - Bidwell and Bauer, 1987). The fact that the rocks in this area underwent multiple phases of deformation suggests that (1) is the most likely explanation. However, data from areas or rock units affected only by one phase of deformation ($D_B$ or $D_{BC}$) are necessary to fully understand the origin of the finite strains. In addition, more data from other localities are needed in order to draw meaningful conclusions concerning the nature and significance of regional variations in strain magnitude.

# Appendix C. Chemical Analyses

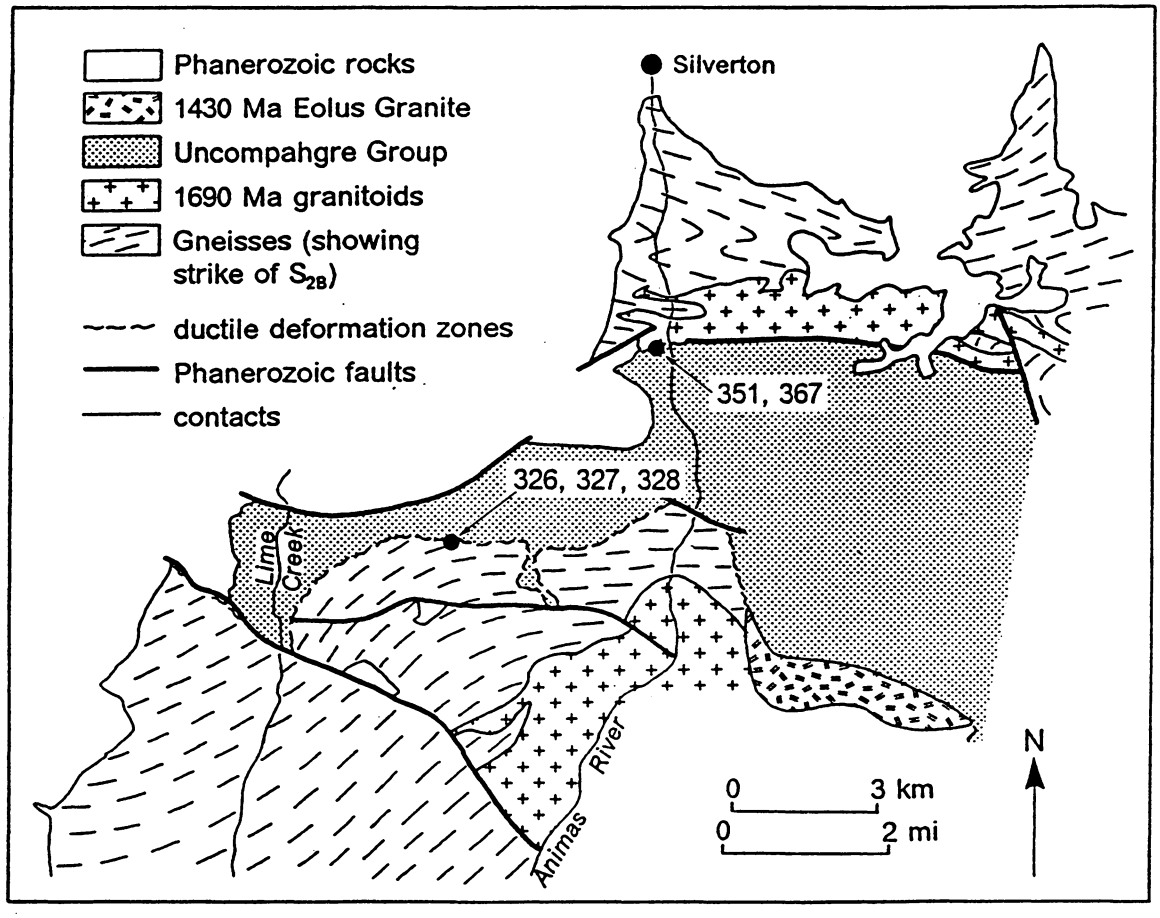


Figure C-1: Approximate locations of samples analyzed for major elements; UTM grid coordinates for each sample locality are given in Appendix D.

Table C-1: Major element analyses of rocks near basement-cover contacts: ICP analyses by Chemex Labs, Sparks, Nevada; detection limits 0.01 wt % for all oxides except $K_2O$ (0.1 wt %).

| Oxide | 327 | 328 | 326 | 351 | 367 |
|---|---|---|---|---|---|
| $SiO_2$ | 69.93 | 69.77 | 68.64 | 68.04 | 65.92 |
| $Al_2O_3$ | 13.75 | 14.41 | 14.98 | 19.13 | 20.52 |
| $Fe_2O_3$ | 4.09 | 3.95 | 4.21 | 2.71 | 3.24 |
| MgO | 1.07 | 2.01 | 2.23 | 0.17 | 0.22 |
| CaO | 3.23 | 1.72 | 0.58 | 0.32 | 0.70 |
| $Na_2O$ | 4.02 | 3.76 | 0.52 | 0.48 | 1.25 |
| $K_2O$ | 2.20 | 0.90 | 3.90 | 5.00 | 4.50 |
| $TiO_2$ | 0.22 | 0.22 | 0.23 | 0.63 | 0.32 |
| $P_2O_5$ | 0.29 | 0.25 | 0.30 | 0.26 | 0.21 |
| MnO | 0.07 | 0.18 | 0.04 | 0.02 | 0.01 |
| LOI | 1.65 | 2.30 | 3.22 | 2.78 | 2.87 |
| TOTAL | 100.5 | 99.47 | 98.33 | 99.54 | 99.76 |

327 - unaltered pl + qtz + bt gneiss, approximately 50m south of sample 326

328 - partially altered felsic gneiss, approximately 10m south of sample 326

326 - ms + qtz + chl phyllite with $S_{2B}$ foliation, approximately 2m south of contact with Uncompahgre Group.

351 - non-foliated ms + qtz + ctd rock, approximately 20cm north of contact with Uncompahgre Group in outcrop illustrated in Figure 3-4b.

367 - ms + qtz rock with relict $S_{2B}$ foliation, approximately 50cm north of contact with Uncompahgre Group.

# Appendix D. Sample Locations

Table D-1: Universal Transverse Mercator (UTM) coordinates for samples and locations cited in the text and appendices; all locations are within grid zone 13, subzone S, grid square BM.

| Sample | Coordinates |
|---|---|
| 15 | $65^{080}$E, $80^{380}$N |
| 26 | $59^{950}$E, $76^{390}$N |
| 28 | $59^{860}$E, $76^{300}$N |
| 29 | $60^{630}$E, $76^{310}$N |
| 55 | $65^{350}$E, $82^{940}$N |
| 83 | $65^{520}$E, $84^{050}$N |
| 118 | $56^{360}$E, $69^{720}$N |
| 141 | $56^{220}$E, $74^{000}$N |
| 162 | $66^{070}$E, $76^{810}$N |
| 165 | $65^{590}$E, $74^{960}$N |
| 165A | $65^{600}$E, $74^{890}$N |
| 166 | $65^{420}$E, $75^{670}$N |
| 173 | $57^{810}$E, $74^{040}$N |
| 180 | $59^{390}$E, $76^{250}$N |
| 183 | $62^{530}$E, $76^{320}$N |
| 213 | $72^{310}$E, $83^{020}$N |
| 220A | $65^{210}$E, $80^{320}$N |
| 220B | $65^{210}$E, $80^{320}$N |
| 228 | $59^{560}$E, $78^{680}$N |
| 294 | $65^{970}$E, $80^{430}$N |
| 315 | $65^{370}$E, $77^{050}$N |
| 316 | $65^{370}$E, $77^{050}$N |
| 317 | $65^{180}$E, $77^{000}$N |
| 326 | $61^{000}$E, $76^{420}$N |
| 327 | $61^{000}$E, $76^{370}$N |
| 328 | $61^{000}$E, $76^{410}$N |
| 334 | $69^{450}$E, $83^{070}$N |
| 350 | $65^{080}$E, $80^{380}$N |
| 351 | $65^{130}$E, $80^{380}$N |
| 355 | $72^{820}$E, $83^{230}$N |
| 367 | $65^{220}$E, $80^{320}$N |
| 381 | $70^{550}$E, $81^{390}$N |
| 412 | $63^{570}$E, $76^{320}$N |

| Outcrop | Coordinates |
|---|---|
| I | $64^{890}$E, $80^{400}$N |
| II | $62^{530}$E, $76^{320}$N |
| III | $65^{970}$E, $80^{430}$N |
| IV | $65^{080}$E, $80^{380}$N |
| V | $57^{810}$E, $74^{040}$N |
| VI | $59^{340}$E, $76^{200}$N |
| VII | $61^{000}$E, $76^{420}$N |
| CB-380 | $56^{200}$E, $68^{850}$N |
| HM-151 | $73^{510}$E, $83^{720}$N |
| NA-51 | $65^{550}$E, $81^{530}$N |

The vita has been removed from the scanned document